CORONA OF MAGNETARS

Andrei M. Beloborodov[1]

Physics Department and Columbia Astrophysics Laboratory, Columbia University, 538 West 120th Street New York, NY 10027; amb@phys.columbia.edu

Christopher Thompson

Canadian Institute for Theoretical Astrophysics, University of Toronto, 60 St. George Street, Toronto, ON M5S 3H8, Canada; thompson@cita.utoronto.ca

ABSTRACT

We develop a theoretical model that explains the formation of hot coronae around strongly magnetized neutron stars — magnetars. The starquakes of a magnetar shear its external magnetic field, which becomes non-potential and is threaded by an electric current. Once twisted, the magnetosphere cannot untwist immediately because of its self-induction. The self-induction electric field lifts particles from the stellar surface, accelerates them, and initiates avalanches of pair creation in the magnetosphere. The created plasma corona maintains the electric current demanded by curl $\mathbf{B}$ and regulates the self-induction e.m.f. by screening. This corona persists in dynamic equilibrium: it is continually lost to the stellar surface on the light-crossing time $\sim 10^{-4}$ s and replenished with new particles. In essence, the twisted magnetosphere acts as an accelerator that converts the toroidal field energy to particle kinetic energy. Using a direct numerical experiment, we show that the corona self-organizes quickly (on a millisecond timescale) into a quasi-steady state, with voltage $e\Phi_e \sim 1$ GeV along the magnetic lines. The voltage is maintained near threshold for ignition of pair production, and pair production occurs at a rate just enough to feed the electric current. The heating rate of the corona is $\sim 10^{36}$ erg/s, in agreement with the observed persistent, high-energy output of magnetars. We deduce that a static twist that is suddenly implanted into the magnetosphere will decay on a timescale of 1-10 yrs. The particles accelerated in the corona impact the solid crust, knock out protons, and regulate the column density of the hydrostatic atmosphere of the star. The transition layer between the atmosphere and the corona may be hot enough to create additional $e^{\pm}$ pairs. This layer is the likely source of the observed 100 keV emission from magnetars. The corona emits curvature radiation up to 10^{14} Hz and can supply the observed IR-optical luminosity. We outline the implications of our results for the non-thermal radiation in other bands, and for the post-burst evolution of magnetars.

[1]Also at Astro-Space Center of Lebedev Physical Institute, Profsojuznaja 84/32, Moscow 117810, Russia

Subject headings: plasmas — stars: coronae, magnetic fields, neutron — X-rays: stars

1. INTRODUCTION

At least 10% of all neutron stars are born as magnetars, with magnetic fields $B > 10^{14}$ G. Their activity is powered by the decay of the ultrastrong field and lasts about 10^4 years. They are observed at this active stage as either Soft Gamma Repeaters (SGRs) or Anomalous X-ray Pulsars (AXPs) (see Woods & Thompson 2006 for a recent review). Twelve active magnetars are currently known, and all of them have similar parameters: spin period $P \sim 10$ s, persistent X-ray luminosity $L \sim 10^{35} - 10^{36}$ erg/s, and surface temperature $k_{\rm B}T \sim 0.5$ keV. The large-scale (dipole) component of the magnetic field $B_{\rm dipole} > 10^{14}$ G has been inferred from the measurement of rapid spindown in several AXPs, and more recently in two SGRs (Kouveliotou et al. 1998, 1999). However, there is evidence for even stronger magnetic field inside the star, as was originally deduced from considerations of magnetic field transport (Thompson & Duncan 1996). In particular, the occurence of enormously energetic X-ray flares in SGRs points to internal magnetic fields approaching $\sim 10^{16}$ G (Hurley et al. 2005). Bursting activity has also been detected in two AXPs (Kaspi et al. 2003), which strongly supports the hypothesis that active rearrangement of the magnetic field takes place in AXPs as well as SGRs, although at differing rates.

Besides the sporadic X-ray outbursts, a second, persistent, form of activity has been discovered by studying the emission spectra of magnetars. Until recently, the spectrum was known to have a thermal component with temperature $k_{\rm B}T \sim 0.5$ keV, interpreted as blackbody emission from the star's surface. The soft X-ray spectrum also showed a tail at $2 - 10$ keV with photon index $\Gamma = 2 - 4$. Intriguingly, the hardness of the $2 - 10$ keV spectrum correlates with long-term activity as a transient burst source (Marsden & White 2001). This deviation from pure surface emission already suggested that energy is partially released above the star's surface. Recently, observations by RXTE and INTEGRAL have revealed even more intriguing feature: magnetars are bright, persistent sources of 100 keV X-rays (Kuiper et al. 2004; Molkov et al. 2005; Mereghetti et al. 2005; den Hartog et al. 2006; Kuiper et al. 2006). This high-energy emission forms a separate component of the magnetar spectrum, distinct from the soft X-ray component that was known before. The new component becomes dominant above 10 keV, has a very hard spectrum, $\Gamma \simeq 1$, and peaks above 100 keV where the spectrum is unknown. The luminosity in this band, $L \sim 10^{36}$ erg s^{-1}, even exceeds the thermal luminosity from the star's surface. These hard X-rays can be emitted only in the exterior of the star and demonstrate the presence of an active plasma corona.

Our goal in this paper is to understand the origin and composition of the magnetar corona. The starting point of our analysis is the fact that an evolving magnetar experiences strong deformations of its crust, due to a shifting configuration of the internal magnetic field. These "starquakes" shear the magnetic field that is anchored in the crust, thereby injecting an electric current into the stellar magnetosphere. This process bears some resemblence to the formation of current-carrying structures in the Solar corona, although there are important differences which shall be discussed below. We investigate how the starquakes and twisting of the magnetosphere can lead to the formation of a plasma corona around a magnetar.

The persistence of magnetospheric twists can explain several observed properties of the AXPs and SGRs (Thompson, Lyutikov, & Kulkarni 2002; hereafter TLK). TLK investigated the observational consequences using a static, force-free model, idealizing the magnetosphere as a globally twisted dipole. They showed that a twist affects the spindown rate of the neutron star: it causes the magnetosphere to flare out slightly from a pure dipole configuration, thereby increasing the braking torque acting on the star. The force-free configuration is independent of the plasma behavior in the magnetosphere. It does rely, however, on the presence of plasma that can conduct the required current $\mathbf{j}_B = (c/4\pi)\nabla \times \mathbf{B}$. This requires a minimum density $n_c = j_B/ec$. TLK showed that even this minimum density significantly modifies the stellar radiation by multiple resonant scattering, which can explain the tail of the surface emission at $2 - 10$ keV.

In this paper, we formulate the problem of plasma dynamics in the closed twisted magnetosphere and find a simple solution to this problem, which allows one to understand the observed energy output of the magnetar corona and the evolution of magnetic twists. Plasma behavior around neutron stars has been studied for decades in the context of radio pulsars, and that problem remains unsolved. The principle difference with radio pulsars is that their activity is caused by *rotation*, and dissipation occurs on *open magnetic lines* that connect the star to its light cylinder. Electron-positron pairs are then created on open field lines (e.g. Ruderman & Sutherland 1975; Arons & Scharlemann 1979; Harding & Muslimov 2002). By contrast, the formation of a corona around a magnetar does not depend on rotation of the neutron star. All observed magnetars are slow rotators ($\Omega = 2\pi/P \sim 1$ Hz), and their rotational energy cannot feed the observed coronal emission. (The bolometric output of some magnetars is $\sim 10^4$ times larger than the spindown luminosity, as deduced from the rotational period derivative!) The open field lines form a tiny fraction $R_{\rm NS}\Omega/c \sim 3 \times 10^{-5}$ of the magnetic flux threading the neutron star. Practically the entire plasma corona is immersed in the *closed* magnetosphere and its heating must be caused by some form of dissipation on the closed field lines. In contrast with canonical radio pulsars, the magnetar corona admits a simple solution.

Plasma near a neutron star is strongly constrained compared with many other forms of plasma encountered in laboratory and space, and therefore easier to model. The relative simplicity is due to the fact that the magnetic field is strong and fixed — its evolution timescale is much longer than the residence time of particles in the corona. Furthermore, particles are at the lowest Landau level and move strictly along the magnetic field lines, which makes the problem effectively one-dimensional. Finally, the magnetic lines under consideration are closed, with both ends anchored in the highly conducting stellar material. The basic questions that one would like to answer are as follows. How is the magnetosphere populated with plasma? The neutron star surface has a temperature $k_{\rm B}T \lesssim 1$ keV and the scale-height of its atmospheric layer (if it exists) is only a few cm. How is the plasma supplied above this layer and what type of particles populate the corona?

How is the corona heated, and what are the typical energies of the particles? If the corona conducts a current associated with a magnetic twist $\nabla \times \mathbf{B} \neq 0$, how rapid is the dissipation of this current, i.e. what is the lifetime of the twist? Does its decay imply the disappearance of the corona?

An outline of the model proposed in this paper is as follows. The key agent in corona formation is an electric field $E_\parallel$ parallel to the magnetic field. $E_\parallel$ is generated by the self-induction of the gradually decaying current and in essence measures the rate of the decay. It determines the heating rate of the corona via Joule dissipation. If $E_\parallel = 0$ then the corona is not heated and, being in contact with the cool stellar surface, it will have to condense to a thin surface layer with $k_{\rm B}T \lesssim 1$ keV. The current-carrying particles cannot flow upward against gravity unless a force $eE_\parallel$ drives it. On the other hand, when $E_\parallel$ exceeds a critical value, $e^\pm$ avalanches are triggered in the magnetosphere, and the created pairs screen the electric field. This leads to a "bottleneck" for the decay of a magnetic twist, which implies a slow decay.

The maintenance of the corona and the slow decay of the magnetic twist are intimately related because both are governed by $E_\parallel$. In order to find $E_\parallel$, one can use Gauss' law $\nabla \cdot \mathbf{E} = 4\pi\rho$, where ρ is the net charge density of the coronal plasma. This constraint implies that $\mathbf{E}$ and ρ must be found self-consistently. We formulate the problem of plasma dynamics in a twisted magnetic field and the self-consistent electric field, and investigate its basic properties. The problem turns out to be similar to the classical double-layer problem of plasma physics (Langmuir 1929) with a new essential ingredient: $e^\pm$ pair creation.

We design a numerical experiment that simulates the behavior of the 1-D plasma in the magnetosphere. The experiment shows how the plasma and electric field self-organize to maintain the time-average magnetospheric current $\bar{\mathbf{j}} = \mathbf{j}_B$ demanded by the magnetic field, $(4\pi/c)\bar{\mathbf{j}} = \nabla \times \mathbf{B}$. The electric current admits no steady state on short timescales and keeps fluctuating, producing $e^\pm$ avalanches. This state may be described as a self-organized criticality. Pair creation is found to provide a robust mechanism for limiting the voltage along the magnetic lines to $e\Phi_e \lesssim 1$ GeV and regulate the observed luminosity of the corona.

The paper is organized as follows. We start with a qualitative description of the mechanism of corona formation, and show that it can be thought of as an electric-circuit problem (§ 2). A careful formulation of the circuit problem and the set up of numerical experiment are described in § 3. In § 4 we find that the circuit without $e^\pm$ creation does not provide a self-consistent model. Pair creation is found to be inevitable and described in detail in § 5. In § 6 we discuss the transition layer between the corona and the relatively cold surface of the star. The maintenance of a dense plasma layer on the surface is addressed in § 7. Observational implications and further developments of the model are discussed in § 8.

2. MECHANISM OF CORONA FORMATION

2.1. Ejection of Magnetic Helicity from a Neutron Star

A tightly wound-up magnetic field is assumed to exist inside magnetars (e.g. Thompson & Duncan 2001). The internal toroidal field can be much stronger than the external large-scale dipole component.[1] The essence of magnetar activity is the transfer of magnetic helicity from the interior of the star to its exterior, where it dissipates. This involves rotational motions of the crust, which inevitably twist the external magnetosphere that is anchored to the stellar surface. The magnetosphere is probably twisted in a catastrophic way, when the internal magnetic field breaks the crust and rotates it. Such starquakes are associated with observed X-ray bursts (Thompson & Duncan 1995). The most interesting effect of a starquake for us here is the partial release of the winding of the internal magnetic field into the exterior, i.e., the injection of magnetic helicity into the magnetosphere.

Since the magnetic field is energetically dominant in the magnetosphere, it must relax there to a force-free configuration with $\mathbf{j} \times \mathbf{B} = 0$. The effective footpoints of the force-free field lines sit in the inner crust of the star. At this depth currents may flow across the magnetic lines because the deep crust can sustain a significant Ampère force $\mathbf{j} \times \mathbf{B}/c \neq 0$: this force is balanced by elastic forces of the deformed crust. The ability of the crust to sustain $\mathbf{j} \nparallel \mathbf{B}$ quickly decreases toward the surface, and it is nearly force-free where[2] $\rho \lesssim 10^{13} B_{15}^{2.5}$ g/cm^3 (Thompson & Duncan 2001). The build-up of stresses in the crust from an initial magnetostatic equilibrium has been studied recently by Braithwaite & Spruit (2006).

The ejection of helicity may be thought of as directing an interior current (which previously flowed across the field and applied a $\mathbf{j} \times \mathbf{B}/c$ force) into the force-free magnetosphere. The ejected current flows along the magnetic lines to the exterior of the star, reaches the top of the line and comes back to the star at the other footpoint. The currents emerging during the starquake may percolate through a network of fractures in the crust. Then large gradients in the field are initially present which can be quickly erased. A relatively smooth magnetospheric twist of scale $\sim R_{\rm NS}$ will have the longest lifetime.

Globally twisted magnetic fields are observed to persist in the Solar corona over many Alfvén crossing times. Twisted magnetic configurations have also been studied in laboratory experiments. In particular, the toroidal pinch configuration has been studied in detail and is well explained as a relaxed plasma state in which the imparted magnetic helicity has been nearly conserved (Taylor 1986). The toroidal pinch relaxes to the minimum-energy state which has a uniform helicity density:

[1]Existing calculations of the relaxation to magnetostatic equilibrium in a fluid star (e.g., a nascent magnetar) assume that the initial toroidal and poloidal fluxes are comparable (Braithwaite & Spruit 2004). The initial toroidal flux can, in fact, be substantially stronger due to the presence of rapid differential rotation in the newly formed star.

[2]Throughout this paper we use the notation $X = X_n \times 10^n$, where quantity X is measured in c.g.s. units.

$\nabla \times \mathbf{B} = \mu\,\mathbf{B}$ with $\mu =$ const. This state is achieved because the experiment has toroidal geometry and the current is isolated from an external conductor. The relaxation process is then free to redistribute the current between neighboring magnetic flux tubes via small-scale reconnection, which leads to a uniform μ. The geometry is different in the case of a magnetar (or the sun) — the field lines are anchored to the star and their configuration depends on the footpoint motion (for related calculations of the relaxed state of a driven plasma see, e.g., Tang & Boozer [2005]). The long lifetime ($\gtrsim 1$ year) of a twisted configuration around magnetars is supported by observations of long-lived changes in the spindown rate and X-ray pulse profiles (Woods & Thompson 2006; TLK) as well as persistent nonthermal X-ray emission.

The shape of a twisted force-free magnetosphere may be calculated given the boundary conditions at the footpoints. An illustrative model of a globally twisted dipole field was considered by TLK. It has one parameter — twist angle $\Delta\phi$ — and allows one to see the qualitative effects of increasing twist on the magnetic configuration. The current density in this configuration is

$$\mathbf{j}(r,\theta) = \frac{c}{4\pi}\nabla \times \mathbf{B} \simeq \frac{c\mathbf{B}}{4\pi r}\sin^2\theta\,\Delta\phi \qquad (r > R_{\rm NS}), \tag{1}$$

where r, θ, ϕ are spherical coordinates with the polar axis chosen along the axis of the dipole. Even for strong twists, $\Delta\phi \sim 1$, the poloidal components B_r and B_θ are found to be close to the normal dipole configuration, although the magnetosphere is somewhat inflated. The main difference is the appearance of a toroidal field B_ϕ.

The global structure of a real twisted magnetosphere may be complex. The displacement ξ of the magnetosphere's footpoints during a starquake may be described as a 2D incompressible motion with $\nabla \cdot \xi = 0$ and $\nabla \times \xi \neq 0$. Suppose that the yielding behavior of the crust produces a motion $\xi \neq 0$ that is localized within a plate S, and this plate is connected by magnetospheric field lines to another plate on the opposite side of the star. Then $\int \nabla \times \xi \,\mathrm{d}S = \int \xi \cdot \mathrm{d}\mathbf{L} = 0$ where L is the boundary of S. Hence $\nabla \times \xi$ must change sign within S. For example, for an axially symmetric rotational motion, the ejection of current in the center of the plate is accompanied by initiation of an opposite current on its periphery that screens the ejected current from the unmoved footpoints with $\xi = 0$.

In this paper, we study the plasma dynamics in a flux tube dS with a given twist current $j_B = (c/4\pi)|\nabla \times \mathbf{B}|$. The magnetosphere may be thought of as a collection of such elementary flux tubes, whose currents j_B vary from footpoint to footpoint. The variation of j_B is expected to be gradual, so that the characteristic thickness of a flux tube with a given j_B is comparable to $R_{\rm NS}$.

The emerging currents are easily maintained during the X-ray outburst accompanying a starquake. A dense, thermalized plasma is then present in the magnetosphere, which easily conducts the current. Plasma remains suspended for some time after the starquake because of the transient thermal afterglow with a high blackbody temperature, up to ~ 4 keV. The cyclotron resonance of the ions is at the energy $\hbar eB/m_pc = 6.3B_{15}$ keV and, during the afterglow, the radiative flux at the resonance is high enough to lift ions from the surface against gravity (Ibrahim et al. 2001).

Eventually the afterglow extinguishes and the radiative flux becomes unable to support the plasma outside the star. The decreasing density then threats the capability of the magnetosphere to conduct the current of the magnetic twist. A minimal "corotation" charge density $\rho_{\rm co} = -\boldsymbol{\Omega}\cdot \mathbf{B}/2\pi c$ is always maintained because of rotation of the star with frequency Ω (Goldreich & Julian 1969), but it is far smaller than the minimal density that is needed to supply the current $\mathbf{j}$ (eq. 1):

$$\frac{|\rho_{\rm co}|}{|\mathbf{j}|/c} \sim \frac{1}{\Delta\phi}\left(\frac{\Omega R_{\rm max}}{c}\right) \ll 1. \tag{2}$$

Here $R_{\rm max}(r,\theta) = r/\sin^2\theta$ is the maximum radius of a dipolar field line that passes through coordinates (r,θ). The current, however, will be forced to continue to flow by its self-induction, and the magnetosphere finds a way to re-generate the plasma that can carry the current (see § 2.2). So, the twisted force-free configuration persists.

The stored energy of non-potential (toroidal) magnetic field associated with the ejected current is subject to gradual dissipation. In our model, this dissipation feeds the observed activity of the corona. The stored energy is concentrated near the star and carried by closed magnetic lines with a maximum extension radius $R_{\rm max} \sim 2R_{NS}$. Thus, most of the twist energy will be released if these lines untwist, and we focus in this paper on the near magnetosphere $R_{\rm max} \sim 2R_{NS}$.

2.2. Bottleneck for the Twist Decay and Plasma Supply to the Corona

Consider a magnetic flux tube[3] with cross section $S \lesssim R_{\rm NS}^2$ and length $L \sim R_{\rm NS}$ which carries a current $I = Sj$. The stored magnetic energy of the current per unit length of the tube is

$$\frac{\mathcal{E}_{twist}}{L} \sim \frac{I^2}{c^2}\, S. \tag{3}$$

The decay of this energy is associated with an electric field parallel to the magnetic lines $\mathbf{E}_\parallel$: this field can accelerate particles and convert the magnetic energy into plasma energy. Conservation of energy can be expressed as

$$\frac{\partial}{\partial t}\left(\frac{B^2}{8\pi}\right) = -\,\mathbf{E}\cdot\mathbf{j} - \nabla\cdot\left(c\frac{\mathbf{E}\times\mathbf{B}}{4\pi}\right), \tag{4}$$

as follows from Maxwell's equations with $E \ll B$ (e.g. Landau & Lifshitz 1975). The first term on the right-hand side is the Joule dissipation caused by $\mathbf{E}_\parallel$. The second term — the divergence of the Poynting flux — describes the redistribution of magnetic energy in space.

The decay of the twist is related to the voltage between the footpoints of a magnetic line,

$$\Phi_e = \int_A^C \mathbf{E}\cdot {\rm d}\mathbf{l}. \tag{5}$$

---

[3]In an axisymmetric magnetosphere, we could equally well focus on a flux surface of revolution which sits within a range $\Delta\theta$ of polar angle θ and has a cross section $S = 2\pi r^2 \sin\theta\Delta\theta$.

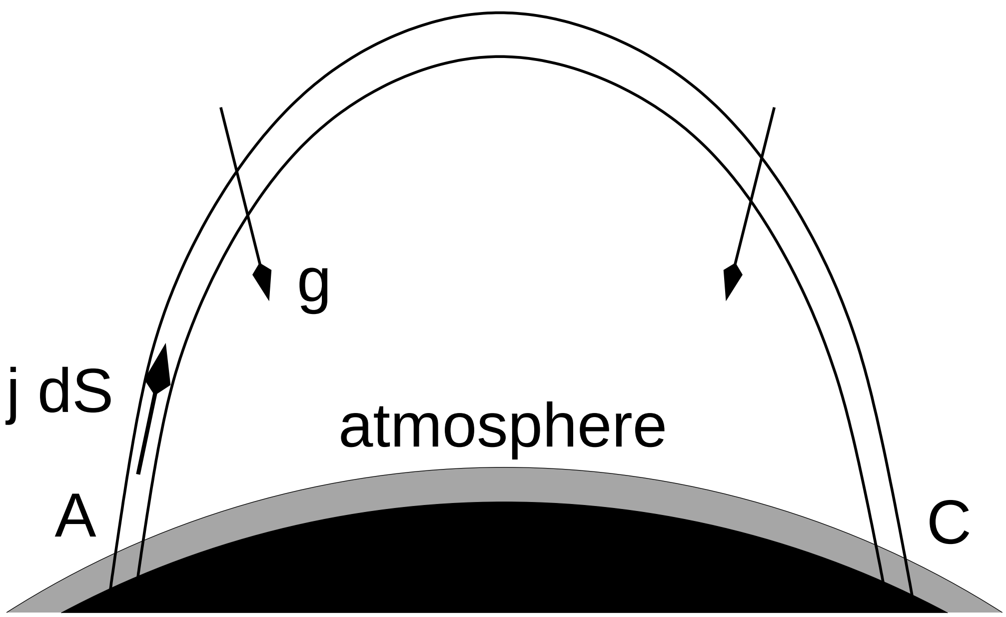

Fig. 1.— Schematic picture of a current-carrying closed magnetic flux tube, anchored to the star's surface. The current is initiated by a starquake that twists one (or both) footpoints of the tube. The current flows along the tube into the magnetosphere and returns to the star at the other footpoint, where it enters the atmosphere and the crust, following the magnetic field lines ($\mathbf{j} \parallel \mathbf{B}$). Sufficiently deep in the crust, the current can flow across the field lines and change direction, so that it can flow back to the twisted footpoint through the magnetosphere (or directly through the star, depending on the geometry of the twist). A self-induction voltage is created along the tube between its footpoints, which accompanies the gradual decay of the current. The voltage is generated because the current has a tendency to become charge-starved above the atmospheric layer whose scale-height $h = k_{\rm B}T/gm_p$ is a few cm.

Here A and C are the anode and cathode footpoints and d$\mathbf{l}$ is the line element; the integral is taken along the magnetic line outside the star (Fig. 1). The product $\Phi_e I$ approximately represents the dissipation rate $\dot{\mathcal{E}}$ in the tube. (The two quantities are not exactly equal in a time-dependent circuit.) The instantaneous dissipation rate is given by

$$\dot{\mathcal{E}} = \int_A^C \mathbf{E} \cdot \mathbf{I}(l) \mathrm{d}\mathbf{l}, \tag{6}$$

where $\mathbf{I}(l) = S\mathbf{j}$ is the instantaneous current at position l in the tube. The current is fixed at the footpoints A and C, $I = I_0$; it may, however, fluctuate between the footpoints.

Note that the true scalar potential Φ is different from Φ_e and not related to the dissipation rate. Φ is the 0-component of the 4-potential $\Phi^\mu = (\Phi, \mathbf{A})$ which is related to the electric field by

$$\mathbf{E} = -\nabla\Phi - \frac{1}{c}\frac{\partial \mathbf{A}}{\partial t}. \tag{7}$$

If anode and cathode are connected by an ideal conductor then $\Phi(C) - \Phi(A) = 0$ while the voltage Φ_e may not vanish.

The voltage Φ_e is entirely maintained by the self-induction that accompanies the gradual untwisting of the magnetic field. Thus, Φ_e reflects the gradual decrease of the magnetic helicity in the tube,

$$\dot{\mathcal{H}} = \frac{\partial}{\partial t}\int_A^C \mathbf{A} \cdot \mathbf{B}\, \mathrm{d}V = -\int_A^C \mathbf{E} \cdot \mathbf{B}\, S(l)\, \mathrm{d}l. \tag{8}$$

(Here $\mathrm{d}V = S(l)\mathrm{d}l$ is the volume element.) It also determines the effective resistivity of the tube: $\mathcal{R} = \Phi_e/I$. The self-induction voltage passes the released magnetic energy to charged particles, and a higher rate of untwisting implies a higher energy $e\Phi_e$ gained per particle. A huge magnetic energy is stored in the twisted tube, and a quick untwisting would lead to extremely high Lorentz factors of the accelerated particles.

There is, however, a bottleneck that prevents a fast decay of the twist: the tube responds to high voltages through the copious production of $e^\pm$ pairs. Runaway pair creation is ignited when electrons are accelerated to a certain Lorentz factor $\gamma_\pm \sim 10^3$. (We describe the microphysics of pair creation in § 5.) The created $e^\pm$ plasma does not tolerate large $E_\parallel$ — the plasma is immediately polarized, screening the electric field. This provides a negative feedback that limits the magnitude of Φ_e and buffers the decay of the twist.

A minimum Φ_e is needed for the formation of a corona. Two mechanisms can supply plasma: (1) Ions and electrons can be lifted into the magnetosphere from the stellar surface. This requires a minimum voltage,

$$e\Phi_e \sim g m_i R_{\rm NS} \sim 200 \ \ \mathrm{MeV}, \tag{9}$$

corresponding to $E_\parallel$ that is strong enough to lift ions (of mass m_i) from the anode footpoint and electrons from the cathode footpoint. (2) Pairs can be created in the magnetosphere if

$$e\Phi_e \sim \gamma_\pm mc^2 = 0.5\gamma_\pm \ \ \mathrm{MeV}, \tag{10}$$

which can accelerate particles to the Lorentz factor $\gamma_{\pm}$ sufficient to ignite $e^{\pm}$ creation. A third possible source — thermal $e^{\pm}$ production in a heated surface layer — will be discussed in § 6; the corresponding minimum voltage is currently unknown.

If Φ_e is too low and the plasma is not supplied, a flux tube is guaranteed to generate a stronger electric field. The current becomes slightly charge-starved: that is, the net density of free charges becomes smaller than $|\nabla\times\mathbf{B}|/4\pi e$. The ultrastrong magnetic field, whose twist carries an enormous energy compared with the energy of the plasma, does not change and responds to the decrease of $\mathbf{j}$ by generating an electric field: a small reduction of the conduction current $\mathbf{j}$ induces a displacement current $(1/4\pi)\partial\mathbf{E}/\partial t = (c/4\pi)\nabla\times\mathbf{B} - \mathbf{j}$. The longitudinal electric field $E_{\parallel}$ then quickly grows until it can pull particles away from the stellar surface and ignite pair creation.

The limiting cases $E_{\parallel}\to 0$ (no decay of the twist) and $E_{\parallel}\to\infty$ (fast decay) both imply a contradiction. The electric field and the plasma content of the corona must regulate each other toward a self-consistent state, and the gradual decay of the twist proceeds through a delicate balance: $E_{\parallel}$ must be strong enough to supply plasma and maintain the current in the corona; however, if plasma is oversupplied $E_{\parallel}$ will be reduced by screening. A cyclic behavior is possible, in which plasma is periodically oversupplied and $E_{\parallel}$ is screened. Our numerical experiment will show that such a cyclic behavior indeed takes place.

3. ELECTRIC CIRCUIT

3.1. Basic Properties

Three facts facilitate our analysis of plasma dynamics in the electric circuit of magnetars:

1. The ultrastrong magnetic field makes the particle dynamics 1-D. The rest-energy density of the coronal plasma is $\sim mcj/e$, where m is the mass of a plasma particle. It is much smaller than the magnetic energy density $B^2/8\pi$: their ratio is $\sim mc^2/eBR_{\rm NS}\sim 10^{-15}(m/m_p)\,B_{15}^{-1}$. The magnetic field lines are not perturbed significantly by the plasma inertia, and they can be thought of as fixed "rails" along which the particles move. The particle motion is confined to the lowest Landau level and is strictly parallel to the field.

2. The particle motion is collisionless in the magnetosphere. It is governed by two forces only: the component of gravity projected onto the magnetic field and a collective electric field $E_{\parallel}$ which is determined by the charge density distribution and must be found self-consistently.

3. The star possesses a dense and thin atmospheric layer.[4] Near the base of the atmosphere, the required current $\mathbf{j}_B = (c/4\pi)\nabla\times\mathbf{B}$ is easily conducted, with almost no electric field. Therefore the circuit has simple boundary conditions: $E_{\parallel}=0$ and fixed current. The atmosphere is much

[4]Such a layer initially exists on the surface of a young neutron star. Its maintenance is discussed in § 7.

thicker than the skin depth of the plasma and screens the magnetospheric electric field from the star.

Our goal is to understand the plasma behavior above the screening layer, where the atmospheric density is exponentially reduced and an electric field $E_\parallel$ must develop. The induced electric field $\mathbf{E}$ and conduction current $\mathbf{j}$ satisfy the Maxwell equation,

$$\nabla \times \mathbf{B} = \frac{4\pi}{c}\mathbf{j} + \frac{1}{c}\frac{\partial \mathbf{E}}{\partial t}. \tag{11}$$

Here $\mathbf{j}$ is parallel to the direction of the magnetic field. Projection of equation (11) onto the magnetic field gives

$$\frac{\partial E_\parallel}{\partial t} = 4\pi(j_B - j), \qquad j_B \equiv \frac{c}{4\pi}\,|\nabla \times \mathbf{B}|, \tag{12}$$

where we have taken into account the force-free condition $\nabla \times \mathbf{B} \parallel \mathbf{B}$. If the conduction current j is smaller than j_B, then $\partial E_\parallel/\partial t > 0$ and an electric field appears that tends to increase the current. Alternatively, if $j > j_B$ then an electric field of the opposite sign develops which tends to reduce the current. Thus, j is always regulated toward j_B. This is the standard self-induction effect.

The timescale of this regulation, τ, is very short. Consider a deviation $|j - j_B| \sim j_B$; then equation (12) gives

$$\frac{E_\parallel}{\tau} \sim 4\pi j_B. \tag{13}$$

The current $j = env$ (carried by particles with charge e and mass m) responds to the induced $E_\parallel$ by changing v,

$$\frac{v}{\tau} \sim \frac{eE_\parallel}{m}. \tag{14}$$

From equations (13) and (14) we get

$$\frac{1}{\tau^2} \sim \frac{4\pi e^2 n}{m} = \omega_P^2. \tag{15}$$

Thus the timescale of the current response to deviations of j from j_B is simply the Langmuir plasma timescale ω_P^{-1}, which is very short. Taking the characteristic density of the corona,

$$n \sim n_c \equiv \frac{j_B}{ec}, \tag{16}$$

and $j_B \sim (c/4\pi)(B/r)$ (eq. 1), we estimate $n \sim 10^{17} B_{15} r_6^{-1}\mathrm{cm}^{-3}$. The corresponding electron plasma frequency ($m = m_e$) is $\omega_P \sim 10^{13}$ Hz. The current relaxes to j_B on the timescale $\omega_P^{-1} \sim 10^{-13}$ s, which is tiny compared with the light crossing timescale of the circuit.

Local deviations from charge neutrality tend to be erased on the same plasma timescale. When the corotation charge density is neglected, the net charge imbalance of the corona must be extremely small, i.e. the corona is neutral. Indeed, the total number of paricles in the corona is $N_c \sim n_c R_{\rm NS}^3 \sim 10^{35}$ and a tiny imbalance of positive and negative charges $\delta N_c/N_c \sim 10^{-14}$ would create an electric field $E \sim e\delta N_c/R_{\rm NS}^2 > GMm_p/eR_{\rm NS}^2$ that easily pulls out the missing charges from the surface.

Adopting a characteristic velocity $v \sim c$ of the coronal particles, the Debye length of the plasma $\lambda_{\rm D} = v/\omega_P$ is essentially the plasma skin depth c/ω_P. An important physical parameter of the corona is the ratio of the Debye length to the circuit size $L \sim R_{\rm NS}$.

$$\zeta = \frac{\lambda_{\rm D}}{L} = \frac{c}{L\omega_P}. \tag{17}$$

In the case of the twisted dipolar magnetosphere (eq. [1]), this becomes

$$\zeta = 3\times 10^{-9}\, B_{15}^{-1/2}\left(\Delta\phi\,\sin^2\theta\right)^{-1/2}. \tag{18}$$

The same parameter may be expressed using a dimensionless current $j_B/j_* \sim 10^{17}B_{15}\Delta\phi\sin^2\theta$. Here j_* corresponds to the plasma density $n_* = j_*/ec$ such that $\lambda_{\rm D} = L$,

$$\frac{j_B}{j_*} = \zeta^{-2}, \qquad j_* = \frac{m_e c^3}{4\pi e L^2}. \tag{19}$$

Note that equation (15) for the plasma frequency is valid only for non-relativistic plasma. We will use the above definition of ω_P, however, one should keep in mind that plasma oscillations in the corona may have a smaller frequency because of relativistic effects.

3.2. Quasi-Neutral Steady State?

Suppose for now that no $e^\pm$ are created in the corona, so that the circuit must be fed by charges lifted from the stellar surface. May one expect that a steady current $j = j_B$ is maintained in the neutral corona by a steady electric force $eE_\parallel \sim gm_i$ or $eE_\parallel \sim gm_e$? It turns out that such a balance between gravitational and electric forces is impossible in the circuit for the following reason: $E_\parallel$ exerts opposite forces on positive and negative charges while the force of gravity has the same sign. This precludes a steady state where $E_\parallel$ lifts particles into the magnetosphere without a significant deviation from neutrality appearing somewhere in the circuit. The point is illustrated by the following toy model.

Suppose positive charges e (mass m_+) flow with velocity $v_+ > 0$ and negative charges $-e$ (mass m_-) flow with velocity $v_- < 0$. The flow of each species is assumed to be cold in this illustration, with a vanishing velocity dispersion at each point, and the total current is $j = j_+ + j_-$ where $j_\pm = \pm e n_\pm v_\pm$. The continuity equation for $+/-$ charges reads

$$\frac{\partial(\pm e n_\pm/B)}{\partial t} + \frac{\partial(j_\pm/B)}{\partial l} = 0, \tag{20}$$

where l is the coordinate along the field line. Suppose the circuit is steady, $\partial/\partial t = 0$, and no strong deviation from neutrality occurs, i.e. $n_+ \simeq n_-$ everywhere. Then one finds $j_+/j_i = -v_+/v_- =$

const, that is the ratio of velocities must remain constant along the field line. Hence v_+ and v_- must *both* vanish at the footpoints. This cannot be: for example, at the anode $E_{\|}$ must lift ions against gravity, and hence it is accelerating the electrons downward rather than stopping them[5]

So, if the current-carrying particles are supplied by the star, we expect either a significant charge separation at some places in the circuit, or a time-dependent behavior (or both). One must also allow for the creation of $e^{\pm}$ pairs if the light charges are accelerated to high enough energies, which will be discussed in § 5. Our approach to this problem is a direct numerical experiment that simulates the time-dependent behavior of plasma particles in the circuit.

3.3. Numerical Simulation of a One-Dimensional Circuit

We shall describe below a time-dependent simulation of a circuit operating along a thin magnetic tube with given $j_B = (c/4\pi)|\nabla\times\mathbf{B}|$ that is fixed in time. Strictly speaking, j_B is *quasi*-steady: it will be found to decay on a long resistive timescale ($\sim$ yrs), much longer than the dynamic time of the current $t_{\rm dyn} = L/c \sim 10^{-4}$ s. The purpose of the simulation is to understand how plasma is supplied above the star's surface layer, and to find the electric field that develops along the tube.

The electric field may be decomposed as $\mathbf{E} = \mathbf{E}_{\|} + \mathbf{E}_{\perp}$ where $\mathbf{E}_{\|}$ is parallel to the magnetic field. It is $\mathbf{E}_{\|}$ that governs the plasma motion and determines the release of magnetic energy in the circuit. In the fixed magnetic configuration, $\nabla\times\mathbf{B}$ does not vary with time and remains parallel to $\mathbf{B}$ (the force-free condition). Then equation (11) implies that $\partial\mathbf{E}/\partial t$ is parallel to $\mathbf{B}$, i.e. no perpendicular field $\mathbf{E}_{\perp}$ is created by the induction effect, and $\nabla\cdot\mathbf{E}_{\perp} = 0$ may be assumed. Then Gauss' law reads

$$4\pi\rho = \nabla\cdot\mathbf{E}_{\|} = \frac{{\rm d}E_{\|}}{{\rm d}l}, \tag{21}$$

where l is length measured along the magnetic tube. The condition $\nabla\cdot\mathbf{E}_{\perp} = 0$ significantly simplifies the problem: it becomes strictly 1-D since $\mathbf{E}_{\perp}$ has no relation to charge density and falls out from the problem. Hereafter we assume $\mathbf{E} = \mathbf{E}_{\|}$ and drop the subscript $\|$.

We note that the approximation of 1D circuit, $j_B(t) = const$, excludes the excitation of transverse waves in the magnetosphere, which in reality can exist. These waves are described by the coupled fluctuations δj_B and $\mathbf{E}_{\perp}$ on scales much smaller than the circuit size L. (Wavelengths $\lambda \sim c/\omega_P$ can be excited by plasma oscillations.) These fluctuations may be expected to have a small effect on the circuit solution unless δj_B becomes comparable to j_B.

With $j_B(t) = const$, the particle motions on different magnetic lines are decoupled. Indeed, the particle dynamics is controlled by electric field $E = E_{\|}$ which is related to the instantaneous

---

[5]A static plasma configuration is possible with the electric and gravitational forces balancing each other at each point of the circuit. However, $j = 0$ in this configuration and it is not relevant to our circuit problem. Besides, such a configuration would be unstable.

charge distribution by Gauss' law (21).[6] Thus, $E(l)$ on a given magnetic line is fully determined by charge density $\rho(l)$ *on the same line*. The plasma and electric field evolve along the line as if the world were 1-D.

The force-free condition $\mathbf{j}_B \times \mathbf{B}$ together with $\nabla \cdot \mathbf{j}_B = 0$ requires that $j_B(l) \propto B(l)$ along the magnetic line. We can scale out this variation simply dividing all local quantities (charge density, current density, and electric field) by B. This reduces the problem to an equivalent problem where $j_B(l) = const$. Furthermore, only forces along magnetic lines control the plasma dynamics, and the curvature of magnetic lines falls out from the problem. Therefore, we can set up the experiment so that plasma particles move along a straight line connecting anode and cathode (Fig. 2). We designated this line as the z-axis, so that $l = z$.

This one-dimensional system may be simulated numerically. Consider N particles moving along the z-axis ($N \sim 10^6$ in our simulations). Their positions z_i and velocities v_i evolve in time according to

$$\frac{\mathrm{d}z_i}{\mathrm{d}t} = v_i, \qquad \frac{\mathrm{d}p_i}{\mathrm{d}t} = g\gamma_i m_i + e_i E, \qquad i = 1, ..., N, \tag{22}$$

where e_i and m_i are charge and mass of the i-th particle, $p_i = \gamma_i m_i v_i$, and $\gamma_i = (1-v_i^2/c^2)^{-1/2}$. Also, $g(z)$ is the projection of the gravitational acceleration onto the magnetic line. In the simulations, we assume $g = g_0(2z/L-1)$ where L is the distance between the anode and cathode; then $g = \pm g_0$ at the cathode/anode surfaces and $g = 0$ in the middle $z = L/2$. The true gravitational acceleration depends on γ and could be refined at large γ by a factor ~ 2 using the exact geodesic equation. However, the crude Newtonian model is sufficient for our purposes. The electric field appearing in equation (22) is given by

$$E(z) = 4\pi \int_0^z \rho \, \mathrm{d}z, \tag{23}$$

where $E(0) = E(L) = 0$ are the boundary condition discussed above. Since the current $j = j_B$ is fixed at both ends, the net charge between anode and cathode does not change with time and remains zero (in agreement with Given the instantaneous positions z_i of charges e_i we immediately find $E(z)$ from Gauss's law (eq. [23]). Thus, we have a well-defined 1-D problem of particle motion in a self-consistent electric field and the fixed gravitational field. To find a quasi-steady state of such a system we start with an initial state and let it relax by following the particle motion.

The evolution of the system may be followed without calculating ρ or j: the equations contain only integrated charge $Q(z) = \int_0^z \rho dz$. In contrast with usual particle-in-cell simulations, no grid or cells are needed. We find the *exact* E at any point z simply by counting the net charge of particles between z and anode. The only source of numerical error is caused by the finite timestep of particle dynamics, and we keep it small, $\Delta t = 10^{-5} - 10^{-4}(L/c)$.

---

[6]The Maxwell equation (12) and Gauss' law (21) are equivalent when charge conservation $\partial j/\partial l = -\partial\rho/\partial t$ is taken into account.

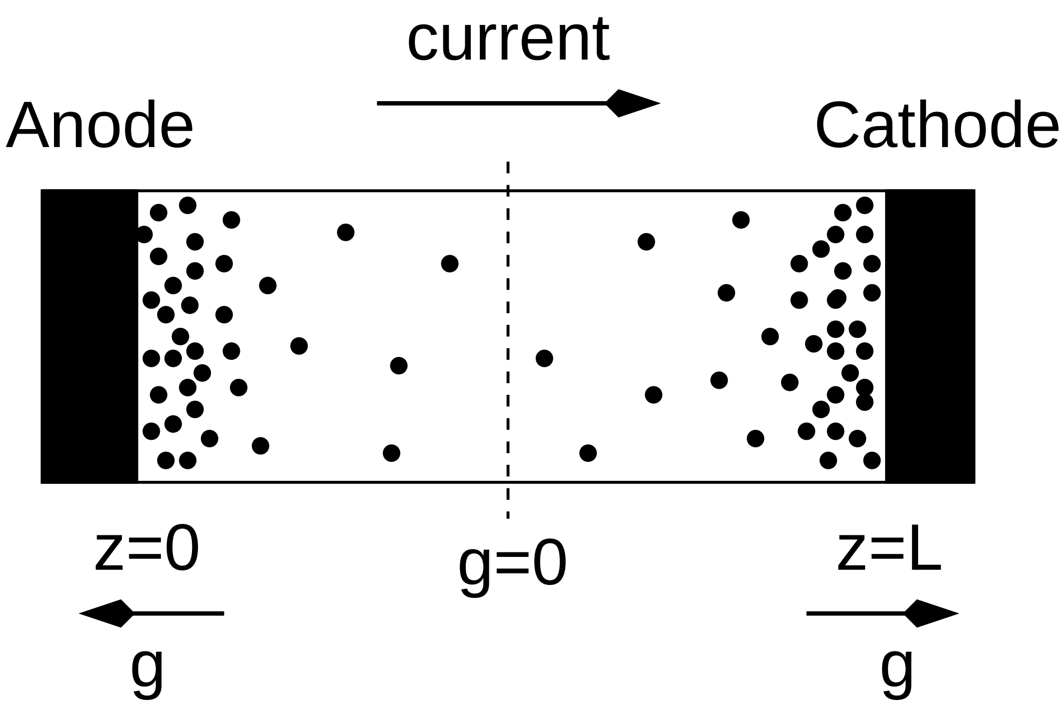

Fig. 2.— Set up of numerical experiment. Thin and dense plasma layers are maintained near the cathode and anode by injecting cold particles through the boundaries of the tube (the footpoints of a magnetic flux tube). The electric current is kept constant at the boundaries and the system is allowed to evolve in time until a quasi-steady state is reached. Without voltage between anode and cathode, the current cannot flow because gravity g traps the particles near the boundaries. The constant current at the boundaries, however, implies that voltage is immediately generated should the flow of charge stop in the tube. The experiment aims to find the induced voltage that keeps the current flowing.

The main dimensionless parameter of the problem is $\zeta = c/\omega_P L \sim 3 \times 10^{-9}$ (see § 3.1). Although it is not possible to simulate circuits with such a low value of ζ, we can experiment with a similar system with $\zeta \simeq 10^{-2}$. This allows one to understand the mechanism of the circuit and find plasma parameters that will be easy to scale to a real magnetosphere. A large number of particles $N \gtrsim 10^6$ may be followed with modern computers in a reasonable time, and $\zeta \ll 1$ may be achieved by choosing an appropriate charge per particle. Two other basic requirements must be satisfied in the simulations: (1) the number of particles within the Debye length is much larger than one; and (2) the timestep is much smaller than ω_P^{-1} and small enough to follow accurately the particle dynamics. Finally, we require the particle charge e to be sufficiently small, so that its electric field in our 1-D problem satisfies $eE = 4\pi e^2 \ll m_e g$. Given a number of particles N, this last condition constrains ζ from below. The minimum ζ achieved in our numerical experiment is $\sim 5 \times 10^{-3}$.

The ions and electrons in the simulated circuit have different masses m_i and m_e. The ratio m_i/m_e is smaller than it would be in a real magnetosphere. Below we will show models with $m_i/m_e = 10$ and 30. Hereafter subscripts i and e refer to ions and electrons, respectively, and subscript p will refer to positrons.

The neutral atmospheric layers near the boundaries of the computational box $z = 0, L$ are created by injecting a flux of positive and negative charges with small temperatures T_e and T_i. Although most charges are bound to the star, some of them must be lifted by the electric field into the magnetosphere. The numerical simulation will show precisely how this happens. The boundary conditions $E = 0$ and $j = j_B$ are imposed *beneath* the atmospheric layers. The condition $j = j_B$ implies keeping track of the flux of leaving charges, and injecting new particles with the correct imbalance between the positive and negative charges. Thus the required current is fed at a constant rate at the conducting boundaries. If net charge escaping through the cathode boundary during timestep dt is smaller than $j_B dt$, we inject electrons to maintain the required j_B, otherwise we inject the needed number of ions. Similarly, $j = j_B$ is enforced at the anode boundary. This maintains the current, but does not determine the contributions to j_B from different types of particles. The plasma self-organizes during the experiment and decides itself what the contributions must be.

The forced injection of net positive charge at anode and net negative charge at cathode would immediately create a long range electric field if the current were not flowing in the system. A deviation of j from j_B at any point of the circuit leads to appearance of E at that point. Thus, the boundary conditions $j(0) = j(L) = j_B$ are equivalent to equation (12).

The electric field does a net positive work on the current-carrying particles. In our experiment, the deposited kinetic energy sinks through the boundaries and never comes back. We envision dense radiatively efficient layers just outside the simulation box and assume that the lost energy is emitted there. The surface layers maintained in the experiment have density only $\sim 20 - 100$ times $n_0 = j_B/ce$, which is just sufficient to screen the electric field and avoid interference of the boundaries in the circuit solution. A future full simulation may include radiative losses *in situ* in the tube and allow one to track the fate of released energy and the spectrum of produced radiation.

Our final choice regards the initial plasma state in the tube. We tried different initial states and got same results. In the runs shown below we take as initial conditions $j(z) = j_B$, a mildly relativistic bulk velocity $v_e = v_i = 0.4c$ and Maxwellian momentum distribution with temperature equal to the bulk kinetic energy.

The problem has four scales: tube length L, electron plasma scale $\lambda_{\mathrm{D}e} = c/\omega_{Pe}$, ion plasma scale $\lambda_{\mathrm{D}i} = (m_i/m_e)^{1/2}\lambda_{\mathrm{D}e}$, and scale-height of the atmospheric layer $h = k(T_e + T_i)/g(m_i + m_e)$. For a real magnetosphere, $\lambda_{\mathrm{D}e} < \lambda_{\mathrm{D}i} < h < L$. We choose the parameters of the experiment so that these relations are satisfied. The inclusion of pair production in the simulation brings a new scale: mean free path l (see § 3.5 below).

A numerical code implementing the described method was developed and first tested on simple plasma problems without gravity, $g = 0$. For example, we calculated the two-stream instability starting with two oppositely directed cold beams of positive and negative charges, and found the correct development of Langmuir oscillations on the plasma timescale. Various technical tests have been done, e.g. independence of the results of timestep and charge of individual particles e. The main parameter of the problem is ζ, and circuits with equal ζ and different N, e, dt gave the same result. Another test passed is the agreement of the linear-accelerator state obtained by the code (§ 5) with the solution of Carlqvist (1982).

As we shall see below, $e^{\pm}$ creation is inevitable in the magnetospheric circuit. However, first we investigate what happens in the circuit with if pair creation "switched-off," when the current-carrying charges must be supplied by the atmospheric layers.

4. CIRCUIT WITHOUT PAIR CREATION

The circuit model has the following parameters: (1) dimensionless current $j_B/j_* = \zeta^{-2}$ (see § 3.1), (2) gravitational potential barrier Φ_g (we will assume $\Phi_g = c^2/4$ in numerical examples), (3) density of the hydrostatic boundary layer n_{atm} (which is regulated in the numerical experiment by the particle injection rate at the boundaries), and (4) injection temperatures of ions, T_i, and electrons, T_e.

Note that T_i and T_e may be well above the surface temperature of the star $k_{\mathrm{B}}T \sim 0.5$ keV because the atmosphere is heated from above by the corona. The vertical temperature profile that is established below the corona is a separate problem which we do not attempt to solve in this paper. T_i and T_e serve as parameters of our model, and we explore first how the mechanism of the circuit depends on these parameters.

4.1. Thermally-Fed Circuit

If the hydrostatic atmosphere is sufficiently hot, its Boltzmann tail at large heights may be able to conduct the current without the need to lift particles by an electric field. The plasma must remain quasi-neutral in the Boltzmann tail. One may think of the neutral atmosphere as a gas of composite particles $m = m_i + m_e$ with effective temperature $T = T_i + T_e$. Its scale-height is given by

$$h = \frac{k_B T}{g_0 m} = \frac{k_B(T_i + T_e)}{g_0(m_i + m_e)}. \tag{24}$$

The plasma density is reduced exponentially on scale h. The reduced density remains high enough to conduct the current j_B all the way to the top of the gravitational barrier if

$$n_{\rm atm} \exp\left(-\frac{m\Phi_g}{k_B T}\right) > n_c = \frac{j_B}{ec}. \tag{25}$$

One example of a circuit that satisfies condition (25) is shown in Figure 3. The electrons and ions are injected at the boundaries with $k_B T_i = k_B T_e = 0.5 m_e c^2$ and $m_i = 10 m_e$; this gives a scale-height $h = 0.09L$. After several light-crossing times L/c, the circuit develops the Boltzmann atmosphere that conducts the required current $j_B = 10^3 j_*$. The electric field remains small and dynamically unimportant, $eE < g_0 m_i$.

The thermally-fed regime requires too high a temperature for the pure ion-electron circuit. Indeed, $mc^2 = (m_i + m_e)c^2 \simeq 1$ GeV and then $k_B T > 1$ GeV$/\log(n_{\rm atm}/n_c)$ would be required. Pair creation would take place at much lower temperatures (see § 6.3 below). Therefore, the thermally-fed pair-free circuit solution cannot apply to a real magnetosphere. The rest of this section focuses on circuits that do not satisfy condition (25).

4.2. Linear Accelerator

When the condition (25) is not satisfied, the circuit becomes plasma-starved and an electric field develops that lifts particles from the dense surface layer. We find that such a circuit quickly relaxes to a state where it acts as an ultra-relativistic linear accelerator. One example is shown Figure 4. The parameters of this particular model are $j_B/j_* = 10^4$, $k_B T_e = 0.1 k_B T_i = 0.04 m_e c^2$, and $n_{\rm atm}/n_c \simeq 20$. We obtained similar solutions for various combinations of T_e, T_i, and $n_{\rm atm}/n_0$ that do not satisfy condition (25) of a thermally-fed regime. In all cases, the circuit reached the quasi-steady state at $t \lesssim 5L/c$. In this state, oscillations of electric field (on the plasma timescale ω_P^{-1}) are confined to the thin atmospheric layers. A static accelerating electric field is created above the layers where the atmosphere density is exponentially reduced. The striking result is that on top of each layer, a large charge builds up, which is positive $(+Q)$ at the anode and negative $(-Q)$ at the cathode. The two charges create a long-range electric field $E = 4\pi Q$.

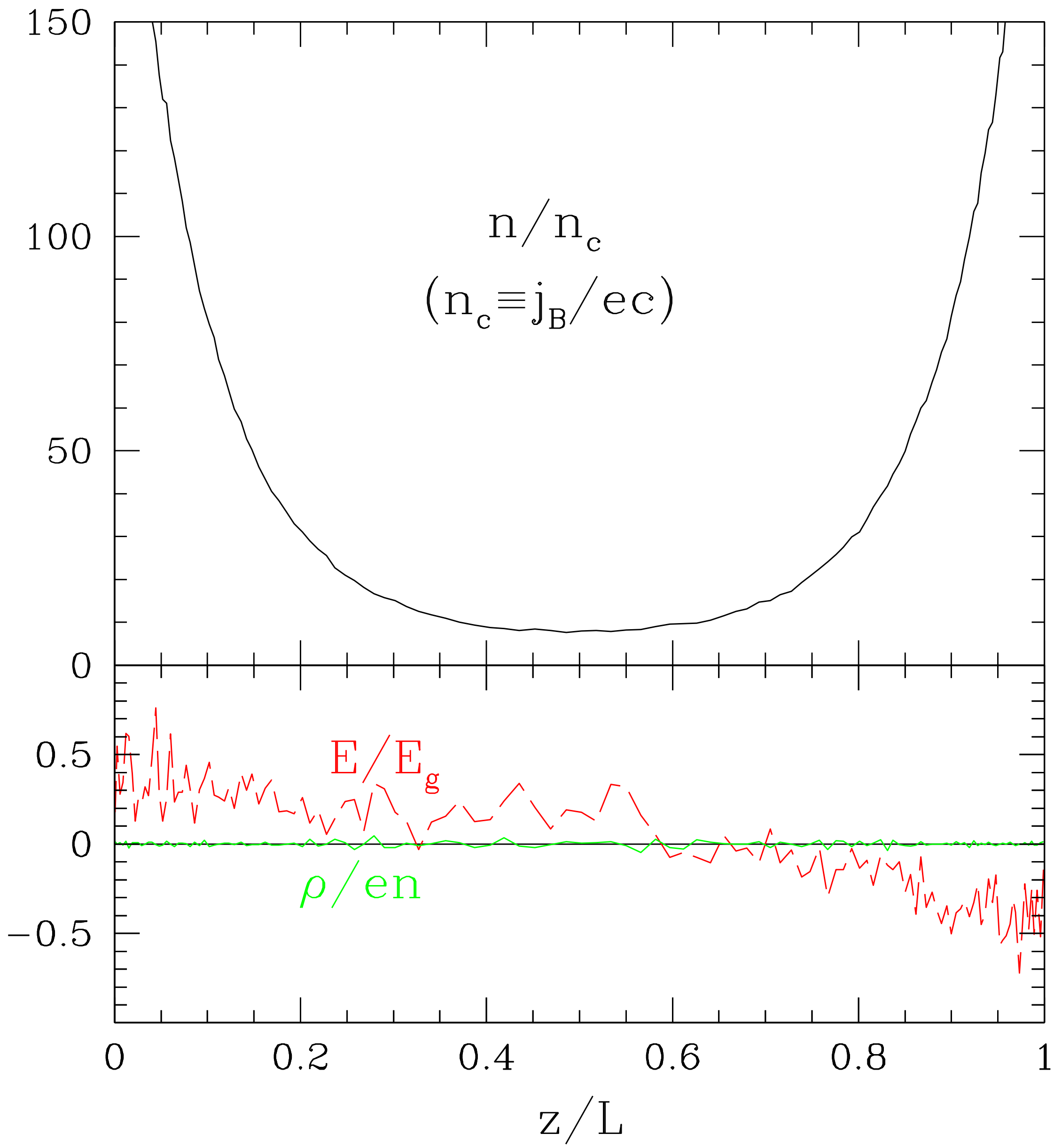

Fig. 3.— Thermally-fed circuit without $e^{\pm}$ production. Upper panel: the plasma density $n = n_e + n_i$ in units of $n_c = j_B/ec$. Lower panel: deviation from neutrality ρ/en, and electric field in units of E_g defined by $eE_g = m_i g_0$. In this simulation, $m_i = 10 m_e$ and $\zeta = c/\omega_P L \simeq 0.03$. The snapshot is taken at $t = 20L/c$, after the system has reached the quasi-steady state.

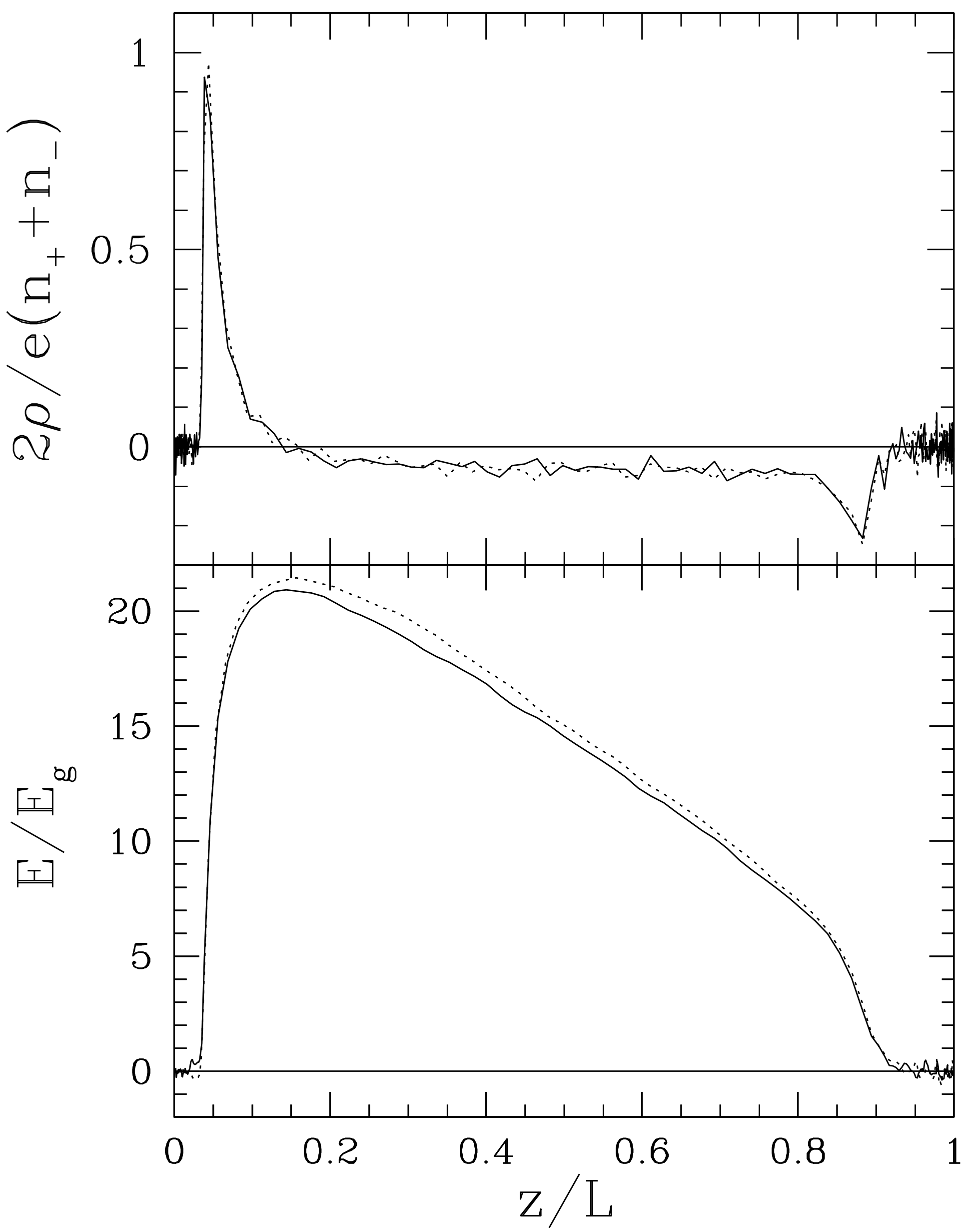

Fig. 4.— Circuit without $e^{\pm}$ production. Upper panel shows the normalized charge density and lower panel shows the electric field in units of E_g defined by $eE_g = m_i g_0$. Solid and dotted curves correspond to two different moments of time, demonstrating that a quasi-steady state has been reached. In this simulation, $m_i = 10m_e$ and $\zeta = c/\omega_P L \simeq 0.01$. The final state is the relativistic double layer described analytically by Carlqvist (1982).

This configuration is a relativistic double layer (Carlqvist 1982). It is well described by Carlqvist's solution, which has no gravity in the circuit and assumes zero temperature at the boundaries, so that particles are injected with zero velocity. According to this solution, the potential drop between anode and cathode, in the limit $e\Phi_e \gg m_i c^2$, is given by

$$e\Phi_e = \frac{1}{2}\left[\left(\frac{m_i}{Zm_e}\right)^{1/2} + 1\right] L\omega_P\, m_e c, \qquad \omega_P \equiv \left(\frac{4\pi je}{m_e c}\right)^{1/2}, \tag{26}$$

where Z is the charge number of the ions (in our experiment $Z = 1$ was assumed). In the limit $m_i \gg Zm_e$, this expression depends only on the ion and not the electron mass.

The established voltage is much larger than is needed to overcome the gravitational barrier Φ_g. It does not even depend on Φ_g as long as Φ_g is large enough to prohibit the thermally-fed regime. Gravity causes the transition to the linear-accelerator state, but the state itself does not depend on Φ_g. The asymmetry of the double-layer solution (Fig. 4) is caused by the difference between the electron and ion masses. A similar but symmetric configuration is obtained for $m_i = m_e$.

The symmetric double layer with $m_e = m_i$ is especially simple and can be qualitatively understood as follows. The currents carried by ions and electrons are equal by symmetry, $j_i = j_e = \frac{1}{2}j$, and hence plasma is approximately neutral between the anode and cathode where $v_i \simeq v_e \simeq c$. A significant deviation from neutrality $|n_e - n_i| \sim n_i + n_e$ takes place in the acceleration regions Δz near anode and cathode because here v_i differs from v_e. For instance, near the anode the ions are not accelerated yet to c, and their charge density $\rho_i = j_i/v_i$ is larger than that of the incoming electron beam, $\rho_e = j_e/v_e \simeq j_e/c$, so the net charge density is positive. One can show that the anode charge $Q(z) = \int_0^z (j_i/v_i - j_e/v_e)dz$ peaks at height $z \sim \Delta z$ where ions move with a mildly relativistic velocity $v_i \sim c/2$. Similarly, at cathode end, where the emitted electron flow is still slow, the net charge density is negative, and the charge $-Q$ peaks at the distance Δz from the cathode. The thickness Δz and the characteristic electric field E in the mildly relativistic region are related by $eE\Delta z \sim m_e c^2$. Combining this with $E = 4\pi Q \sim 4\pi e n_c \Delta z$, one finds $\Delta z \sim \lambda_{\rm D}$ and $Q \sim e n_c \lambda_{\rm D}$. This is the only possible self-consistent static solution for a double layer (besides the trivial solution $E = 0$ which is prohibited in our case by gravity). $E = 4\pi Q$ must be this large in a static double layer because a smaller E would accelerate the particles more slowly, which would imply larger non-neutral regions Δz near the ends of the circuit and larger Q. Gauss' law would then imply a larger E, leading to inconsistency with the assumed smaller E.

Similar estimates may be made for the asymmetric double layer with $m_i > m_e$. In the limit $e\Phi_e \gg m_i c^2$, one again finds $j_i \simeq j_e$ from the Langmuir condition (see Carlqvist 1982),

$$\frac{j_i}{j_e} = \left(\frac{e\Phi_e + 2m_e c^2}{e\Phi_e + 2m_i c^2/Z}\right)^{1/2} \simeq 1. \tag{27}$$

There is only one qualitative difference from the symmetric case. Now the mildly relativistic region near the anode ($v_i \sim c/2$) has a thickness $\Delta z_A \sim \lambda_{{\rm D}i}$, and near the cathode ($v_e \sim c/2$) — $\Delta z_C \sim \lambda_{{\rm D}e}$. The spikes of charge near anode and cathode are now different: the cathode spike is smaller by a factor of $\lambda_{\mathrm{D}e}/\lambda_{\mathrm{D}i} = Z(m_e/m_i)^{1/2}$. The net charge of a double layer, however, must vanish to satisfy the boundary conditions $E = 0$. The "missing" negative charge is distributed between the two spikes, throughout the circuit. This behavior is observed in Fig. 4 and derived analytically by Carlqvist (1982).

The static double-layer solution has been much studied previously, but its possible astrophysical applications remained unclear. Our numerical experiment shows that an ion-electron circuit in a gravitational field relaxes to the double layer of the macroscopic size L and huge voltage Φ_e. The system does not find any state with a lower Φ_e, even though it is allowed to be time-dependent. The experiment shows that, regardless the initial state, the charges $\pm Q$ near the anode/cathode build up with time in spite of the strong fluctuations that persist in the atmospheric layers (reversing the sign of E), and Q grows until the Carlqvist solution is reached.

The effective boundaries of the double layer in our experiment are not exactly at $z = 0, L$ because the atmosphere has a finite scale-height. Height z_* where the circuit becomes plasma-starved may be estimated from the condition $n_{\mathrm{atm}} \exp(-z_*/h) \sim n_c$.

If the linear accelerator were maintained in the twisted magnetosphere, the twist would be immediately killed off. The huge voltage implies a large untwisting rate and a fast dissipation of the toroidal magnetic energy (§ 2). The electron Lorentz factor developed in the linear accelerator is (taking the real $m_i/m_e = 1836$ and $\zeta \sim 3 \times 10^{-9}$),

$$\gamma_e = \frac{e\Phi_e}{m_e c^2} \simeq \frac{20}{\zeta} \sim 6 \times 10^9. \tag{28}$$

However, new processes will become important before the particles could acquire such high energies: production of $e^\pm$ pairs will take place. Therefore, the linear-accelerator solution cannot describe a real magnetosphere. We conclude that pair creation is a key ingredient of the circuit that will regulate the voltage to a smaller value.

5. PAIR CREATION IN THE CORONA

In the magnetospheres of canonical radio pulsars with $B \sim 10^{12}$ G, $e^\pm$ pairs are created when seed electrons are accelerated to large Lorentz factors $\gamma_e \sim 10^7$. Such electrons emit curvature gamma rays that can convert to $e^\pm$ off the magnetic field.

In stronger fields, another channel of $e^\pm$ creation appears. It is also two-step: an accelerated particle resonantly upscatters a thermal X-ray photon, which subsequently converts to a pair. This channel is dominant in radio pulsars with relatively strong magnetic fields (e.g. Hibschman & Arons 2001). A similar channel of $e^\pm$ creation operates in the super-QED field of a magnetar. Because of the large magnetic field an accelerated electron can resonantly upscatter the ambient X-rays and produces $e^\pm$ pairs when its Lorentz factor is $\gamma_e \sim 10^3$, much smaller than in a normal pulsar.

5.1. Resonant Channel of Pair Creation

Consider an electron moving along a magnetic line with Lorentz factor $\gamma_e \gg 1$ and an ambient X-ray photon $\hbar\omega_X$ propagating at an angle θ_{kB} with respect to the electron velocity. In the electron frame, the photon is strongly aberrated and moves nearly parallel to the magnetic field with an energy $\hbar\omega'_X = \gamma_e(1-\cos\theta_{kB})\hbar\omega_X$. The resonant scattering may be viewed as a two-step process: the excitation of the electron into the first Landau level with energy

$$E_B = \left(\frac{2B}{B_{\rm QED}}+1\right)^{1/2} m_e c^2, \tag{29}$$

followed rapidly by a de-excitation. Here $B_{\rm QED} = m_e^2 c^3/e\hbar \approx 4.4\times 10^{13}$ G.

The resonant condition on photon energy $\hbar\omega'_X$ is obtained from energy and momentum conservation,

$$\hbar\omega'_X + m_e c^2 = \gamma E_B, \qquad \frac{\hbar\omega'_X}{c} = \gamma\beta\frac{E_B}{c}. \tag{30}$$

Here β is the velocity along $\mathbf{B}$ acquired by the excited electron (relative to its initial rest frame) and $\gamma = (1-\beta^2)^{-1/2}$. The photon $\hbar\omega'_X$ is assumed to propagate parallel to $\mathbf{B}$, which is a very good approximation since we consider ultrarelativistic electrons and the ambient radiation is strongly beamed in the electron frame. From these equations one finds $\gamma = \frac{1}{2}(E_B/m_e c^2 + m_e c^2/E_B)$ and

$$\hbar\omega'_X = \frac{1}{2}\left[\left(\frac{E_B}{m_e c^2}\right)^2 - 1\right] = \frac{B}{B_{\rm QED}}\, m_e c^2 = \hbar\,\frac{eB}{m_e c}. \tag{31}$$

This resonant condition may also be written as a condition on γ_e for given $\hbar\omega_X$ and θ_{kB},

$$\gamma_{\rm res} = \frac{B/B_{\rm QED}}{1-\cos\theta_{kB}}\left(\frac{\hbar\omega_X}{m_e c^2}\right)^{-1} \approx 10^3\, B_{15}\left(\frac{\hbar\omega_X}{10{\rm keV}}\right)^{-1}. \tag{32}$$

De-excitation is examined conveniently in the frame where the parallel momentum of the excited electron vanishes (Herold, Ruder, & Wunner 1982). The energy of de-excitation photon E_γ depends on its emission angle $\theta_{\rm em}$ with respect to the magnetic field. This angle determines how the released energy E_B is shared between the emitted photon and the electron recoil. The relation $E_\gamma(\theta_{\rm em})$ is found from energy and momentum conservation,

$$E_\gamma + (c^2 p_e^2 + m_e^2 c^4)^{1/2} = E_B, \qquad E_\gamma \cos\theta_{\rm em} = -c p_e. \tag{33}$$

Here p_e is recoil momentum of the electron, which is directed along B. Eliminating p_e, one finds

$$E_\gamma(\theta_{\rm em}) = \frac{E_B}{\sin^2\theta_{\rm em}}\left[1 - \left(\cos^2\theta_{\rm em} + \frac{m_e^2c^4}{E_B^2}\sin^2\theta_{\rm em}\right)^{1/2}\right]. \tag{34}$$

In the super-critical field, $B \gg B_{\rm QED}$, this simplifies to

$$E_\gamma(\theta_{\rm em}) \approx \frac{E_B}{1+|\cos\theta_{\rm em}|}. \tag{35}$$

The de-excitation photon has the maximum energy $E_\gamma = E_B$ when it is emitted at $\theta_{\rm em} = \pi/2$ (no recoil) and the minimum energy $E_\gamma = E_B/2$ when $\theta_{\rm em} = 0$ (maximum recoil).

Photons have two polarization states in the strongly magnetized background: O-mode and E-mode. These eigenmodes are determined by the effect of vaccuum polarization in response to an electromagnetic wave. Both modes are linearly polarized: the O-mode has its electric vector in the plane of the wave vector **k** and the background magnetic field **B**. The electric vector of the E-mode is perpendicular to this plane. De-excitation photons are emitted in either the O or E mode: the gyrational motion of the excited electron overlaps both linear polarization states.

O-mode photons can convert to a pair with both particles in the lowest Landau state (Daugherty & Harding 1983). The threshold condition for this process is

$$E_\gamma > E_{\rm thr} = \frac{2m_e c^2}{\sin\theta_{\rm em}}. \tag{36}$$

The threshold energy becomes $2m_ec^2$ when transformed to the frame where the photon propagates perpendicular to **B**. Using equation (35), we find the interval of emission angles $\theta_{\rm em}$ for which the O-mode photon will immediately convert to a pair,

$$1 - |\cos\theta_{\rm em}| < 8\left(\frac{m_e c^2}{E_B}\right)^2, \qquad B \gg B_{\rm QED}. \tag{37}$$

O-mode photons emitted below the threshold still have huge energy in the lab frame, $\sim \gamma_{\rm res} E_B$, and will convert to $e^\pm$ after propagating a small distance $\Delta l \sim R_{\rm NS}/\gamma_{\rm res}$. Indeed, even a photon emitted with $\theta_{\rm em} = 0$ will quickly build up a sufficient pitch angle for conversion because of the curvature of magnetic lines and/or gravitational bending of the photon trajectory.

The threshold energy for an E-mode photon is E_B in the frame where the photon propagates normally to the field. Therefore, an E-mode de-excitation photon cannot immediately convert to $e^\pm$. It will, however, quickly split in two daughter photons, at least one of which will be in O-mode (Adler et al. 1970) and will convert to a pair.[7]

Thus, resonant scattering in the ultrastrong field always leads to $e^\pm$ creation, sometimes multiple because E-mode may split repeatedly and give multiple O-mode photons that convert to $e^\pm$. The average multiplicity $\mathcal{M}$ is not much larger than unity, and $\mathcal{M} = 1$ may be taken as a first approximation. The rate of pair creation by an accelerated electron is then determined by the cross section of resonant scattering and the number density of the target photons. The cross section of resonant absorption for a photon propagating parallel to **B** in the rest frame of the electron is given by (Daugherty & Ventura 1978),

$$\sigma_{\rm res}(\omega_X') = 2\pi^2 r_e c\,\delta\left(\omega_X' - \frac{eB}{m_e c}\right) = \sigma_{\rm res\,0}\,\omega_X'\,\delta\left(\omega_X' - \frac{eB}{m_e c}\right), \tag{38}$$

[7]Splitting of the O-mode is kinematically forbidden. All three components of the momentum are conserved in the splitting process. This allows splitting only for the mode with the smaller index of refraction, which is the E-mode in a super-QED magnetic field.

where $r_e = e^2/m_e c^2$ and $\sigma_{\mathrm{res}\,0} = 2\pi^2 e/B$. This expression is valid for any B/B_{QED}.

Magnetic Compton scattering has also been calculated for arbitrary B/B_{QED} by Herold (1979) and Melrose & Parle (1983). The calculations must be modified at the resonance to take into account the finite lifetime Γ^{-1} of the intermediate resonant state (e.g. Ventura 1979; Harding & Daugherty 1991). Using the results of Herold (1979) and Herold et al. (1982), we find the resonant Compton cross section that agrees with equation (38) within a factor of 2 (details will be given elsewhere). Below we use the cross section (38). Note also that at $B \gg B_{\mathrm{QED}}$, there are equal probabilities for the photon to end up in the E-mode or O-mode in the final state, independent of θ_{em}.

The number density of target photons for resonant scattering is

$$n_X \approx \frac{\mathrm{d}L_X/\mathrm{d}\ln\omega_X}{4\pi R_{\mathrm{NS}}^2 \hbar\omega_X c} \approx 2\times 10^{20} \left(\frac{\mathrm{d}L_X/\mathrm{d}\ln\omega_X}{10^{35}\ \mathrm{erg\ s^{-1}}}\right)\left(\frac{\hbar\omega_X}{\mathrm{keV}}\right)^{-1}\ \ \mathrm{cm^{-3}}. \tag{39}$$

The mean free path of an electron to scattering a photon is then

$$l_{\mathrm{res}} = \frac{1}{n_X\sigma_{\mathrm{res}\,0}}\left|\frac{d\ln B}{d\ln l}\right| \approx \frac{3}{n_X\sigma_{\mathrm{res}\,0}} \sim 10^3\, B_{15}\left(\frac{\mathrm{d}L_X/\mathrm{d}\ln\omega_X}{10^{35}\ \mathrm{erg\ s^{-1}}}\right)^{-1}\left(\frac{\hbar\omega_X}{\mathrm{keV}}\right)\ \ \mathrm{cm}. \tag{40}$$

The upscattered photons produce pairs at a small distance from the scattering site compared with l_{res}. So, the distance over which an accelerated electron creates a pair is approximately equal to the free path to scattering. It depends only on B and the spectrum of target photons. While being accelerated, an electron with initially low γ_e may first experience a resonance with a high-energy photon. Therefore it is important to know the radiation spectrum at high energies, above the blackbody peak. It is possible that the transition region between the corona and the star emits 100 keV photons (Thompson & Beloborodov 2005; see §§ 6 and 8.5 below), which may be targets for resonant scattering by electrons with relatively low $\gamma_e \sim 100$. Photons with energy much above ~ 100 keV are not good targets for resonant scattering in the strong-B region near the star because then l_{res} becomes comparable to R_{NS}.

5.2. Inconsistency of the Linear Accelerator

Now we can show that the linear accelerator discussed in § 4.2 becomes inconsistent in the presence of pair creation and cannot be established in the magnetosphere. Suppose it is established. Electrons in the accelerator will be in resonance with photons at the peak of the stellar blackbody spectrum, $\hbar\omega_X \sim 1$ keV, when they have Lorentz factors $\gamma_{\mathrm{res}} \sim 10^4\, B_{15}$. Using the Carlqvist solution for the electron Lorentz factor $\gamma_e(z)$, we find the characteristic distance from cathode where electrons reach γ_{res}. This distance is given by

$$a_{\mathrm{res}} \simeq \gamma_{\mathrm{res}}\lambda_{\mathrm{D}e}. \tag{41}$$

Here we have used $\lambda_{\mathrm{D}e} \ll a_{\mathrm{res}} \ll (m_i/m_e)^{1/2}L$; the electric field of the double layer varies little across this region and equals $E = 4\pi(j/c)\lambda_{\mathrm{D}e}$, where j is the current flowing through the circuit.

The resonance region is at the distance $a_{\rm res} \sim 30$ cm from cathode and its thickness is $\sim a_{\rm res}$. The mean free path of an electron in this region is $l_{\rm res} \sim 10^3$ cm (see eq. [40]), which is much larger than $a_{\rm res}$. This means that only a small fraction $f = a_{\rm res}/l_{\rm res}$ of the flowing electrons will upscatter a photon and the bulk of them pass through the resonance region without any interaction.

In sum, $f \ll 1$ positrons are created per unit electron flowing through the circuit. The created positrons will flow to the cathode. This backflow carries a current fj and charge density $\rho_+ = fj/c$. The charge density ρ_+ creates a potential drop between the resonance region and cathode,

$$\Delta\Phi = 2\pi \, \frac{a_{\rm res}^3}{l_{\rm res}} \, \frac{j}{c}. \tag{42}$$

The linear-accelerator configuration becomes inconsistent if $e\Delta\Phi > \gamma_{\rm res} m_e c^2$ — then the created positrons will screen the assumed electric field. This condition may be written as

$$l_{\rm res} < \frac{1}{2} \, \gamma_{\rm res}^2 \zeta L. \tag{43}$$

We can evaluate it by substituting $L = R_{\rm NS} = 10$ km and equation (40) for $l_{\rm res}$. Using the example of a twisted dipole magnetosphere with the corresponding expression (18) for ζ, one finds

$$\frac{{\rm d}L_X}{{\rm d}\ln\omega_X} > 7 \times 10^{32} \, B_{15}^{-1/2} \, (\Delta\phi)^{1/2} \sin\theta \, \left(\frac{\hbar\omega_X}{1 \text{ keV}}\right)^3 \quad \text{erg s}^{-1}. \tag{44}$$

The linear accelerator configuration is inconsistent if this condition is satisfied at some $\hbar\omega_X$. It is easily satisfied at $\hbar\omega_X \sim 1$ keV (the observed luminosity in this range is $\sim 10^{35}$ erg/s).

Even if the linear-accelerator state were formally allowed as a self-consistent solution, the coronal circuit would not have to evolve to this state. Indeed, if the voltage in the circuit evolves gradually to higher and higher values, an $e^\pm$ discharge occurs well before the linear accelerator could be established. We now consider the circuit that operates on $e^\pm$ discharge, at a much lower voltage compared to the linear accelerator.

5.3. Discharge via Pair Breakdown

The development of pair breakdown may be illustrated with the following toy model. Suppose a uniform electric field E is fixed in the tube of size L. To start, we introduce one seed electron at the cathode with zero velocity. The electron accelerates toward the anode and its Lorentz factor γ_e grows. The toy model assumes that the electron creates a pair when it reaches a certain threshold $\gamma_{\rm res}$. At this point, the electron energy is shared between three particles, so the energy of the original electron is reduced. In this illustration we use a random energy distribution between the three particles with the mean values of 1/2, 1/4, and 1/4 of $\gamma_{\rm res} m_e c^2$. This introduces stochasticity in the pair breakdown.[8]

[8]In reality there are other sources of stochasticity, in particular, the random free-path to resonant scattering with a mean value $l_{\rm res}(\gamma_e)$. It is taken into account in the numerical experiment described below (§ 5.3). For the illustrative

The key parameter is $a_{\rm res}/L$ where

$$a_{\rm res} = \frac{(\gamma_{\rm res} - 1)m_e c^2}{eE}$$

is the length of electron (or positron) acceleration to the energy $\gamma_{\rm res} m_e c^2$, starting from rest. The necessary condition for breakdown is $a_{\rm res}/L < 1$ — otherwise the seed electron reaches the anode before gaining enough energy for pair creation.

The development of the pair breakdown is shown in a spacetime diagram in Figure 5. Each pair-creation event gives two new particles of opposite charge, which initially move in the same direction. One of them is accelerated by the electric field and lost at the boundary after a time $< L/c$, while the other is decelerated and can reverse direction before reaching the boundary. After the reversal, the particle is accelerated toward the opposite boundary and creates at least two new particles, one of which can reverse direction etc. This reversal of particles in the tube and repeated pair creation allows the $e^{\pm}$ plasma to be continually replenished. In the super-critical regime (left panel in Fig. 5) more than one reversing particle is created per passage time L/c and an avalanche develops exponentially on a timescale $\sim a_{\rm res}/c$. In the near-critical regime shown in the right panel of Fig. 5, just one reversing particle is created per passage time L/c. This critical state is unstable: sooner or later the avalanche will be extinguished.

This toy model is very idealized because it assumes a fixed electric field E. In reality, the behavior of E is coupled to the charge density in the tube, which is determined by the particle dynamics and the boundary conditions $j = j_B$. E changes on a timescale much shorter than L/c and the behavior of the coupled plasma and electric field is complicated.

The toy model, however, shows an essential property of the $e^{\pm}$ breakdown: it is a critical stochastic phenomenon. Above a critical voltage pair creation proceeds in a runway manner, and the current and the dissipation rate would run away if the voltage were fixed. Below the critical voltage pair creation does not ignite. The criticality parameter is $L/a_{\rm res} = e\Phi_e/(\gamma_{\rm res} - 1)m_e c^2$. The tube with enforced current at the boundaries must self-organize to create pairs in the near-critical regime $e\Phi_e \sim \gamma_{\rm res} m_e c^2$ and maintain the current.

If the current demanded by $\nabla \times \mathbf{B}$ is not maintained, the self-induction voltage will grow until it exceeds the critical value $e\Phi_e \sim \gamma_{\rm res} m_e c^2$ (corresponding to $a_{\rm res} \sim L$) and a pair breakdown develops. Avalanches of $e^{\pm}$ then supply plasma that tends to screen the electric field by conducting the necessary current, and the voltage in the tube is reduced. The discharging tube is similar to other phenomena that show self-organized criticality, e.g., a pile of sand on a table (Bak, Tang, & Weisenfeld 1987). If sand is steadily added, a quasi-steady state is established with a characteristic mean slope of the pile. The sand is lost (falls from the table) intermittently, through avalanches — a sort of "sand discharge." In our case, charges of the opposite signs are added steadily instead

purposes of this section, it is sufficient to introduce any random element in the pair creation process to make it stochastic.

of sand (fixed j at the boundaries), and voltage $\Phi_e = EL$ plays the role of the mean slope of a pile. The behavior of the discharging system is expected to be time-dependent, with stochastic avalanches.

A steady state is not expected for a pair-creating circuit for two reasons: (1) The created pairs may not maintain a static electric field. Like the Carlqvist double layer, a self-consistent static voltage must be huge, much above the critical value tolerated by pair discharges. No static solution exists at modest voltages because it implies a slow particle acceleration and a large charge imbalance in a broad region, leading to inconsistency (see the end of § 4.3). (2) The near-critical behavior is unstable: either a runaway is ignited or pair creation extinguishes soon after a seed particle is injected.

Discharges are well known in tubes with low-temperature plasma, which is weakly ionized. In that case, the critical voltage accelerates electrons to the ionization threshold and avalanches of ionization develop. Charge carriers are then supplied by ionization rather than pair creation. Another difference is that the fast electrons are lost to the cylindrical wall of the tube, so the problem is not 1-D, and coherent waves of ionization can develop.

5.4. Numerical Simulations

5.4.1. Setup

We implement the pair-creation process in our numerical experiment in a simple way: electrons (or positrons) can create pairs if their Lorentz factors are in a specified range $\gamma_1 < \gamma_e < \gamma_2$. The mean free-path for $e^{\pm}$ emission by an accelerated electron in this window, $l_{\rm res}$, is a parameter of the experiment. It determines the probability of pair creation by the electron during a timestep dt: this probability is $c dt/l_{\rm res}$. Note that $\lambda_{\rm De} \ll l_{\rm res} \ll R_{\rm NS}$.

In a real magnetosphere, the resonance window $\gamma_1 < \gamma_e < \gamma_2$ is shaped by the spectrum of target photons F_ω and the local magnetic field B. In our simplified model, this window is constant along the magnetic line. It is possible to use a more realistic resonance condition that takes into account variations in B and F_ω along a magnetospheric field line. However, our major goal is to see whether $e^{\pm}$ creation leads to a qualitatively different state of the circuit. We shall see that the new state weakly depends on the details of the resonance condition when $B > B_{\rm QED}$ and $\gamma_{\rm res} \gg 1$ everywhere in the circuit.

We consider here only circuits with boundary temperatures too low for plasma to be supplied thermally (§ 4.1). Then the circuit solution weakly depends on the chosen values of T_i and T_e. In this section, we show a sequence of models with $k_{\rm B}T_e = 0.04 m_e c^2$ and $k_{\rm B}T_i = 0.04 m_i c^2$. The corresponding scale height of the surface layers is $h = 0.04L$.

To illustrate the weak dependence on details of the pair creation process we consider two extreme cases of very efficient and very inefficient $e^{\pm}$ creation. Pair creation is less efficient if the resonant window (γ_1, γ_2) is narrow and the mean free-path $l_{\rm res}$ is large even in this window. We therefore focus on two models: Model A: an infinitely wide resonance window $(\gamma_{\rm res}, \infty)$ with free path $l_{\rm res} = 0$ and Model B: a narrow resonance window $(\gamma_{\rm res}, 2\gamma_{\rm res})$ with a large mean free path $l_{\rm res} = L/3$. The inclusion of pair creation brings two new parameters into the experiment: $\gamma_{\rm res}$ and $l_{\rm res}$. We are especially interested in values of $\gamma_{\rm res}$ that are comparable to or below m_i/m_e, which corresponds to a real magnetosphere.

5.4.2. Results

The results of the numerical experiments are shown in Figures 6-14. Figure 6 displays the relation between current j and voltage Φ_e in a circuit with $m_i = 10m_e$ and $\gamma_{\rm res} = 10$. The current is normalized to a minimum current j_* for which the characteristic Debye length $\lambda_{\rm De} = c/\omega_P$ equals the size of the system L (see eq. [19]). At small j_B, the double layer configuration is established in the circuit; its voltage is not sufficient to ignite $e^{\pm}$ production. With increasing j_B, the voltage of the double layer increases as $(j_B/j_*)^{1/2}$ and reaches $\gamma_{\rm res} m_e c^2$ at $j_1 \simeq j_* \gamma_{\rm res}^2$; then it stops growing. At $j_B > j_1$ the voltage saturates at the characteristic $e\Phi_e \sim \gamma_{\rm res} m_e c^2$ in both Models A and B. This asymptotic regime $j_B \gg j_1$ is of interest to us because magnetars are in this regime. All subsequent figures show the asymptotic behavior at $j_B \gg j_1$.

Each point in Fig. 6 is obtained by running a time-dependent simulation that relaxes to a quasi-steady state. Figures 7 and 8 show the relaxation history in two simulations with $j_B = 10^4 j_*$. The voltage Φ_e is zero in the initial state and grows on the dynamical timescale $t_{\rm dyn} = L/c$ while the plasma and electric field self-organize to maintain the required current. The voltage grows until electrons in the circuit get accelerated to Lorentz factors $\gamma_e \sim \gamma_{\rm res}$ and pair production begins. One can see that after a few dynamical times the voltage Φ_e stops growing and the circuit enters an oscillatory regime. During each oscillation, an increased voltage leads to a higher $e^{\pm}$ production rate $\dot{N}_+$, then too many $e^{\pm}$ are produced which screen the voltage (discharge), $\dot{N}_+$ drops, and Φ_e begins to grow again. The oscillations persist until the end of the simulation $(40L/c)$, with a constant amplitude.

We see that a quasi-steady state is reached after a few $t_{\rm dyn}$. This state is time-dependent on short timescales, but it has a well-defined steady voltage when averaged over a few $t_{\rm dyn}$. Models A and B have similar histories of Φ_e and $\dot{N}_+$ (cf. Figs. 7 and 8) except that Model A is noisier on short timescales and shows less coherent oscillations. (The quasi-periodic oscillations are, however, pronounced in the Fourier spectra of $\Phi_e[t]$ and $\dot{N}_+[t]$.) It is not surprising that Φ_e may vary on short timescales $t \ll t_{\rm dyn}$. For example, if the current suddenly stopped, a characteristic voltage $e\Phi_e = m_e c^2$ that is able to accelerate electrons would be created after time $t = m_e c^2/4\pi e L j_B = (j_B/j_*)^{-1}(L/c) \ll L/c$.

In all circuits of interest ($j_B \gg j_1$) we found the time-average voltage,

$$e\bar{\Phi}_e \sim \gamma_{\rm res} m_e c^2. \tag{45}$$

This relation applies even to circuits with $\gamma_{\rm res} m_e c^2 \gg m_i c^2$, where lifting of the ions is energetically preferable to pair creation. We conclude that *the voltage along the magnetic tube is self-regulated to a value just enough to maintain pair production and feed the current with* $e^\pm$ *pairs*. The robustness of this result is illustrated in Figure 9, which shows circuits with $m_i/m_e = 10, 30$ and various $\gamma_{\rm res}$. In all cases, $e\Phi_e \sim \gamma_{\rm res} m_e c^2$ is established, and the pair creation rate $2\dot{N}_+ \sim j_B/e$ is maintained. Thus, the near-critical state is self-organized as expected. Avalanches of $e^\pm$ creation are observed to happen anywhere in the circuit between the dense boundary layers.

The current is carried largely by $e^\pm$ everywhere in the tube. The ion fraction in the current depends on the ratio $e\Phi_e/m_i c^2 \simeq \gamma_{\rm res} m_e/m_i$ (Fig. 10). If this ratio is small, pairs are easily produced with a small electric field, too small to lift the ions, and the ion current is suppressed. In the opposite case, ions carry about 1/2 of the current. For typical parameters expected in the magnetosphere, $\gamma_{\rm res} \lesssim m_i/m_e$, ions carry $\lesssim 10\%$ of the current.

The simulations show that the released energy sinks through the anode and cathode boundaries at approximately equal rates, and that their sum equals $j_B\bar{\Phi}_e$. For magnetars, this implies that both footpoints of a twisted magnetic tube will radiate energy bolometrically at comparable rates.

5.4.3. Sample Model

We now describe in more detail the plasma behavior in one sample experiment. It assumes Model A for $e^\pm$ creation and $\gamma_{\rm res} = m_i/m_e = 10$.[9] The relaxation history of this experiment is shown in Figure 7, and a snapshot of the circuit is shown in Figure 11.

The charge density $\rho = e(n_i + n_p - n_e)$ and electric field are found to fluctuate significantly in time, while the densities n_i, n_p, and n_e are approximately steady. Deviations from charge neutrality are small: $\rho/e(n_i + n_p + n_i) \ll 1$ and $E^2/8\pi U_{pl} \ll 1$ where U_{pl} is the plasma kinetic energy density. The plasma turbulence may then be described as a superposition of Langmuir waves. We do not, however, attempt a development of analytical theory in this paper.

The anode current $j_e + j_i + j_p$ is dominated by electrons. The anode value of j_e even exceeds j_B by 17%. Together with ions ($j_i \simeq 0.13 j_B$), electrons balance the negative current of positrons $j_p \simeq -0.3 j_B$ so that the net current $j_e + j_i + j_p$ equals j_B. Positrons contribute negative j_p at the anode because they move in the "wrong" direction (they are created by accelerated electrons, and some of them leave the box against the mean electric field). The cathode current is dominated by positrons (64%); electrons contribute 23%, and ions 13%.

[9] A similar solution is obtained for $\gamma_{\rm res} = m_i/m_e = 30$. We expect the same circuit solution to apply to $\gamma_{\rm res} = m_i/m_e = 1836$ or any other $\gamma_{\rm res} = m_i/m_e \gg 1$.

Bulk speeds of the three plasma components, v_e, v_i, v_p, and the dispersions of their dimensionless momenta $p/mc = \gamma\beta$ are shown in Figures 12 and 13. The dispersions are significant, i.e. the corresponding distribution functions are broad. The time-averaged distribution of pair creation over z is shown in Figure 14. It has two peaks that correspond to pair production by accelerated e^- and e^+. The net rate of pair creation by e^- is about 2 times higher than that by e^+ in this model.

A complicated kinetic state self-organizes in the phase space of electrons, ions, and positrons. The state keeps oscillating. The oscillations might be related to the fact that positrons move in a wrong direction at creation (negative current) and have to reverse direction to maintain the net $j = j_B$ without strong deviations from neutrality. This requires an extra voltage which leads to "overshooting" in the pair creation rate followed by a temporary screening of the electric field.

6. TRANSITION LAYER

A transition layer must be established between the corona and the relatively cold optically thick atmosphere of the star. It may play a crucial role for two reasons. (1) The layer is able to radiate away the energy received from the corona because it is dense enough for efficient bremsstrahlung emission. The corona itself may not efficiently radiate the dissipated power because its bremsstrahlung output is negligible, and Compton cooling is inefficient as upscattered photons cannot escape — they convert to pairs in the ultra-strong magnetic field. (2) The layer may be hot enough to maintain thermal pair creation at an interesting rate and feed the charge flow in the coronal circuit (Thompson & Beloborodov 2005). A detailed analysis of the transition layer is left for future work. Below we describe some key mechanisms by which energy is deposited and redistributed within the layer, and by which $e^{\pm}$ pairs may be created.

6.1. Heating by Beam Instability

The particles accelerated in the corona enter the hydrostatic atmosphere with high Lorentz factors $\gamma_b \sim e\Phi_e/m_ec^2$. This relativistic beam drives an electrostatic instability with the growth length (e.g. Godfrey, Shanahan, & Thode 1975),

$$l_b \sim \gamma_b \left(\frac{n_e}{n_b}\right)^{1/3} \frac{c}{\omega_{Pe}} = \frac{\gamma_b}{(4\pi n_b r_e)^{1/2}} \left(\frac{n_b}{n_e}\right)^{1/6}. \tag{46}$$

Here $\omega_{Pe} = (4\pi n_e e^2/m_e)^{1/2}$ is the electron plasma frequency in the atmosphere with density n_e, and $r_e = e^2/m_ec^2 \simeq 2.8\times10^{-13}$ cm. The beam exponentially amplifies a seed Langmuir wave whose phase speed is in resonance with the beam. The exchange of energy with the atmospheric plasma occurs on a scale comparable to l_b. As the beam propagates a distance $\sim l_b$ into the layer, the amplified Langmuir waves feed back on the beam and flatten its distribution function to a plateau.

If the initial distribution function of the beam is idealized by δ-function, $f_b(\gamma_e) = \mathrm{const}\, \delta(\gamma_e - \gamma_b)$, its relaxation to the plateau $1 < \gamma_e < \gamma_b$ implies the deposition of $\frac{1}{2}$ of the beam energy into plasma turbulence. Since the relaxation occurs in a strong magnetic field, the particle momentum distribution remains one-dimensional. This is different from beam relaxation in a normal plasma — in that case a large dispersion of perpendicular momenta develops before relaxing to the plateau in energy.

The coronal beam has a density $n_b \sim n_c = j_B/ec \sim 10^{16} - 10^{17}$ cm^{-3} and Lorentz factor $\gamma_b \simeq \gamma_{\rm res} \sim 10^3$ (see § 5; this would correspond to a total energy deposition rate of $10^{36}\, \gamma_{b,3} n_{16}$ erg s^{-1} if integrated over the entire surface of the star). Substituting these values to equation (46) one finds $l_b \sim 1$ cm. The beam relaxation occurs at a much larger depth than the skin depth of the atmospheric plasma, $l_b \gg c/\omega_P$. Therefore, the beam instability may heat the atmosphere only well below the screening layer, i.e. well below the region where the induced electric field develops and particles are lifted to the corona.

In our numerical experiments $l_b \sim 10(c/\omega_P) \sim 0.1L$ was larger than the scale height of the atmosphere, h, so heating by beam instability could not possibly operate in the computatonal box. The possible atmospheric heating at larger depths was regulated in the experiment by hand, by setting the boundary temperatures T_e and T_i. Further investigation of beam heating is deferred to a future work.

Comparing the expected l_b and h, one has

$$\frac{l_b}{h} \sim \left(\frac{n_b}{n_e}\right)^{1/6} \left[\frac{k_{\rm B}(T_e + T_i)}{\rm keV}\right]^{-1}. \tag{47}$$

Note that l_b/h is reduced if the plasma temperature grows. It is possible that the atmosphere develops a hot layer with $l_b \ll h$, which absorbs a significant part of the beam energy. The excited Langmuir turbulence heats mostly electrons and T_e may grow to $k_{\rm B}T_e \gtrsim 100$ keV. Then hard X-ray emission and thermal pair creation may occur as discussed below.

6.2. Thermal Conduction and Radiative Losses

Dissipation without losses of energy would imply an unlimited growth of temperature. If the twisted magnetosphere were thermally insulated, it would quickly heat up and remain filled with a hot plasma that would steadily conduct the current with no further dissipation. Losses of the dissipated energy are therefore crucial in the regulation of the state of the circuit. In our numerical experiment we simply allowed the released energy to sink through the anode and cathode boundaries, assuming that it is radiated away outside our boundaries. Here we discuss a possible mechanism of the energy loss.

We expect the energy of the accelerated coronal particles to be deposited in an optically thin atmospheric layer by collisionless processes (such as beam instability discussed in § 6.1). This layer is still unable to cool radiatively, and the deposited heat will be conducted to deeper and denser layers that can radiate the heat away by bremsstrahlung (Thompson & Beloborodov 2005). The radiation flux emitted at that depth is $F_\gamma \sim h\epsilon_{\rm ff}$ where h is a characteristic scale-height and $\epsilon_{\rm ff}$ is the free-free emissivity. Plasma with temperature T_e and density n_e has the bremsstrahlung emissivity

$$\epsilon_{\rm ff} \approx \alpha\,\theta_e^{1/2} n_e^2 \sigma_{\rm T} m_e c^3, \qquad \theta_e \equiv \frac{k_{\rm B} T_e}{m_e c^2}, \tag{48}$$

where $\alpha = e^2/\hbar c = 1/137$ is the fine structure constant. The characteristic scale-height on which density and temperature change in the layer is the hydrostatic scale-height, $h = k_{\rm B} T_e / m_i g$ (we assume here $T_e < T_i$ since the collisionless dissipation heats mostly electrons). Then the emitted radiation flux is

$$F_\gamma = h\epsilon_{\rm ff} \approx \alpha\,\frac{m_e}{m_i}\,\theta_e^{3/2}\frac{c^2}{g} n_e^2 \sigma_{\rm T} m_e c^3. \tag{49}$$

It carries away a significant fraction of the energy flux received from the corona when $F_\gamma \sim F = n_c \gamma_b m_e c^3$, where $\gamma_b = e\Phi_e/m_e c^2 \simeq \gamma_{\rm res}$. This gives one relation between temperature θ_e and Thomson optical depth $\tau_{\rm T} = h\sigma_{\rm T} n_e$ at which the heat flux is converted to radiation,

$$\theta_e^{-1/2} \tau_{\rm T}^2 \simeq \frac{\tau_c \gamma_b}{\alpha}\,\frac{m_e}{m_i}\,\frac{c^2}{g R_{\rm NS}}, \tag{50}$$

where

$$\tau_c \equiv R_{\rm NS} \sigma_{\rm T} n_c \sim 0.01 - 0.1. \tag{51}$$

Equation (50) is not sufficient to determine θ_e and $\tau_{\rm T}$ of the emitting layer because the mechanism of heat transport to this layer has not been specified yet. A second relation is needed, which is the equation of thermal conductivity (Thompson & Beloborodov 2005). It relates the heat flux $F_c \sim F \sim F_\gamma$ to the temperature gradient: $F_c = \kappa dT_e/dz$ where $\kappa = n_e v_e \ell k_{\rm B}$, $v_e = (k_{\rm B} T_e/m_e)^{1/2}$, and ℓ is the mean free path of electrons. In the absence of plasma turbulence, the mean free path is determined by Coulomb collisions,

$$\ell_{\rm Coul} = \frac{\theta_e^2}{n_e \sigma_{\rm T}}. \tag{52}$$

If strong plasma turbulence develops with energy density above the thermal level, $U_{\rm turb} = (\delta E_\|)^2/8\pi \gg k_{\rm B} T_e/\lambda_{\rm De}^3$, the fluctuating electric field suppresses the mean free path. It is then given by

$$\ell \simeq \lambda_{\rm De} \left(\frac{U_{\rm turb}}{n_e k_{\rm B} T_e}\right)^{-1}. \tag{53}$$

(We here assumed that the turbulence develops at frequencies $\omega \sim \omega_{Pe}$.) We will keep ℓ as a parameter in our estimates. It is bounded from above and below by $\lambda_{\rm De} < \ell < \ell_{\rm Coul}$.

Estimating $dT_e/dz \sim T_e/h$, one finds

$$F_c = n_e v_e \ell \frac{k_{\rm B} T}{h} = n_e\, v_e\, \ell\, g m_i, \tag{54}$$

$$\theta_e^{-3}\tau_{\rm T}^2 \simeq \frac{1}{\alpha}\left(\frac{\ell}{\ell_{\rm Coul}}\right). \tag{55}$$

Combining equations (50) and (55), one finds the temperature of the radiating layer,

$$\theta_e \approx \left(\tau_c\gamma_b\,\frac{m_e}{m_i}\,\frac{c^2}{gR_{\rm NS}}\,\frac{\ell_{\rm Coul}}{\ell}\right)^{2/5}, \qquad k_{\rm B}T_e \approx 200\left(\frac{\tau_c}{0.1}\right)^{2/5}\left(\frac{\gamma_b}{10^3}\right)^{2/5}\left(\frac{\ell}{\ell_{\rm Coul}}\right)^{-2/5}\ {\rm keV}. \tag{56}$$

If $\ell < \ell_{\rm Coul}$ (suppressing heat conduction) the emission temperature will grow above 200 keV. The growth, however, will be quickly stopped at $\theta_e \sim 1$ because the hot layer starts to generate $e^\pm$ pairs which can short out the circuit (see § 6.3).

6.3. Heated Atmospheric Layer as a Possible Source of $e^\pm$

6.3.1. Channels of Pair Creation

The dominant channels of thermal pair creation in a hot atmosphere involve an electron-ion collision. Three such channels are summarized below.

1. An $e^\pm$ pair can be created directly in a collision between an ion and an energetic electron (or positron), $e^- + Z \rightarrow e^- + Z + e^- + e^+$. This reaction is possible when the kinetic energy of the incident electron exceeds a threshold $E_{\rm thr} = 2m_ec^2$ (both e^- and e^+ can be created in the lowest Landau state). When the temperature $k_{\rm B}T_e \ll 2m_ec^2$, the reaction occurs in the high-energy tail of the electron distribution.

2. A bremsstrahlung photon can be emitted in an electron-ion collision, almost always in the O-mode. The photon converts to an $e^\pm$ pair if satisfies the threshold condition $E_\gamma > 2m_ec^2/\sin\theta_{\rm em}$ where $\theta_{\rm em}$ is the emission angle (cf. § 5.1).

This second channel of pair creation is similar to the first one, where a virtual photon converts directly to a pair during the electron-ion collision. The emission of a real bremsstrahlung photon makes the process two-step and increases its threshold from $2m_ec^2$ to $2m_ec^2/\sin\theta_{\rm em}$. The exact cross sections of these processes in the ultrastrong magnetic field have not been calculated, to our knowledge. They may be roughly estimated using the nonmagnetic formulae (e.g. Berestetskii, Lifshitz, & Pitaevskii 1982): $\sigma_{\rm bremss} \sim 0.3\,Z^2\alpha\,\sigma_T$ and $\sigma_{\rm direct} \sim \alpha\sigma_{\rm bremss}$.

Note that relativistic bremsstrahlung emission is preferentially beamed along **B**, in the direction of the incident electron, so $\theta_{\rm em}$ is small. Then the threshold is substantially higher than $2m_ec^2$ and the bremsstrahlung photon will be unable to convert to $e^\pm$ in situ. If the photon propagates away from the emission site where **B** has a different direction, the threshold may be reduced because the pitch angle of the photon increases. Gravitational bending of the photon trajectory also helps to increase the pitch angle. Thus, pair creation by bremsstrahlung photons can be non-local and take place above the hydrostatic atmosphere.

3. An electron can be excited to the first Landau state by a Coulomb collision with an ion. The excited electron rapidly de-excites and emits an energetic photon that may convert to a pair (or split, see § 5.1). This channel requires the initial electron to have a minimum energy $E_{\rm thr} = E_B \approx 6.7\,B_{15}^{1/2}\,m_ec^2$ (eq. 29). The side-scattering into the first Landau state involves a perpendicular momentum transfer $p_\perp = (2B/B_{\rm QED})^{1/2}m_ec$, and the corresponding Coulomb cross section may be estimated as

$$\sigma_{\rm Coul}(0\rightarrow 1) \approx \frac{4\pi Z^2e^4}{(p_\perp c)^2} = \frac{3Z^2}{4}\left(\frac{B}{B_{\rm QED}}\right)^{-1}\sigma_T. \qquad (57)$$

6.3.2. *Feeding the Corona with Atmospheric Pairs*

The rate of pair creation in the atmosphere may be roughly estimated as the rate of electron-ion collisions above the threshold $E_{\rm thr}$,

$$\dot{n}_+ \sim n_i\,f_{\rm thr}\,n_e\,\sigma\,c, \qquad (58)$$

where $f_{\rm thr} \sim \exp(-E_{\rm thr}/k_{\rm B}T_e)$ is the fraction of thermal 1-D electrons that have energy $E_e > E_{\rm thr}$; σ and $E_{\rm thr}$ are the cross section and the threshold energy of the relevant channel. Atmospheric pair production is able to feed the coronal current j_B if $h\dot{n}_+ > j_B/e$ or, equivalently,

$$f_{\rm thr}\,\tau_{\rm T}n_i\left(\frac{\sigma}{\sigma_{\rm T}}\right) > n_c, \qquad (59)$$

where $\tau_T = \sigma_{\rm T}n_eh$. This condition may be rewritten using $\tau_c = R_{\rm NS}\sigma_{\rm T}n_c$ and $h = \theta_e(m_e/m_i)(c^2/g)$,

$$\theta_e^{-1}\tau_{\rm T}^2 > \frac{m_e}{m_p}\left(\frac{c^2}{R_{\rm NS}g}\right)\frac{\sigma_{\rm T}}{\sigma}\,\frac{\tau_c}{f_{\rm thr}} \approx 2\times 10^{-3}\,\frac{\tau_c}{f_{\rm thr}}\,\frac{\sigma_{\rm T}}{\sigma}. \qquad (60)$$

If this condition is met at some depth $\tau_{\rm T}$, the atmospheric pairs can dominate the charge supply to the coronal circuit. At $\tau_{\rm T} \gg 1$ the parameter $\theta_e\tau_{\rm T}^2 \lesssim 1$ is limited by Compton cooling of the plasma, which implies a low T_e and negligible $f_{\rm thr}$. The condition (60) may be satisfied only at $\tau_{\rm T} \lesssim 1$ and requires at least mildly relativistic T_e. The created pairs have kinetic energies $\sim k_{\rm B}T_e$, so they may elevate, overflow the gravitational barrier, and maintain the current.

6.3.3. *Numerical Models*

In order to see how atmospheric pair production could affect the circuit, we have done a few numerical simulations using the following toy model. We assume that the atmosphere responds to the heat flux from the corona by producing $e^\pm$ pairs. Therefore, in addition to the ion-electron atmosphere, we now maintain a thermal $e^\pm$ atmosphere. Its density at each boundary is regulated in the experiment so that it is proportional to the flux of lost energy through the boundary.

If the atmospheric pairs were cold, the circuit would be in the same regime as in their absence. The fact that positrons are now available at the boundaries to carry the current instead of ions does not lead to any significant reduction of the voltage: it still evolves to the state with $e\Phi_e \simeq \gamma_{\rm res} m_e c^2$, in which energetic $e^\pm$ are supplied via the resonant-scattering channel. We have checked this by running the models with cold $e^\pm$ atmospheres. The key property of atmospheric pairs is, however, that they are created hot enough to feed the current thermally (cf. § 4.1). Their expected kinetic energy is comparable to the height of the gravitational barrier (§ 6.3.2) and they can overflow the barrier. Therefore, the required current j_B can be conducted at a small voltage $e\Phi_e < \gamma_{\rm res} m_e c^2$.

The thermally-driven regime was indeed established in our experiment with a realistic $k_{\rm B}T_\pm = 0.5 m_e c^2$. The established voltage then depends on the efficiency of pair supply in response to the energy flux from the corona. We define the efficiency ξ as the fraction of the energy flux through the boundary that is returned to the corona in the form of $e^\pm$ kinetic and rest-energy. We find that the voltage Φ_e across the circuit adjusts so that the flux of released energy, $j_B\Phi_e$, can generate the minimum flux of atmospheric pairs to feed the coronal current, j_B/e. Then voltage is related to ξ roughly as $e\Phi_e \sim \xi^{-1} m_e c^2$. For example, a maximum efficiency $\xi \sim 1$ would reduce the voltage to $e\Phi_e \sim m_e c^2$. We have done the corresponding experiment that confirmed this estimate. The voltage was found to fluctuate significantly, but it did not get high enough to initiate the resonant channel of $e^\pm$ production ($\gamma_{\rm res} = m_i/m_e = 10$ in the simulation). The ion current was small, $j_i/j_B \simeq 10^{-2}$.

When ξ is reduced, a higher voltage is required in the circuit according to the relation $e\Phi_e \sim \xi^{-1} m_e c^2$. This estimate is applicable as long as $\xi \gtrsim \gamma_{\rm res}^{-1}$, so that $e\Phi_e < \gamma_{\rm res} m_e c^2$. A further reduction of ξ does not lead to an increase of voltage: then the circuit is mainly fed by pairs created via the resonant channel, and $e\Phi_e \sim \gamma_{\rm res} m_e c^2$ as described in § 5. The thermal pair creation in the atmosphere then has a negligible effect on the circuit.

We have also studied one modification of this experiment by allowing only the anode to supply pairs with efficiency $\xi = 1/2$. In this case, the $e^\pm$ atmosphere created by the anode filled the whole tube, and conducted the current. Ions lifted from the anode surface contributed a small fraction to the current $j_i/j_B \simeq 3 \times 10^{-2}$. The established voltage was ~ 5 times higher than in the model with pair supply at both ends. However, the circuit was able to operate without igniting the resonant pair creation (which we checked by setting $\gamma_{\rm res} = \infty$). This shows that the thermally-driven regime can operate even when pair creation takes place at one footpoint of the magnetic tube.

In summary, the coronal current may be fed by atmospheric $e^\pm$ instead of the pair discharge via the resonant channel if $\xi \gtrsim \gamma_{\rm res}^{-1}$. The numerical coefficient in this condition increases if one of the surfaces (anode or cathode) dominates the pair supply.

6.4. Anomalous Resistivity and Hydrostatic Equilibrium

In addition to the heating by the relativistic beam that comes from the corona, the atmosphere may experience anomalous heating in response to the strong electric current. This type of heating is known to occur in astrophysical and laboratory plasmas when the drift speed of the current-carrying electrons, v_d, exceeds the sound speed $c_s = (k_B T_e/m_i)^{1/2}$ (e.g. Bernstein & Kulsrud 1961). If the electron current can be described as a shift of a Maxwellian distribution with respect to the ions in velocity space, $\Delta v_e = v_d$, a positive gradient $df_e/dv_e > 0$ appears in the electron distribution function viewed from the rest-frame of the ion component. The positive gradient exists at $v_e < v_d$ and will amplify slow plasma modes with phase speed along the magnetic field $\omega/k_\parallel < v_d$. The dispersion relation of ion-sound waves gives $\omega/k_\parallel = c_s\,(1+k^2\lambda_{\rm De}^2)^{-1/2}$ and they are easily amplified when $v_d > c_s$. The excited ion-sound turbulence creates the anomalous resistivity and heating.

With an increasing level of turbulence, $U_{\rm turb}/n_e k_B T_e$, the mean free path of the electrons ℓ decreases according to equation (53). This implies a higher resistivity and a lower thermal conductivity. Thus, a reduced ℓ leads to a strong anomalous heating and the suppression of heat conduction out of the layer. It is then possible that the layer is overheated, loses hydrostatic balance, and expands in a runway manner. We now estimate the critical ℓ for this to happen. We neglect the radiative losses in this estimate.

The ohmic heating rate per unit area of the layer is

$$F_{\rm Ohm} \simeq h\,\frac{j^2}{\sigma}, \tag{61}$$

where $h = k_B T_e/m_i g$, $\sigma = n_e e^2 \ell/m_e v_e$ is electrical conductivity, and $v_e = (k_B T_e/m_e)^{1/2}$ is electron thermal speed. The conductive heat loss F_c is given by equation (54), and we find

$$\frac{F_{\rm Ohm}}{F_c} = \left(\frac{m_e}{m_i}\right)^2 \left(\frac{c^2}{gR_{\rm NS}}\right)^2 \frac{\tau_c^2}{\theta_e^3} \left(\frac{\ell}{\ell_{\rm Coul}}\right)^{-2}. \tag{62}$$

Hence the layer must be overheated if

$$\frac{\ell}{\ell_{\rm Coul}} < 2\times 10^{-3}\,\theta_e^{-3/2}\,\tau_c. \tag{63}$$

Here $\tau_c = \sigma_T R_{\rm NS}\, j/ce \sim 10^{-1} - 10^{-2}$ (§ 6.2), and the temperature is limited by pair creation to $\theta_e \lesssim 1$ (see § 6.3). One can see that the ohmic overheating requires a high level of plasma turbulence, when the mean-free path is strongly reduced compared to the Coulomb value. This level is achievable in principle because it is still below the upper limit $U_{\rm turb}/n_e k_B T_e \sim 1$ that corresponds to the minimum $\ell \sim \lambda_{\rm De}$. Indeed,

$$\frac{\lambda_{\rm De}}{\ell_{\rm Coul}} \simeq \frac{4}{3}\,\pi^{1/2} \left(\frac{n_e r_e^3}{\theta_e}\right)^{1/2} = \left(\frac{2}{3}\right)^{1/2} \frac{\tau_{\rm T}^{1/2}}{\theta_e} \left(\frac{g r_e}{c^2}\,\frac{m_i}{m_e}\right)^{1/2} \simeq 2\times 10^{-7}\,\frac{\tau_{\rm T}^{1/2}}{\theta_e}. \tag{64}$$

Note that anomalous heating becomes interesting only when the thermal heat flux is strongly suppressed. In other words, $F_{\rm Ohm}$ may compete with F_c and overheat the layer only when F_c is small. One can derive from the above formulae,

$$\frac{F_{\rm Ohm}}{F_c} \simeq \left(\frac{F_c}{4\times 10^{22}\,\tau_c\theta_e\ \ {\rm erg\ s^{-1}\ cm^{-2}}}\right)^{-2}. \tag{65}$$

Substituting $\tau_c \sim 10^{-1} - 10^{-2}$ and $\theta_e \lesssim 1$ one finds that the maximum energy flux from the ohmically-heated layer is $F_c \sim 10^{21}$ erg s^{-1} cm^{-2}. Even if the layer covers the whole star with area $4\pi R_{\rm NS}^2 \simeq 10^{13}$ cm^2, its total power would not exceed 10^{34} erg s^{-1}. This is two orders of magnitude smaller than the observed luminosity of the corona, and hence the anomalous heating of the atmosphere is unlikely to generate the observed activity.

The marginally stable state $F_{\rm Ohm} = F_c$ has an electrostatic potential drop $e\delta\Phi_e \sim k_{\rm B}T_e$ across the layer, which equals the energy gained by an electron crossing the layer. Since T_e is limited by pair creation, the maximum potential drop that can be sustained by the layer is $\sim m_ec^2$. This is at least 2 orders of magnitude lower than the voltage $\gamma_{\rm res}m_ec^2$ that is developed in the corona with $e^\pm$ discharges. If the turbulence in the transition layer reaches the level required for runaway heating, the plasma may be supplied to the corona at a much lower voltage compared with the pair discharge described in § 5.

Pair creation in the atmosphere (see § 6.3) would tend to reduce its mean molecular weight and increase h. When the expressions for $F_{\rm Ohm}$ and F_c are modified to include the pair density, $n_e \to n_e + n_\pm$, one finds that the critical value of $\ell/\ell_{\rm Coul}$ for runaway heating (eq. 63) increases as $1 + n_\pm/n_e$. The critical value of pair density is $n_* \sim n_c(h/\ell)$, at which the diffusive flux of hot $e^\pm$ out of the atmosphere dominates the corona and shortens out the electric circuit. One finds the relation

$$\frac{F_{\rm Ohm}}{F_c} = \left(\frac{n_*}{n_e + n_\pm}\right)^2 \frac{1}{\theta_e}. \tag{66}$$

If the atmosphere is the main source of charges for the coronal current then $n_\pm \approx n_*$ is expected. Ohmic heating is unimportant in such an "electrically regulated" atmosphere if $n_\pm \approx n_* < n_e$. It can become important if the atmosphere happens to enter the pair-dominated regime, $n_\pm > n_e$. Then the overheating with $F_{\rm Ohm}/F_c \sim \theta_e^{-1} > 1$ is possible, leading to over-production of pairs, $n_\pm > n_*$, which will suppress $F_{\rm Ohm}/F_c$ and quickly shut the instability. Perhaps a cyclic overheating with pair enrichment would occur.

The effects discussed in this section indicate the possibility of an alternative way of forming the corona, through heating and pair creation in the atmosphere. This would require a high level of turbulence in the atmospheric plasma, and it is unclear whether this level is reached. Observations of the high-energy tail of the X-ray spectrum may help constrain the composition and temperature of the transition layer.

7. CRUST EXCAVATION AND FORMATION OF A LIGHT-ELEMENT SURFACE LAYER

7.1. Mass Transfer in the Coronal Circuit

The existence of an ion current in the magnetosphere implies the transfer of mass from the anode footpoint of a magnetic line to its cathode footpoint. The rate of transfer may be easily estimated for the idealized configuration of a twisted dipole (§ 2),

$$\dot{M} \sim m_p \frac{j_i}{e} 4\pi R_{\rm NS}^2 \sim \left(\frac{j_i}{j}\right) \frac{m_p\, c}{e} \varepsilon_j\, BR_{\rm NS} \sim 10^{17} \, \left(\frac{j_i}{j}\right) \varepsilon_j B_{15} \;\; {\rm g\ s^{-1}}. \tag{67}$$

Here the dimensionless coefficient $\varepsilon_j \equiv \Delta\phi \sin^2\theta$ measures the strength of the twist in the dipole magnetosphere (see eq. [1]). During the active life of a magnetar, $t \sim 10^4$ yr, a significant mass is transferred through the magnetosphere, $\Delta M \sim 3 \times 10^{28}\,(j_i/j)\,\varepsilon_j\,B_{15}$ g. It is much larger than the mass of the stellar atmosphere, and the atmosphere is quickly removed from the anode part of the stellar surface.

There is, however, a mechanism which can re-generate the atmosphere and regulate its column density. A thin atmosphere is unable to stop the energetic particles flowing from the corona and these particles will hit the crust and knock out new ions. In a steady state, the atmosphere column density can adjust so that the rate of ion supply equals the rate of their transfer through the corona. Then the rate of crust excavation at the anode footpoints is proportional to the ion current through the corona.

Excavation depends on the chemical composition of the uppermost crust of the neutron star. If it is made of light elements, the atmosphere is easily re-generated by simple knock out of ions from the surface. If it is made of carbon, oxygen, or any heavier elements, the ions are condensed into long molecular chains in a $\sim 10^{15}$ G magnetic field (Neuhauser, Koonin, & Langanke 1987; Lieb, Solovej, & Yngvason 1992; see Thompson et al. 2000 for estimates of the chain binding energy in the case of $\sim 10^{15}$ G magnetic fields). The knock out of light elements by the beam is still possible in this case because of spallation reactions. We discuss the excavation process in more detail below.

7.2. Excavation of Hydrogen and Helium Layers

Light elements — hydrogen and helium — may be present only above a certain depth that may be estimated as follows. The column mass density Σ above a given depth in the crust is related to pressure P at this depth through the equation of hydrostatic equilibrium,

$$\Sigma g = P = \frac{eB_{\rm NS}}{2\pi\hbar^2}\frac{p_F^2}{2\pi}. \tag{68}$$

Here it is taken into account that the pressure is dominated by degenerate electrons that are confined to their lowest Landau state ($E_F < E_B$ in the density range of interest); $p_F \sim m_e c\,\rho_7 B_{15}^{-1}$ and $E_F = [p_F^2c^2 + m_e^2c^4]^{1/2}$ is the Fermi energy. A conservative upper bound on the depth of a hydrogen layer is obtained by balancing E_F with the threshold for electron captures on protons, $E_F \sim 1.3$ MeV. This corresponds to $\rho \sim 10^7$ g cm^{-3}. At larger depths, free protons are rapidly consumed by reaction $e^- + p \rightarrow n + \nu$.

A more realistic upper bound takes into account that hydrogen is burned into helium, and the maximum depth of a helium layer is limited by the triple-alpha reaction $3\alpha \rightarrow {}^{12}$C, which is very temperature-dependent. The interior of a magnetar probably sustains a temperature of $\sim 3\times10^8$ K at an age of $\sim 10^3 - 10^4$ yr (e.g. Arras, Cumming, & Thompson 2004). In the presence of a light-element atmosphere, the crust temperature remains close to the central temperature at depths $\rho > 10^6$ g cm^{-3} (e.g. Potekhin et al. 2003). At such densities and temperatures helium (and hydrogen) cannot be present — its lifetime would be only $\sim 10^{-3}$ $(Y_e\rho_6)^{-2}$ yr where $Y_e \approx 0.5$ is the electron fraction. Helium may survive only in an upper layer of density $\rho < 10^5$ g cm^{-3}, where temperature is below $\sim 1\times10^8$ K.

The maximal layer of light elements will be drained rapidly from the anode surface and deposited at the cathode surface in the presence of a magnetic twist. The excavation time down to a depth with a Fermi momentum p_F is

$$t_{\rm exc} = \frac{\Sigma}{Am_p j_i/e} = 0.3\,\frac{Z/A}{\varepsilon_j}\left(\frac{j_i}{j}\right)^{-1}\left(\frac{p_F}{m_e c}\right)^2\frac{R_{\rm NS,6}}{g_{14}}\quad {\rm yr}. \tag{69}$$

Substituting $j_i/j \sim 0.1$ and $\varepsilon_j \sim 0.1$ shows that the excavation time of the maximal hydrogen layer ($E_F \simeq 1.3$ MeV) is much shorter than the active $\sim 10^4$-yr lifetime of a magnetar. Taking a more realistic maximum density $\rho \sim 10^5$ g cm^{-3} and $p_F/m_e c \simeq 6\times10^{-3}\rho_5 B_{15}^{-1}$, one finds the excavation time of hours or days. It is faster than hydrogen consumption through diffusion to a deeper layer of carbon (Chang, Arras, & Bildsten 2004).

We conclude that the anode surface of the star should be made of heavier elements — carbon or iron. A gaseous atmosphere of light elements may be maintained above such a condensed, heavy-element surface due to the beam of energetic particles from the corona.

7.3. Beam Stopping and Spallation of Nuclei in a Solid Crust

When the coronal beam enters the crust, it is stopped by two-body collisions, and collective processes become negligible. In particular, the growth length of beam instability l_b (eq. [46]) is much larger than the mean free path to two-body collisions (their ratio scales as $n_e^{5/6}$ and is large in condensed matter because n_e is large). The stopping length of the beam is then mainly determined by Coulomb collisions with the nuclei.

Consider a downward-moving electron with an energy $E_e = \gamma m_e c^2 \gg E_B$ (eq. [29]). Collision with an ion can excite the electron to any Landau level $n > 0$ with energy $E_n = (2nB/B_{\rm QED} + 1)^{1/2} < E_e$. Most frequently, it will be the first level $E_1 = E_B$ because this process has the largest cross section (eq. 57). The probability of excitation to levels $n' \geq n$ is reduced by a factor $\sim \frac{1}{n}$ (it requires a smaller impact parameter; see also Kotov & Kelner 1985). One may assume a two-level system $n = 0, 1$ in simplified estimates.

The excited electron moves along the magnetic line with a new Lorentz factor $\gamma_{\|}$, which is found from the energy conservation, $\gamma_{\|}E_B = E_e$. It immediately de-excites and emits a photon at pitch angle $\theta_{\rm em}$ with energy $E_\gamma(\theta_{\rm em})$ (§ 5.1). The normal modes of radiation in the uppermost crust are determined by both vaccuum and matter polarization, which gives elliptical polarization states. A photon in either elliptical mode immediately converts to $e^{\pm}$ off the magnetic field if it is above the threshold, $E_\gamma > 2m_ec^2/\sin\theta_{\rm em}$. This condition is satisfied for a fraction f_B of de-excitation photons, which is estimated using the results of Herold et al. (1982). When $B \gg B_{\rm QED}$, the angular distribution of the emitted photons is proportional to $E_\gamma^2\,\exp[-\frac{1}{2}(B/B_{\rm QED})^{-1}\,(E_\gamma/m_ec^2)^2]$ in both polarization modes. Combining this expression with $E_\gamma(\theta_{\rm em})$ (eq. [36]), we find that f_B can be well approximated by

$$f_B \approx 1 - \frac{2e}{(e-1)}\left(\frac{B}{B_{\rm QED}}\right)^{-1} \approx 1 - 0.14\,B_{15}^{-1}, \qquad B \gg B_{\rm QED}. \tag{70}$$

The net result of collisional excitation, de-excitation, and photon conversion to $e^{\pm}$ is the sharing of initial electron energy E_e between three particles, and each of them will again collide with an ion and produce more $e^{\pm}$. Thus, a pair cascade develops as a beam with initial $\gamma = \gamma_0$ propagates into the crust, giving more $e^{\pm}$ with lower Lorentz factors $\gamma < \gamma_0$.

This branch of the cascade operates for a large fraction of the de-excitation photons. Photons that cannot immediately convert off the field (a fraction $1 - f_B$) will wait until they interact with an ion in the crust (photon splitting is slow compared with photon-ion interaction). Normally, such a photon will convert to $e^{\pm}$ in the Coulomb field of the nucleus. Less frequently, it can knock out a neutron, proton, or (rarely) alpha particle. This second branch of the cascade is most important for us, since it produces light elements.

The probability of proton knockout instead of normal conversion to $e^{\pm}$ may be roughly estimated using the known nonmagnetic cross sections for photon-nucleous collision. Knockout requires a minimum photon energy of $\sim 15-20$ MeV, and its cross section typically peaks at $\sim 20-30$ MeV (e.g. Dietrich & Berman 1988). The cross section for proton knockout from oxygen is $\sigma(\gamma,^{16}{\rm O} \to p,^{15}{\rm N}) \approx 12$ mb at $E_\gamma \simeq 25$ MeV. It scales approximately in proportion to Z, and so we take

$$\sigma\,(\gamma, Z \to p, Z-1) = 1.5\,Z \;\;{\rm mb}. \tag{71}$$

The cross section for pair creation is

$$\sigma^Z_{e^+e^-} = \frac{7}{6\pi}\,Z^2\alpha\left[\ln\left(\frac{2E_\gamma}{m_ec^2}\right) - \frac{109}{42}\right]\sigma_{\rm T} \approx 3.2\,Z^2 \;{\rm mb}. \tag{72}$$

We can now estimate the number of protons knocked out per incident energetic electron. We will assume in this estimate an idealized surface layer that is composed of ions of a single charge Z. We roughly estimate the number of generations in the cascade down to an energy of ~ 25 MeV $\simeq 50m_ec^2$ as $N_g \sim \log_2(\gamma_0/50) \sim 5$. The number of ~ 25 MeV photons created per incoming electron is about $\gamma_0/50$. A fraction $1 - f_B$ of these photons hit a nucleus, yielding a proton with a probability $\sigma\,(\gamma, Z \to p, Z-1)\,/\sigma^Z_{e^+e^-}$. The resulting yield of protons per incident primary electron is

$$N_p \approx (1 - f_B)\,B_{15}^{-1}\left(\frac{\gamma_0}{50}\right)\frac{\sigma\,(\gamma, Z \to p, Z-1)}{\sigma^Z_{e^+e^-}} \sim 0.1\left(\frac{\gamma_0}{10^3}\right)\left(\frac{Z}{26}\right)^{-1}. \tag{73}$$

The $e^{\pm}$ cascade develops at a significant depth that buries the created positrons — they annihilate in the crust and cannot escape back through the surface. The first Coulomb collision occurs at a Thomson depth $\tau_{\rm T} \sim Z\sigma_T/\sigma_{\rm Coul} \approx 20\,B_{15}/Z$. The relativistic cascade so initiated is strongly beamed into the star, and noticeable backscattering may occur only after the last stage of the cascade that gives $e^{\pm}$ with $\gamma \sim E_B/2m_ec^2 \sim 3B_{15}^{1/2}$, after $\log_2(\gamma_0 m_e c^2/E_B) \sim 8$ generations. Even the first branch of the cascade, which involves immediate pair creation off the magnetic field, ends at a significant $\tau_{\rm T} \gtrsim 100Z^{-1}B_{15}$. This layer is optically thick to positron annihilation. Therefore, the anode surface can supply positive charges only by emitting light ions, mostly protons that have been produced by spallation.

Spallation reactions occur down to a Thomson depth $\tau_{\rm T} \sim N_g\,Z\sigma_T/\sigma^Z_{e^+e^-} \sim 10^3/Z$. The knocked-out protons diffuse through the spallation layer on a short timescale, much shorter than the excavation time of this layer, and are quickly sublimated to the atmosphere.[10] Thus, excavation of the crust is driven by spallation followed immediately by sublimation.

Our preferred circuit model has voltage $e\Phi_e \sim 1$ GeV and ion current $j_i \sim 0.1j$ (§ 5). If the gaseous atmosphere does not decelerate the particles flowing from the corona, they will impact the solid crust with $\gamma_0 \sim 10^3$. The estimated proton yield $N_p \sim 0.1(Z/26)^{-1}$ is then sufficient to feed $j_i \sim 0.1j$ and can supply more ions than transferred through the corona. Then the column density of the atmosphere will grow until it is able to damp the relativistic beam from the corona and reduce the crustal excavation rate.

The profile of the atmosphere is determined by its efficiency of stopping the relativistic $e^{\pm}$. If collisionless processes do not decelerate the relativistic beam but just form a plateau in its distribution function (§ 6.1), then a thick atmosphere must be accumulated to decelerate the beam through Coulomb collisions. Collisions initiate a cascade similar to that in the crust: the beam particles collide with ions and emit photons that convert to pairs.[11] The crustal spallation rate will be reduced if the beam is decelerated to $\gamma \lesssim 50$ before reaching the solid surface. This requires $\log_2(\gamma_{\rm res}/50) \sim 5$ generations of pair-creation, and so the optical depth to Coulomb collisions should be ~ 5. Thus, the column density of the atmosphere will be regulated to the value

$$N_{\rm atm} \sim \frac{\log_2(\gamma_{\rm res}/50)}{\sigma_{\rm Coul}} \sim 100\,B_{15}\,\sigma_{\rm T}^{-1}. \tag{74}$$

If $N_p/(1+N_p) < j_i/j$, the crust will not supply the ion flux implied by our circuit solution with $e\Phi_e \sim \gamma_{\rm res} m_e c^2$. We then expect the voltage to grow, giving a higher spallation rate of the crust. We leave this regime for a future study.

---

[10] Protons have a binding energy E_I of a few keV and are easily sublimated at the temperature $k_{\rm B}T \sim 0.5$ keV, in contrast to the heavy elements that are locked in molecular chains with $E_I \sim 10^2$ keV.

[11] The relatively low density of the atmosphere implies two differences with the cascade in the crust: (1) The polarization states of photons are now linear — vaccuum O- and E-modes – and the E-mode does not convert to $e^{\pm}$ off the field. (2) Splitting of E-mode occurs faster than photon-ion interaction. This leaves only one branch for the cascade, with $e^{\pm}$ production off the magnetic field.

The thickness of the plasma layer that is accumulated near the cathode surface is limited by burning processes and diffusion to greater depths (Chang et al. 2004).

8. DISCUSSION

The basic finding of this paper is that an $e^{\pm}$ corona must be maintained around a magnetar. It exists in a state of self-organized criticality, near the threshold for $e^{\pm}$ breakdown. The stochastic $e^{\pm}$ discharge continually replenishes the coronal plasma, which is lost on the dynamic time $t_{\rm dyn} \sim 10^{-4}$ s.

The solution for the plasma dynamics in the corona is strongly non-linear and time-dependent. It is essentially global in the sense that the plasma behavior near one footpoint of a magnetospheric field line is coupled to the behavior near the other footpoint. Remarkably, this complicated global behavior may be described as essentially one-dimensional electric circuit that is subject to simple boundary conditions $E \approx 0$ on the surface of the star and can be studied using a direct numerical experiment.

The established voltage across the entire magnetospheric circuit is marginally sufficient to accelerate an electron (or positron) to the energy where collisions with ambient X-ray photons spawn new pairs. This physical condition determines the rate of energy dissipation in the corona. The voltage is maintained by small deviations from charge neutrality in the coronal plasma as required by Gauss' law. The generation of this voltage is precisely the self-induction effect of the gradually decaying magnetic twist, and the energy release in the corona is fed by the magnetic energy of the twisted field.

8.1. Comparison With Canonical Radio Pulsars

Canonical radio pulsars are usually assumed to have a magnetosphere that is almost everywhere potential, $\nabla\times\mathbf{B} = 0$, except for narrow bundles of open field lines that connect the polar caps of the star to its light cylinder. The plasma content of the magnetosphere then depends on its rotation: the charge density $\rho_{\rm co} = -\mathbf{\Omega}\cdot\mathbf{B}/2\pi c$ must be maintained to screen the electric field induced by rotation (Goldreich & Julian 1969). In this picture, the persistent current of a canonical pulsar only flows along the open field lines out to the light cylinder. The sign of this current $I_{\rm open}$ is determined by the corotation charge density. The closure of the electric circuit back to the star remains poorly understood.

Previous studies of plasma near neutron stars focused on open magnetic lines. It was shown that pair discharge can be sparked near the polar cap (Ruderman & Sutherland 1975; Arons & Scharlemann 1979; Muslimov & Tsygan 1992), and the created pairs carry the current $I_{\rm open}$ toward the light cylinder. Recent calculations of the discharge (Harding & Muslimov 2002) employ an approximate analytic prescription for the decay of the electric field with distance from the star. (Self-consistent calculations of the electric field and pair creation are now available for the outer gap, see Takata et al. 2006.) The global dynamics of the plasma on open magnetic lines is poorly understood because of the complicated behavior at the light cylinder, so only one boundary condition is known — at the polar cap.

The solution presented in this paper applies to currents along *closed* magnetic lines of the inner magnetosphere. In this case, it is easier to find the global solution for the plasma dynamics because both boundary conditions are defined at the two footpoints of the magnetic lines. This problem has important applications to the magnetar physics for two reasons: (1) The observed radiative output is generated in the closed magnetosphere — the dissipation rate on the open field lines is orders of magnitude smaller and cannot explain the observed emission. (2) A current is naturally created on closed magnetic lines because they are twisted by the starquakes of magnetars, and our solution shows that such twists have a long lifetime.

One may compare the twist of open magnetic lines at the polar cap, as sustained by the rotation of the star, $B_\phi/B_P \sim (R_{\rm NS}/R_{\rm lc})^3$, with the twist that can be created in the closed magnetosphere by the starquakes. Consider a current I flowing along a magnetic flux tube of radius a and let B_ϕ be the twisted component of the field. Then

$$I = \frac{c}{2} a B_\phi = \frac{c}{2} a^2 B_P \frac{\mathrm{d}\phi}{\mathrm{d}l}, \qquad (75)$$

where l is the length measured along the tube. Since the current I and the poloidal magnetic flux $\pi a^2 B_P$ are constants along the tube, the twist angle ϕ satisfies $\mathrm{d}\phi/\mathrm{d}l = const$. Hence,

$$\frac{\mathrm{d}\phi}{\mathrm{d}l} \sim \frac{\Delta\phi}{R_{\rm max}}, \qquad (76)$$

where $R_{\rm max}$ is the maximum radius to which the tube extends and $\Delta\phi$ is the net twist angle integrated along the tube. The net twist angle is limited by the global stability of magnetosphere to $\Delta\phi \lesssim 1$. On the star's surface one then finds $B_\phi/B_P = a\mathrm{d}\phi/\mathrm{d}l \lesssim a/R_{\rm max}$. This implies that the closed field lines with $R_{\rm max} \sim 2R_{\rm NS}$ and $a \sim R_{\rm NS}$ can bear much stronger twists than the open lines.

Note also one more differrence of the magnetar currents: they impact the stellar surface with a modest Lorentz factor $\gamma_b \sim 10^3$. Such a beam can deposit its energy in an optically thin atmospheric layer through a plasma instability (§ 6.1). By contrast, $e^\pm$ from the discharge in an ordinary radio pulsar impact the star with high $\gamma_b = 10^6 - 10^7$, which suppresses the beam instability in the atmosphere: its length scale l_b is proportional to γ_b (eq. 46) and becomes much larger than the atmosphere scale-height. Such a beam must be stopped by Coulomb collisions and relativistic bremsstrahlung in the solid crust. Therefore, the polar cap of an ordinary pulsar is expected to release the beam energy in the form of blackbody radiation, in agreement with observations (e.g. De Luca et al. 2005). By contrast, magnetars may have a strongly overheated hydrostatic atmosphere, with $k_{\rm B}T > 100$ keV (§ 6.2).

8.2. Comparison with Solar Corona

The corona of a magnetar may be viewed as a collection of closed current-carrying flux tubes with footpoints anchored in a relatively cold stellar surface. As in the Solar corona, a current is created by the twisting motions of the footpoints. Another similarity with the Solar corona is the important interaction of the coronal plasma with a dense atmospheric layer on the stellar surface where the plasma becomes collisional and can efficiently radiate the energy flux received from the corona.

However, the magnetar corona is distinguished from the Solar corona in a few important respects. The differences in the behavior of the magnetic field are as follows.

1. The footpoints of magnetic lines of the Solar corona are constantly pushed and twisted because the outer envelope of the Sun is convective and in constant motion. In addition, magnetic flux tubes are observed to emerge from the Solar convection zone with a twist already implanted in them. By contrast, the neutron star's rigid crust is subject only to rare and sporadic yielding events (starquakes). Because the crust is stably stratified, the transfer of a toroidal magnetic field to the exterior occurs through a differential rotation of the crustal material along the gravitational equipotential surfaces.

2. The magnetic twists have long lifetimes between starquakes, and their evolution differs from the evolution of twists in the Solar corona. Once a current $\mathbf{j} = (c/4\pi)\nabla \times \mathbf{B}$ is created in the magnetosphere of a neutron star, it lives a long time because the net current $I \sim R_{\rm NS}^2 j$ is enormous and maintained by its self-induction. The gradual decay of the current induces an e.m.f. along the magnetic field lines, which forces the plasma and electric field to self-organize into a quasi-steady electric circuit. The ease with which charges can be supplied by $e^{\pm}$ production when the induced voltage exceeds $e\Phi_e \sim 1$ GeV implies a "bottleneck" for the decay of the twist (§§ 2 and 5).

3. The evolution of the magnetic field between the starquakes involves a gradual release of the twist energy through Joule dissipation and spreading of the twist toward the magnetic polar axis. The latter process causes a gradual flaring of the poloidal field lines. Explosive magnetic reconnection similar to Solar flares is likely to be triggered by starquakes, but not during the following slow-dissipation stage.

4. The external magnetic field of a magnetar is likely to have less small-scale structure compared with the Solar corona. The small-scale braiding of magnetic lines followed by reconnection and dissipation is one of the possible heating mechanisms for the Solar corona (Parker 1979). Precisely what creates this structure is unclear: it could be driven by the hydrodynamic turbulence that is excited at the top of the Solar convection zone or by the Taylor relaxation of a helical magnetic field (e.g. Diamond & Malkov 2003). In magnetars, the small-scale structure of magnetic field can be expected to dissipate quickly after the starquakes if it is created in these events. The dissipation timescale is longest for the large-scale twists expected from large-scale motions of the crust. Indirect evidence that small-scale instabilities are less important comes from the observed distribution of

energies of SGR bursts: the cumulative energy in bursts $E^2 dN/dE \sim E^{0.4}$ is weighted toward the largest events (Cheng et al. 1996; Gogus et al. 2001). By contrast, several recent measurements of the distribution of Solar flare energies suggest a power-law $dN/dE = E^k$ with $k < -2$, and are therefore consistent with the basic picture of coronal heating by 'nano-flares' (Walsh & Ireland 2003).

Let us also note a few differences in the plasma behavior.

5. The rapid cooling of the transverse motion of charged particles in the ultra-strong magnetic field of magnetars makes the particle distribution functions one-dimensional. This reduces the number of relevant plasma modes in the corona.

6. The coronal plasma of magnetars is continually lost to the surface and re-generated. By contrast, the Solar corona is in hydrostatic equilibrium. Its density n is much higher than the minimum needed to maintain the current, and the mean drift speed j/en of the coronal currents is much below the electron and ion thermal speeds. So, the *mean* current does not experience a strong anomalous resistivity. Strong plasma turbulence is expected in localized current sheets and can develop explosively, giving rise to the Solar flares. In the magnetar corona, a strong turbulence is maintained routinely, everywhere where current flows. The very mechanism of the current supply involves a strongly non-linear phenomenon — $e^\pm$ discharge.

7. The magnetar corona is dominated by relativistic $e^\pm$ pairs. As indicated by our numerical experiments, ions lifted from the surface contribute a modest fraction, perhaps $\sim 10\%$, to the charge flow.

8.3. Magnetospheric Circuit as a Double-layer Problem

From the plasma physics point of view, there is an interesting connection between the magnetospheric circuit and the double-layer problem that was first studied by Langmuir (1929) and later by many authors (for reviews see Radau 1989; Block 1978). The magnetospheric current flows along a magnetic tube with footpoints on a cold conductor and is subject to the boundary condition $E \simeq 0$ at the footpoints. We argued that the tube curvature is not essential to understanding many features of the circuit, and studied the charge flow in a straight tube where gravity is replaced by a force $m\mathbf{g}$ that attracts plasma to the anode and cathode boundaries. The longitudinal electric field must develop between the two boundaries because of gravity. This is a significant difference from the normally invoked mechanisms for double-layer formation (such as current-driven instability). In our case, gravity traps the thermal particles at the magnetic footpoints and impedes the flow of the current that is required by the self-induction of the twisted magnetic field.

Thus, perfect conditions for double-layer formation are created. And indeed, our numerical experiment showed the formation of a huge relativistic double layer between the footpoints, of size $L \sim R_{\rm NS}$. This result is obtained if the current can be maintained only by particles lifted from the anode and cathode surfaces. It could have dramatic consequences for the magnetar physics because of the huge dissipation rate in the double layer: the energy of magnetic twist would be quickly released in a powerful burst.

However, there is one more ingredient in the problem, which again makes the magnetar circuit different from the previously studied double layers: new charges ($e^{\pm}$) can be created by accelerated particles in the tube. This process qualitatively changes the problem because voltage is now limited by $e^{\pm}$ discharge (§ 5). As a result, the circuit enters the new state of self-organized criticality where voltage repeatedly builds up and is screened by the $e^{\pm}$ creation. This allows the current to flow and maintain the required $\nabla \times \mathbf{B}$.

8.4. Observational Implications

Two important observational implications of the magnetospheric twist were already pointed out by TLK, based on the force-free model of a twisted dipole:

1. The poloidal field lines are inflated compared with a pure dipole, so that a larger magnetic flux connects the star to its light cylinder $R_{\rm lc}$. This implies a higher spin-down torque. Thus, the twisting leads to a higher spindown rate $\dot{P}$.

2. The minimum particle density needed to maintain the currents, $n_c = j/ec$, is high enough to make the magnetosphere semi-opaque. The main source of opacity is resonant cyclotron scattering. If the magnetic field lines are twisted, then the optical depth to scattering happens to be $\sim n/n_c$ (independent of r, B, and nature of the flowing charges). Scattering by the magnetospheric charges must modify the X-ray spectrum and pulse profile.

TLK also pointed out that if the magnetospheric current is carried by ions and electrons lifted from the stellar surface by a minimum voltage $e\Phi_e \sim g m_p R_{\rm NS}$, then one expects a dissipation rate comparable to the observed persistent luminosity of magnetars.

Further implications of our model for the coronal electric circuit are as follows.

3. The density of the plasma corona is found to be close to its minimum $n_c = j/ec$ as conjectured by TLK. It is largely made of $e^{\pm}$ pairs rather than electron-ion plasma. This suggests that the optical depth of the corona is determined mostly by the cyclotron resonance of $e^{\pm}$. All species of particles (e^-, e^+, and even ions) flow with relativistic bulk speeds and large temperatures $\sim e\Phi_e$. The cyclotron resonance is very broad, which will have important implications for radiative transfer through the corona. Note, however, that our calculations focused on small radii $r \sim R_{\rm NS}$ where most of the energy release occurs. At larger radii $r \sim (10-20) R_{\rm NS}$, where electron cyclotron energy is in the keV range, $e^{\pm}$ feel a strong radiative drag force and can decelerate to a small velocity. We defer a detailed analysis of this part of the corona to another paper.

4. The voltage $e\Phi_e \simeq \gamma_{\rm res} m_e c^2 \sim 1$ GeV along the twisted magnetic lines of the corona is regulated

by the threshold for $e^{\pm}$ discharge, and its exact value depends on B and the spectrum of target photons involved in $e^{\pm}$ creation, especially on its high-energy tail at $10 - 300$ keV (§ 5). By coincidence, the mean electric field developed along the magnetic lines, $E \sim \Phi_e/R_{\rm NS}$, is marginally sufficient to lift ions from the anode footpoint. Therefore, in addition to $e^{\pm}$ pairs, some ions are present in the corona. Their abundance depends on the exact Φ_e and is about 10% for $e\Phi_e = 1$ GeV (see Fig. 10). The coronal ions may produce interesting features in the magnetar spectrum and likely to play a key role in the low-frequency emission (§ 8.4.2).

5. The rate of energy dissipation in the twisted magnetosphere is given by $L_{\rm diss} = I\Phi_e$ where I is the net current through the corona. The current may be estimated as

$$I \sim j_B a^2 \sim \frac{c}{4\pi}\,\Delta\phi\,\frac{B}{R_{\rm NS}}\,a^2, \tag{77}$$

where a is the size of a twisted region on the stellar surface and $\Delta\phi = |\nabla \times \mathbf{B}|(B/R_{\rm NS})^{-1} \lesssim 1$ characterizes the strength of the twist. The calculated $e\Phi_e$ is comparable to 1 GeV and implies

$$L_{\rm diss} = I\Phi_e \sim 10^{37}\,\Delta\phi\left(\frac{B}{10^{15}\text{ G}}\right)\left(\frac{a}{R_{\rm NS}}\right)^2\left(\frac{e\Phi_e}{\rm GeV}\right)\text{ erg s}^{-1}. \tag{78}$$

The observed luminosity $L_{\rm diss} \sim 10^{36}$ erg s^{-1} is consistent with a partially twisted magnetosphere, $a \sim 0.3R_{\rm NS}$, or a global moderate twist with $\Delta\phi\,(e\Phi_e/{\rm GeV}) \sim 0.1$. (Larger dissipation rates and larger twists are not yet excluded by the data: e.g. the output at 1 MeV is presently unknown.) More precise formulae may be obtained for concrete magnetic configurations. In the simplest case of a twisted dipole (TLK), one can use equation (1) and find I by integrating $\mathbf{j}\cdot d\mathbf{S}$ over one hemisphere of the star. This gives $I = \frac{1}{8}\,\Delta\phi c B_{\rm pole} R_{\rm NS}$ and $L_{\rm diss} = 1.2 \times 10^{37}\Delta\phi B_{\rm pole,15} R_{\rm NS,6}\Phi_{e,\rm GeV}$.

6. Once created, a magnetospheric twist has a relatively long but finite lifetime. The energy stored in it is $\mathcal{E}_{\rm twist} \sim (I^2/c^2)R_{\rm NS}$. This energy dissipates in a time

$$t_{\rm decay} = \frac{\mathcal{E}_{\rm twist}}{L_{\rm diss}} \simeq \frac{IR_{\rm NS}}{c^2\Phi_e} = \frac{R_{\rm NS}}{c^2}\frac{L_{\rm diss}}{\Phi_e^2} \simeq 3\left(\frac{L_{\rm diss}}{10^{36}\text{ erg s}^{-1}}\right)\left(\frac{e\Phi_e}{\rm GeV}\right)^{-2}\text{ yr}. \tag{79}$$

The exact numerical coefficient in this equation again depends on the concrete magnetic configuration. For example, the energy stored in the global twist of a dipole is $\mathcal{E}_{\rm twist} = 0.17(\Delta\phi)^2 E_{\rm dipole}$ (TLK), where $E_{\rm dipole} = \frac{1}{12}\,B_{\rm pole}^2 R_{\rm NS}^3$ is the energy of a normal dipole. In this case, one finds $t_{\rm decay} = 0.8\,(R_{\rm NS}/c^2)\,L_{\rm diss}/\Phi_e^2$.

The characteristic timescale of decay is determined by voltage Φ_e and the corona luminosity $L_{\rm diss}$. Note that a stronger twist (brighter corona) lives longer. Given a measured luminosity and its decay time, one may infer Φ_e and compare it with the theoretically expected value. Since Φ_e does not change as the twist decays in our model, one can solve equation (79) for $\mathcal{E}_{\rm twist}(t)$ and $L_{\rm diss}(t) = -{\rm d}\mathcal{E}_{\rm twist}/{\rm d}t$. This gives

$$L_{\rm diss}(t) = 5 \times 10^{35}\left(\frac{e\Phi_e}{\rm GeV}\right)^{-2}(t_0 - t)\text{ erg s}^{-1}, \tag{80}$$

where time t is expressed in years. The final decay of the twist should occur at a well-defined time $t_0 = t + t_{\rm decay}$. The finite time of decay implies that the emission called "persistent" in this paper is not, strictly speaking, persistent. If the time between large-scale starquakes is longer than $t_{\rm decay}$, the magnetar should be seen to enter a quiescent state and the observed luminosity should then be dominated by the surface blackbody emission.

7. The voltage Φ_e implies a certain effective resistivity of the corona, $\mathcal{R} = \Phi_e/I$. This resistivity leads to spreading of the electric current *across* the magnetic lines. Equivalently, the magnetic helicity is redistributed within the magnetosphere. This spreading is described by the induction equation $\partial\,\mathbf{B}/\partial t = -c\nabla\times\mathbf{E}$. The magnitude of $\nabla\times\mathbf{E}$ depends on the gradient of $E_\parallel$ transverse to the twisted magnetic field lines. Our model of the magnetospheric voltage implies that Φ_e has a gradient on a lengthscale $\sim R_{\rm NS}$, so that $\partial B_{\rm twist}/\partial t \sim cE_\parallel/R_{\rm NS}$. The characteristic spreading time of the twist $B_{\rm twist} = \Delta\phi\, B\,(a/R_{\rm NS})$ is $t_{\rm spread} \sim B_{\rm twist}\,(\partial B_{\rm twist}/\partial t)^{-1}$ and can be roughly estimated as

$$t_{\rm spread} \sim \frac{\Delta\phi\, B}{E_\parallel}\,\frac{R_{\rm NS}}{c}\,\left(\frac{a}{R_{\rm NS}}\right) \sim 300\,\Delta\phi\,\left(\frac{B}{10^{15}\ {\rm G}}\right)\left(\frac{e\Phi_e}{\rm GeV}\right)^{-1}\left(\frac{a}{R_{\rm NS}}\right)\ {\rm yr}. \tag{81}$$

If a twisting event happens near the magnetic equator, it initially does not affect the extended magnetic lines with $R_{\rm max} \sim R_{\rm lc}$. Its impact on spindown may appear with a delay as long as $t_{\rm spread}$. Although the exact numerical coefficient in equation (81) is unknown, the rough estimate suggests a timescale that is comparable to the decay time (eq. [79]). Their ratio is $\propto (a/R_{\rm NS})^{-1}$ and depends sensitively on geometrical factors. It is possible that starquakes occurring far from the poles will have little effect on the spindown.

8. Even a small ion current implies a large transfer of mass through the magnetosphere over the $\sim 10^4$-yr active lifetime of a magnetar. Essentially all hydrogen and helium that could be stored in the upper crust is rapidly transferred from the anode surface to the cathode surface, thereby exposing heavier elements (e.g. carbon) that are strongly bound in molecular chains. A continuing flux of protons can, nonetheless, be maintained in the circuit. The bombarding relativistic electrons from the corona cause the gradual disruption of ions just below the solid surface. They trigger a cascade of $e^\pm$ pairs and gamma-rays that knock out nucleons and occasionally α-particles from the heavier nuclei. This process re-generates the light-element atmosphere on the surface and regulates its column density (§ 7). As a result, the Thomson depth of the atmosphere equilibrates to a value ~ 100. The chemical composition of the upper crust (carbon or heavier elements) and its light-element atmosphere affect radiative transfer and the emerging spectrum of the star's radiation (e.g. Zavlin & Pavlov 2002).

9. Our study of the transition layer between the corona and the star (§ 6) suggests that the energy dissipated in the corona is radiated below it in two forms (see also Thompson & Beloborodov 2005). First, the high-energy radiation with a hard spectrum possibly extending up to ~ 1 MeV; this radiation is caused by collisionless dissipation of the coronal beam in the transition layer. Second, a blackbody radiation component that is caused by thermalization of the remaining energy of the beam when it enters the dense atmosphere and then the crust; two-body collisions and

development of an $e^{\pm}$ cascade are responsible for this thermalization. A crude estimate gives comparable luminosities in the high-energy and blackbody components. Further investigation of the transition layer may show that the collisionless dissipation is more efficient. This would be in a better agreement with observations of SGR 1806-20 whose high-energy component was found more luminous than the blackbody component (Mereghetti et al. 2005; Molkov et al. 2005).

8.5. Emission from the Magnetar Corona

8.5.1. Hard X-ray Emission

The radiative output from the corona is observed to peak above 100 keV (Kuiper, Hermsen & Mendez 2004; Mereghetti et al. 2005; Molkov et al. 2005; den Hartog et al. 2006). It is likely fed by the inner parts of the corona: in the model investigated in this paper, one expects that the bulk of the coronal current is concentrated fairly close to the star, at radii $\lesssim 2R_{\rm NS}$. Currents in the outer region $r \gg R_{\rm NS}$ (even if it is strongly twisted) flow through a small polar cap on the star and therefore are small (§ 8.1).

Emission from the inner corona must be suppressed above ~ 1 MeV, regardless the mechanism of emission, because photons with energy $\gtrsim 1$ MeV cannot escape the ultra-strong magnetic field. There are two possible linear polarizations of photons in the corona: E-mode (electric vector perpendicular to $\mathbf{B}$) and O-mode (electric vector has a component along $\mathbf{B}$). An energetic E-mode photon cannot escape because it splits into two photons. An O-mode photon propagating at angle θ with respect to $\mathbf{B}$ cannot escape when its energy $E_\gamma > 2m_ec^2/\sin\theta$ because it converts to a pair. Therefore, the spectrum escaping the inner corona is limited to ~ 1 MeV. The available data show that the high-energy radiation extends above 100 keV. There is an indication for a cutoff between 200 keV and 1 MeV from COMPTEL upper limits for AXP 4U 0142+61 (den Hartog et al. 2006).

The possible mechanisms of emission are strongly constrained. The corona has a low density $n \sim n_c = j_B/ec \lesssim B(4\pi\, eR_{\rm NS})^{-1} \sim 10^{17}B_{15}$ cm^{-3} and particle collisions are rare, so two-body radiative processes are negligible. The only available emission process in the corona is upscattering of surface X-rays. The scattering can occur resonantly (excitation to the first Landau level followed by de-excitation) or non-resonantly (Compton scattering). The scattering, however, cannot explain the observed 100-keV emission:

1. *Resonant upscattering by electrons (or positrons)* with Lorentz factor γ_e gives high-energy photons with energy $\sim \gamma_e\hbar eB/m_ec \gg 1$ MeV (§ 5.1), which cannot escape. They either split (if E-mode) or convert to pairs (if O-mode). Splitting may give escaping photons below 1 MeV, but their number is not sufficient to explain the observed emission. The voltage along the magnetic lines adjusts so that the coronal particles experience ~ 1 resonant scattering before they are lost to the surface, while the observed emission requires the production of $10^3 - 10^4$ 100-keV photons

per particle.

2. *Resonant upscattering by ions* with Lorentz factors γ_i gives photons of energy $\gamma_i eB/m_p c$, which is too low to explain the 100-keV emission (ions are mildly relativistic in the circuit with $\sim$ GeV voltage, $\gamma_i \sim 1$).

3. *Non-resonant Compton scattering* is negligible for E-mode photons. The cross section of O-mode scattering by electron with Lorentz factor γ_e is $\sim \sigma_T/\gamma_e^2$.[12] This may be seen by transforming the photon to the rest frame of the electron. Then the photon propagates at angle $\sin\theta' \sim 1/\gamma_e$ with respect to the magnetic field and its electric vector is nearly perpendicular to $\mathbf{B}$. Viewing it as a classical wave that shakes the 1D electron, one finds the cross section of scattering $\sigma = \sigma_T \sin^2\theta' = \sigma_T/\gamma_e^2$. The corresponding optical depth of the corona is $\tau = n_c R_{NS}\sigma = \tau_c/\gamma_e^2$. The upscattered photon is boosted in energy by γ_e^2 and the net Compton amplification factor of O-mode radiation passing through the corona is $\tau\gamma_e^2 = \tau_c$, i.e. does not depend on γ_e. Since $\tau_c = \sigma_T R_{NS} n_c$ is small, $\sim 0.1 - 0.01$, one concludes that the energy losses of the corona through non-resonant Compton scattering are a small fraction of the surface O-mode luminosity.

A possible source of observed $20 - 100$ keV emission is the transition layer between the corona and the thermal photosphere (see Thompson & Beloborodov 2005 and § 6). This layer can radiate away (through bremsstrahlung) a significant fraction of the energy received from the corona. Its temperature is $k_B T \sim 100(\ell/\ell_{Coul})^{-2/5}$ keV (eq. [56]), where $\ell/\ell_{Coul} < 1$ parameterizes the suppression of thermal conductivity by plasma turbulence. This suppression is likely to be significant and increase the temperature of the layer. The emitted hard X-ray spectrum may be approximated as single-temperature optically thin bremsstrahlung (Thompson & Beloborodov 2005). Its photon index below the exponential cutoff is close to -1, in agreement with magnetar spectra observed with INTEGRAL and RXTE.

The observed pulsed fraction increases toward the high-energy end of the spectrum and approaches 100% at 100 keV (Kuiper et al. 2004). If the hard X-rays are produced by one or two twisted spots on the stellar surface, the large pulsed fraction implies that the spots almost disappear during some phase of rotation. Then they should not be too far from each other and, in particular, cannot be antipodal because a large fraction of the stellar surface is visible to observer due to the gravitational bending of light: $S_{vis}/4\pi R_{NS}^2 = (2 - 4GM/c^2 R_{NS})^{-1} \approx 3/4$ (Beloborodov 2002). The decreasing pulsed fraction at smaller energies may be explained by contamination of the strongly pulsating component by another less pulsed and softer component of the magnetospheric emission (see § 8.4.2).

Hard X-ray emission may also be produced at about 100 km above the star surface (Thompson & Beloborodov 2005). The magnetic field is about 10^{11} G in this region, and the electrons can experience a significant radiative drag as a result of resonant cyclotron scattering. They cannot close

---

[12]This assumes Thomson regime of scattering, $\gamma_e \hbar\omega \ll m_e c^2$. At larger energies, the electron recoil becomes important (Klein-Nishina regime) and the cross section is reduced.

the circuit unless an additional electric field develops that helps them flow back to the star against the radiative pressure. Then some positrons in this region can undergo a runaway acceleration and Compton scatter keV photons to a characteristic energy $E_\gamma \simeq (3\pi/8)\alpha^{-1} m_e c^2$, where $\alpha = \frac{1}{137}$ is the fine structure constant. Such a photon is immediately converted to an $e^\pm$ pair in the magnetic field, and the created pairs emit a synchrotron spectrum consistent with the observed 20-100 keV emission.

8.5.2. 2-10 keV Emission

A promising emission mechanism for the observed soft X-ray tail of the blackbody component is resonant upscattering of keV photons in the corona (TLK). The emergent soft X-ray spectrum and pulse profile is likely to form at radii where $B \sim 10^{11}$ G and the $e^\pm$ can be decelerated to mildly relativistic speeds by the resonance with keV photons.

Ions flowing through the inner magnetosphere can also upscatter the keV photons. The ions are mildly relativistic and their cyclotron resonance near the star is $6B_{15}$ keV — just in the $2-10$ keV band. On the other hand, the ion current may be suppressed (see Fig. 10), which would imply their small optical depth in the corona, except the first $10^3 - 10^5$ seconds following an SGR flare when many ions are lifted to the magnetosphere (Ibrahim et al. 2001).

8.5.3. Optical and Infrared Emission

The observed infrared (K-band) and optical luminosities of magnetars are $\sim 10^{32}$ erg/s (Hulleman et al. 2004), which is far above the Rayleigh-Jeans tail of the surface blackbody radiation. The inferred brightness temperature is $\sim 10^{13}$ K if the radiation is emitted from the surface of the star. Four principle emission mechanisms may then be considered.

1. Coherent plasma emission. Eichler, Gedalin, & Lyubarsky (2002) proposed that the optical emission is generated as O-mode radiation at a frequency $\sim \omega_{Pe}$. We find that this mechanism gives too low a frequency of emission. The plasma frequency in the corona is suppressed by the large relativistic dispersion of the $e^\pm$, $\omega_{Pe} \sim (4\pi n_c e^2/m_e\gamma_e)^{1/2}$; in addition, it may not be blueshifted by bulk relativistic motion as suggested by pulsar models. A fraction of $\sim \omega_{Pe}$ photons may, however, be upscattered to the optical or higher bands by the coronal $e^\pm$ that have a broad distribution $1 < \gamma_e \lesssim 10^3$.

The plasma frequency is higher in the hydrostatic atmosphere, where the density is higher. For a hydrostatic layer of temperature T_e and Thomson depth τ_T one finds $\hbar\omega_{Pe} = 0.65\,(\tau_{\rm T} m_e c^2/kT_e)^{1/2}\, g_{14}^{1/2}$ eV. In this case, however, the brightness temperature of the O-mode photons is limited to a value $k_{\rm B}T_b \sim m_e c^2/\tau_T$ by induced downscattering in the atmosphere. The corresponding upper limit for K-band luminosity, $\omega L_\omega = (k_{\rm B}T_b\,\omega^3/8\pi^2c^2)\,4\pi R_{\rm NS}^2 \lesssim 10^{29}\,\tau_{\rm T}^{-1}\,(\omega/\omega_{\rm K-band})^3$ erg s^{-1}, is in conflict with observations.

2. Non-thermal synchrotron emission from electrons with high γ_e. This mechanism could work only far from the star, $r \gtrsim 200 R_{\rm NS}\gamma_e^{2/3}$, where the minimum energy of the synchrotron photons, $\sim \gamma_e^2 \hbar eB/m_e c$, is below the optical band ($B < 10^8 \gamma_e^{-2}$ G). The magnetic lines extending to large r form a small cap on the stellar surface and carry a tiny fraction of the total magnetospheric current, $f \sim (r/R_{\rm NS})^{-2} \sim 3\times 10^{-5}\gamma_e^{-4/3}$. If the voltage maintained along the extended lines is comparable to 1 GeV, energy dissipation rate in the region is only $10^{30}\gamma_e^{-4/3}$ erg s^{-1}, orders of magnitude smaller than the observed optical-IR luminosity. Therefore this mechanism appears to be unlikely.

3. Ion cyclotron emission from radii $\sim 20 R_{\rm NS}$, where the ion cyclotron frequency is in the optical band. The observed flux then implies ion temperatures of $\sim 10^{11}$ K. Such temperatures are indeed achieved in the corona. This mechanism also requires a sufficient number of ions in the corona, which is sensitive to the ratio of voltage $e\Phi_e$ to the ion gravitational energy (Fig. 10). The ions will act as a filter for the radio and microwave radiation that is emitted by coherent processes near the star. The radiation reaching $r \gtrsim 500$ km will be partially absorbed by the ions at their cyclotron resonance, pumping their perpendicular energy $E_\perp$. This energy further increases as the ions approach the star since $E_\perp/B$ is an adiabatic invariant. Their cyclotron cooling and transit times become comparable at a radius $r_* \sim\ 200\,(v_i/c)^{-1/5}\,R_{\rm NS,6}^{6/5}\,B_{\rm pole,15}^{2/5}$ km. Then the ions emit cyclotron radiation in the optical-IR range, since $\hbar eB(r_*)/m_p c \approx B_{\rm pole,15}^{-1/5}(v_i/c)^{3/5}R_{\rm NS,6}^{-3/5}$ eV.

4. Curvature emission by pairs in the inner magnetosphere may extend into the optical-IR range. Charges moving on field lines with a curvature radius $R_C \lesssim R_{\rm NS}$ will emit radiation with frequency $\nu_C \sim \gamma_e^3 c/2\pi R_C$, which is in the K-band ($\nu = 10^{14}$ Hz) or optical when $\gamma_e m_e c^2 \gtrsim$ GeV. As in models of pulsar radio emission, bunching of the radiating charges is required to produce the observed luminosity (e.g. Asseo, Pelletier, & Sol 1990). The radio luminosity of a normal pulsar can approach $\sim 10^{-2}$ of its spindown power, and it is not implausible that the observed fraction $\sim 10^{-4}$ of the power dissipated in a magnetar corona is radiated in optical-IR photons by the same coherent mechanism.

There are indications of charge bunching on the Debye scale in our numerical experiment, although this detail of the experiment is difficult to scale to the real corona of magnetars. Suppose a fraction f of the net flow of particles through the corona $\dot{N}_e = I/e \sim 10^{39} L_{\rm diss\,36}\,(e\Phi_e/{\rm GeV})^{-1}$ s^{-1} is carried by bunches of $\mathcal{N}$ electrons (or positrons). The power emitted by one bunch is $\dot{E} = (2/3)(\mathcal{N}e)^2\gamma_e^4 c/R_C^2$, and the total coherent luminosity produced by the corona is given by $L \approx f\mathcal{N}\dot{N}_e\,\gamma_e^4\,e^2/R_C$. Using the relation $\nu_C \sim (c/2\pi R_C)\,\gamma_e^3$ for curvature radiation, we find the number of charges per bunch that is required to explain the observed luminosity $L \sim 10^{32}$ erg s^{-1},

$$\mathcal{N} \sim 10^4\, f^{-1}\, L_{32} \nu_{C,14}^{-4/3}. \tag{82}$$

This is much smaller then the number of charges per Debye sphere, $\mathcal{N}_{\rm D} \sim (n_c r_e^3)^{-1/2} \sim 10^{11}$. Thus, a very weak bunching of charges (or very small bunches, with a scale $\sim 10^{-2}\lambda_{De}$) can generate a significant power in coherent curvature radiation. The required bunching is small compared with what is commonly invoked to explain the emission of radio pulsars.

For example, one can compare with the Crab pulsar. The total flux of $e^{\pm}$ pairs from the pulsar, $\dot{N}_e \sim 10^{39}$ s^{-1}, is comparable to the flux in a magnetar corona. The pulsar $e^{\pm}$ flow is concentrated on the open field lines, and its density is enhanced by a factor $R_{\rm lc}/R_{\rm NS} \sim 10^2$. The curvature radius of the open field lines near the star is $R_C \sim 10 R_{\rm NS}$. These differences are, however, modest compared with the much larger bunching efficiency that is implied by the observed brightness of the radio emission from the Crab pulsar. Supplying its luminosity $L \sim 10^{31}$ erg s^{-1} at $\nu \sim 10^8$ Hz would require $\gamma_e \sim 60$ and $\mathcal{N} \sim 10^{11} f^{-1}$.

The dispersion relation for the IR-optical radiation in the corona is dominated by plasma rather than by vacuum polarization. The curvature radiation is, generally, a superposition of all possible polarization modes (see Arons & Barnard 1986 for a description of the normal modes of a strongly magnetized plasma). Emission of the superluminal O-mode will occur if the bunch size (measured in its rest frame) is smaller than the plasma skin depth. The E-mode also comprises a fraction of the curvature emission when the magnetic field lines are twisted (Luo & Melrose 1995). Curvature emission in the subluminal Alfvén mode is also possible, but this mode is ducted along the magnetic field lines and has a frequency below the ambient plasma frequency.

The spectrum of curvature emission is expected to cut off at frequencies above ν_C that corresponds to the maximum Lorentz factor (a few $\gamma_{\rm res}$) of $e^{\pm}$ in the corona. This cutoff may be observable in the optical or infrared band (cf. Hulleman et al. 2004). Note also that the K-band brightness temperature inferred from observations of AXPs is remarkably close to the effective temperature of the coronal $e^{\pm}$, $T_{\rm eff} \sim \gamma_e m_e c^2/k_{\rm B}$, which is bounded by $\sim 10^{13}$ K by the pair creation process.

8.6. Evolution Following Bursts of Activity

Bursts of magnetar activity are associated with starquakes — sudden crust deformations that release the internal magnetic helicity of the star and impart an additional twist to the magnetosphere. The increase of the twist should lead to a larger luminosity from the corona since the luminosity is simply proportional to the net current flowing through the magnetosphere. Between bursts, the magnetospheric currents persistently dissipate and the corona disappears after the time $t_{\rm decay}$ (eqs. [79] and [80]). If there were no bursts during a long time $t > t_{\rm decay}$ the magnetar should enter the quiescent state with no coronal emission. Such behavior has been observed in AXP J1810-197 (Gotthelf & Halpern 2005). An outburst, which occured between November 2002 and January 2003, was followed by the gradual decay of soft X-ray emission on a time-scale of a few years, and now the source is returning to the quiesent state. It would be especially interesting to observe the evolution of the hard X-ray component, which is not detected in the relatively weak AXP J1810-197.

During periods of high activity, when bursts occur frequently, the growth of the magnetospheric twist may be faster than its decay. The twist may grow to the point of a global instability. When the magnetic lines achieve $\Delta\phi \gtrsim 1$ the magnetosphere becomes unstable and relaxes to a smaller twist angle. A huge release of energy must then occur, producing a giant flare; a model of how this can happen is dicussed by Lyutikov (2006). It is possible that the 27 December 2004 giant flare from SGR 1806-20 was produced in this way — a prolonged period of unusually high activity preceded the flare. If the flare indeed released the external twist energy, then the current through the magnetosphere should have decreased after the flare, and the coronal luminosity now should be smaller than it was prior to the flare.

A possible way to probe the twist evolution is to measure the history of spindown rate $\dot{P}$ of the magnetar. The existing data confirm the theoretical expectations: the spin-down of SGRs was observed to accelerate months to years following periods of activity (Kouveliotou et al. 1998, 1999; Woods et al. 2002). A similar effect was also observed following more gradual, sub-Eddington flux enhancement in AXPs (Gavriil & Kaspi 2004). This "hysteresis" behavior of the spindown rate may represent the delay with which the twist is spreading to the outer magnetosphere.

Since the density of the plasma corona is proportional to the current that flows through it, changes in the twist also lead to changes in the coronal opacity. The opacity should increase following bursts of activity and affect the X-ray pulse profile and spectrum. Such changes, which persist for months to years, have been observed following large X-ray outbursts from two SGRs (Woods et al. 2001).

8.7. Further Developments

1. We focused in this paper on the inner magnetosphere, that is, on field lines that do not extend beyond a radius $R_{\rm max} \sim 2R_{\rm NS}$. This part of the magnetosphere is expected to retain most of the toroidal field energy, and to dominate the non-thermal output of the star. The outer corona may be qualitatively different because it is subject to a strong "cyclotron drag": the resonantly scattered X-rays can escape (rather than convert to $e^{\pm}$), thus providing an efficient sink of energy. This drag will cause a local change of the electric field in the circuit (TLK; Thompson & Beloborodov 2005). At yet larger radii, beyond ~ 200 km from the star, ions may populate higher Landau levels $n > 0$. Then a new degree of freedom appears in the problem: the transverse motion of the ions.

2. Like the Solar transition region, the transition layer at the base of a magnetar corona may respond to the coronal dissipation by increasing the supply of plasma. In particular, pair creation in the transition layer needs further investigation because pairs may feed the coronal current (§ 6.3). The state of this layer and its effect on the corona is determined by the level of plasma turbulence (see §§ 6.2 and 6.4). This layer may partially insulate the star from the hot corona because plasma turbulence suppresses thermal conduction. By trapping the generated heat, the layer may overheat and expand to the corona.

3. The transition layer also plays a crucial role in the energy balance of the corona because it produces radiation that can escape the magnetar. A significant part of the released energy is emitted in the hard X-ray band. The rest of the released energy is deposited in an optically thick surface layer and reprocessed into blackbody radiaton with $k_{\rm B}T \lesssim 1$ keV. An accurate calculation of the ratio of the two emission components (hard X-ray to blackbody) that are fed by the corona remains to be done.

4. The role of transverse waves in the corona, which were suppressed in our numerical experiment, will need to be studied. The waves produce a three-dimensional pattern of magnetic-field fluctuations $\delta(\nabla \times B) \neq 0$ and their study will require 3-D or 2-D simulations.

5. Our plasma model of the corona may be generalized to include the effects of rotation. This can be done by changing the neutrality condition $\rho = 0$ to $\rho = \rho_{\rm co}$. Note that $\rho_{\rm co}$ may be easily maintained by a small polarization of the current-carrying plasma because $\rho_{\rm co} \ll en_c$ (see eq. [2]). It can be taken into account by adding an extra source term $4\pi\rho_{\rm co}$ to the Poisson equation (cf. eq. 21), ${\rm d}E_\parallel/{\rm d}l = 4\pi(\rho - \rho_{\rm co})$. Then $E_\parallel$ vanishes if $\rho = \rho_{\rm co}$ along the magnetic line, so that $\rho_{\rm co}$ is the new equilibrium charge density.

6. It is important to understand the resistive redistribution of the twist in the magnetosphere, in particular its spreading toward the open field lines, because it is a promising source of torque variability in active magnetars (TLK). This would require the construction of a global, time-dependent model of the currents in the magnetosphere.

We thank A. Frolov, P. Goldreich, A. Gruzinov, M. Medvedev, and M. Ruderman for discussions. AMB is supported by NASA ATP and an Alfred P. Sloan Fellowship. CT is supported by the Natural Sciences and Engineering Research Council of Canada.

REFERENCES

Adler, S. L., Bahcall, J. N., Callan, C. G., & Rosenbluth, M. N. 1970, Phys. Rev. Lett., 25, 1061

Arons, J., & Barnard, J. J. 1986, ApJ, 302, 120

Arons, J., & Scharlemann, E. T. 1979, ApJ, 231, 854

Arras, P., Cumming, A., & Thompson, C. 2004, ApJ, 608, L49

Asseo, E., Pelletier, G., & Sol, H. 1990, MNRAS, 247, 529

Bak, P., Tang, C., & Wiesenfeld, K. 1987, Phys. Rev. Lett., 59, 381

Baring, M. G. 2000, Phys. Rev. D, 62, 016003

Baring, M. G., & Harding, A. K. 2001, ApJ, 547, 929

Beloborodov, A. M. 2002, ApJ, 566, L85

Berestetskii, V. B., Lifshitz, E. M., & Pitaevskii, L. P. 1982, Quantum Electrodynamics, Oxford: Pergamon Press.

Bernstein, I. & Kulsrud, R. M. 1961, Phys. Fluids, 4, 1037

Block, L. P. 1978, Ap&SS, 55, 59

Braithwaite, J., & Spruit, H. C. 2004, Nature, 431, 819

Braithwaite, J., & Spruit, H. C. 2006, A&A, in press (astro-ph/0510287)

Carlqvist, P. 1982, Ap&SS, 87, 21

Chang, P., Arras, P., & Bildsten, L. 2004, ApJ, 616, L147

Cheng, B., Epstein, R. I., Guyer, R. A., & Young, C. 1996, Nature, 382, 518

Daugherty, J. K., & Harding, A. K. 1983, ApJ, 273, 761

Daugherty, J. K., & Ventura, J. 1978, Phys. Rev., D18, 1053

De Luca, A., Caraveo, P. A., Mereghetti, S., Negroni, M., & Bignami, G. F. 2005, ApJ, 623, 1051

den Hartog, P. R., Hermsen, W., Kuiper, L., Vink, J., in 't Zand, J. J. M., & Collmar, W. 2006, A&A, in press (astro-ph/0601644)

Diamond, P. H., & Malkov, M. 2003, Physics of Plasmas, 10, 2322

Dietrich, S. S., & Berman, B. L. 1988, Atomic Data and Nuclear Data Tables, 38, 199

Durant, M. & van Kerkwijk, M. H. 2006, ApJ, submitted

Eichler, D., Gedalin, M., & Lyubarsky, Y. 2002, ApJ, 578, L121

Gavriil, F. P., & Kaspi, V. M. 2004, ApJ, 609, L67

Godfrey, B. B., Shanahan, W. R., & Thode, L. E. 1975, Physics of Fluids, 18, 346

Göğüş, E., Kouveliotou, C., Woods, P. M., Thompson, C., Duncan, R. C., & Briggs, M. S. 2001, ApJ, 558, 2

Goldreich, P., & Julian, W. H. 1969, ApJ, 157, 869

Gotthelf, E. V., & Halpern, J. P. 2005, ApJ, 632, 1075

Harding, A. K., & Muslimov, A. G. 2002, ApJ, 568, 862

Harding, A. K., & Daugherty, J. K. 1991, ApJ, 374, 687

Hibschman, J. A., & Arons, J. 2001, ApJ, 554, 624

Herold, H. 1979, Phys. Rev. D, 19, 2868

Herold, H., Ruder, H., & Wunner, G. 1982, A&A, 115, 90

Hulleman, F., van Kerkwijk, M. H., & Kulkarni, S. R. 2004, A&A, 416, 1037

Hurley, K., et al. 2005, Nature, 434, 1098

Ibrahim, A. I., et al. 2001, ApJ, 558, 237

Kaspi, V. M., Gavriil, F. P., Woods, P. M., Jensen, J. B., Roberts, M. S. E., & Chakrabarty, D. 2003, ApJ, 588, L93

Kotov, Y. D., & Kelner, S. R. 1985, Sov. Astron. Lett., 11, 392

Kouveliotou, C., et al. 1998, Nature, 393, 235

Kouveliotou, C., et al. 1999, ApJ, 510, L115

Kuiper, L., Hermsen, W., & Mendez, M. 2004, ApJ, 613, 1173

Lai, D. 2001, Reviews of Modern Physics, 73, 629

Landau, L. D., & Lifshitz, E. M. 1975, Classical Theory of Fields, Oxford: Pergamon Press.

Langmuir, I. 1929, Phys. Rev., 33, 954

Lieb, E. H., Solovej, J. P., & Yngvason, J. 1992, Phys. Rev. Lett., 69, 749

Luo, Q., & Melrose, D. B. 1995, MNRAS, 276, 372

Lyutikov, M. 2006, MNRAS, 367, 1594

Marsden, D., & White, N. E. 2001, ApJ, 551, L155

Melrose, D. B., & Parle, A. J. 1983, Australian Journal of Physics, 36, 799

Mereghetti, S., Götz, D., Mirabel, I. F., & Hurley, K. 2005, A&A, 433, L9

Molkov, S., Hurley, K., Sunyaev, R., Shtykovsky, P., Revnivtsev, M., & Kouveliotou, C. 2005, A&A, 433, L13

Muslimov, A. G., & Tsygan, A. I. 1992, MNRAS, 255, 61

Neuhauser, D., Koonin, S. E., & Langanke, K. 1987, Phys. Rev. A, 36, 4163

Parker, E. N. 1979, Oxford, Clarendon Press; New York, Oxford University Press, 1979, 858 p.

Potekhin, A. Y., Yakovlev, D. G., Chabrier, G., & Gnedin, O. Y. 2003, ApJ, 594, 404

Raadu, M. A. 1989, Phys. Rep., 178, 25

Ruderman, M. A., & Sutherland, P. G. 1975, ApJ, 196, 51

Sturner, S. J., Dermer, C. D., & Michel, F. C. 1995, ApJ, 445, 736

Takata, J., Shibata, S., Hirotani, K., & Chang, H.-K. 2006, MNRAS, 366, 1310

Tang, X. Z., & Boozer, A. H. 2005, Physical Review Letters, 94, 225004

Taylor, J. B. 1986, Reviews of Modern Physics, 58, 741

Thompson, C., & Beloborodov, A. M. 2005, ApJ, 634, 565

Thompson, C., & Duncan, R. C. 1995, MNRAS, 275, 255

Thompson, C., & Duncan, R. C. 1996, ApJ, 473, 322

Thompson, C., & Duncan, R. C. 2001, ApJ, 561, 980

Thompson, C., Duncan, R. C., Woods, P. M., Kouveliotou, C., Finger, M. H., & van Paradijs, J. 2000, ApJ, 543, 340

Thompson, C., Lyutikov, M., & Kulkarni, S. R. 2002, ApJ, 574, 332

Ventura, J. 1979, Phys. Rev., D19, 1684

Woods, P. M., Kouveliotou, C., Göğüş, E., Finger, M. H., Swank, J., Smith, D. A., Hurley, K., & Thompson, C. 2001, ApJ, 552, 748

Woods, P. M., Kouveliotou, C., Göğüş, E., Finger, M. H., Swank, J., Markwardt, C. B., Hurley, K., & van der Klis, M. 2002, ApJ, 576, 381

Walsh, R. W., & Ireland, J. 2003, Astron. Astrophys. Rev., 12, 1

Woods, P. M., & Thompson, C. 2006, in "Compact Stellar X-ray Sources," eds. W. H. G. Lewin and M. van der Klis, Cambridge University Press, astro-ph/0406133

Zavlin, V. E., & Pavlov, G. G. 2002, Neutron Stars, Pulsars, and Supernova Remnants, 263

This preprint was prepared with the AAS LaTeX macros v5.2.

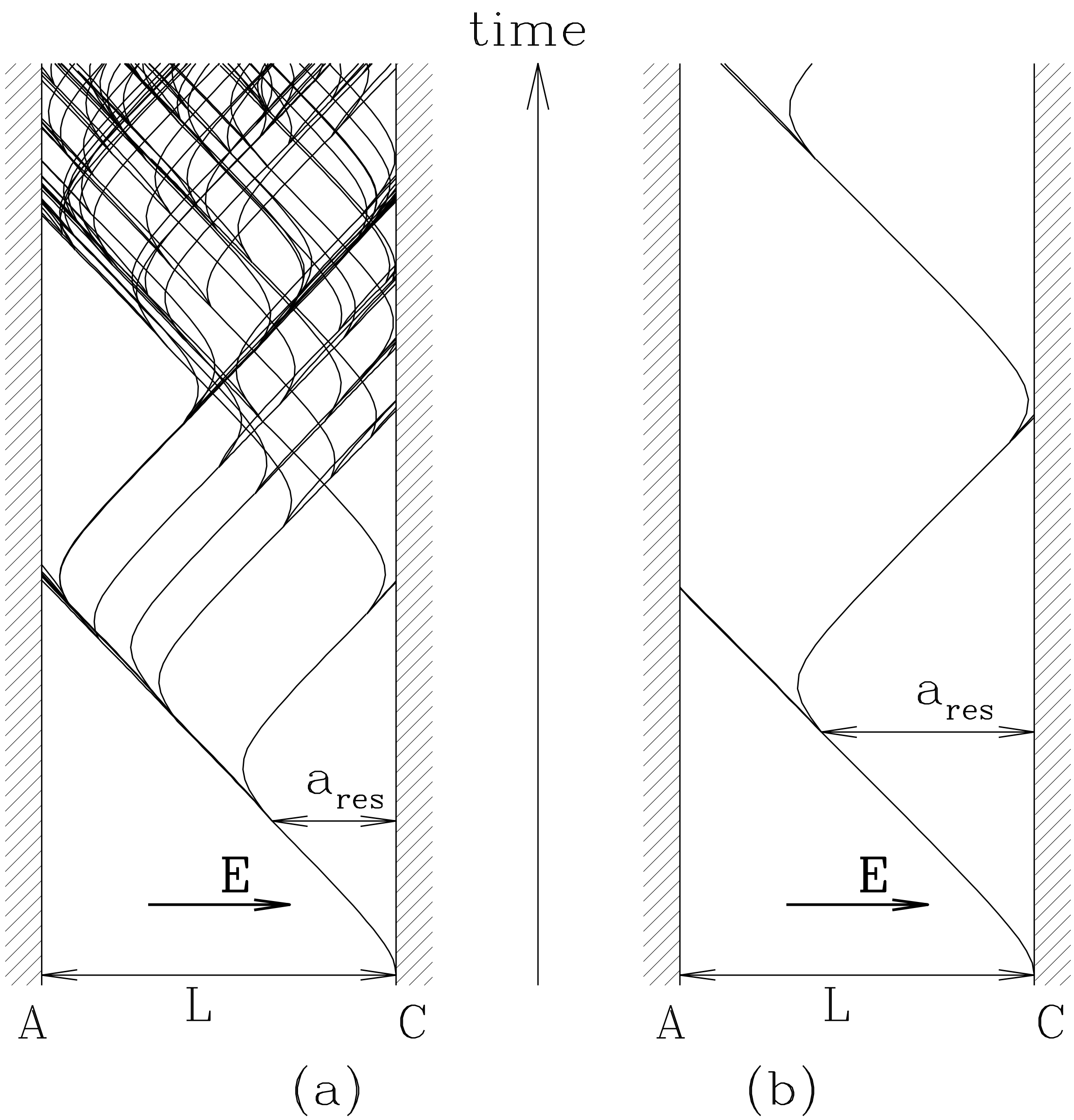

Fig. 5.— Spacetime diagrams illustrating the critical character of the $e^{\pm}$ breakdown and formation of avalanches. The toy model used in this illustration is described in the text; $e\Phi_e = eEL = 11m_ec^2$ is assumed. Worldlines of particles are shown, starting with one seed electron at the cathode. (a) $a_{\rm res}/L = 0.35$ (supercritical case). (b) $a_{\rm res}/L = 0.6$ (critical case). The magnetar corona is expected to evolve close to the threshold for triggering $e^{\pm}$ avalanches, when $a_{\rm res}$ is comparable to but somewhat smaller than L (or, equivalently, when the voltage Φ_e is just above the minimum needed to trigger $e^{\pm}$ creation). The $e^{\pm}$ avalanches are then initiated stochastically in the regime of self-organized criticality. This expectation is confirmed by the numerical experiment described in § 5.4.

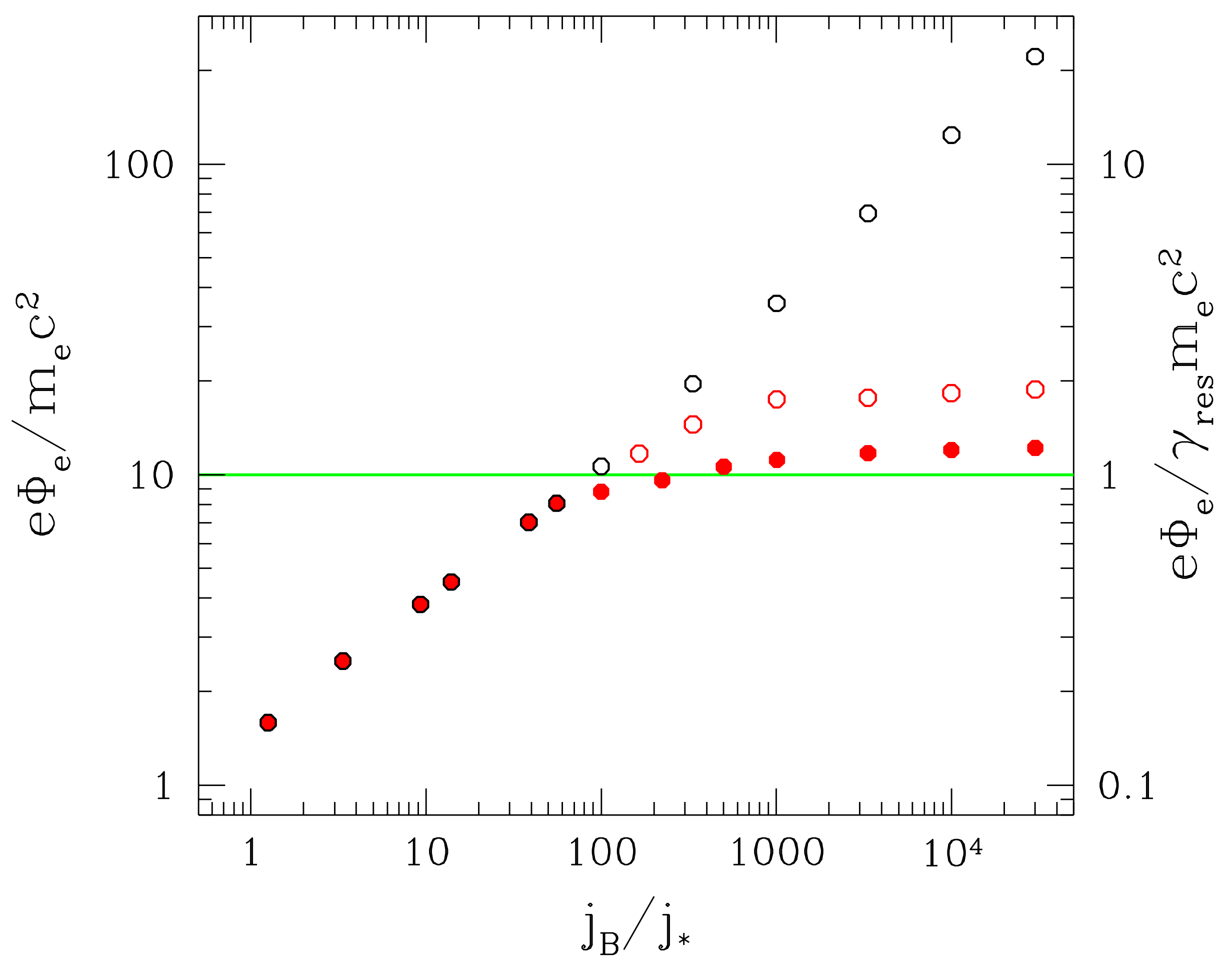

Fig. 6.— Voltage vs. current for circuits with (red circles) and without (black circles) $e^{\pm}$ creation. Model A of pair production is represented by filled red circles and Model B by open red circles; both models have the resonant Lorentz factor $\gamma_{\rm res} = 10$. Each point in the figure represents the result of one experiment and shows the time-averaged voltage Φ_e. The current is expressed in units of j_* (see the text).

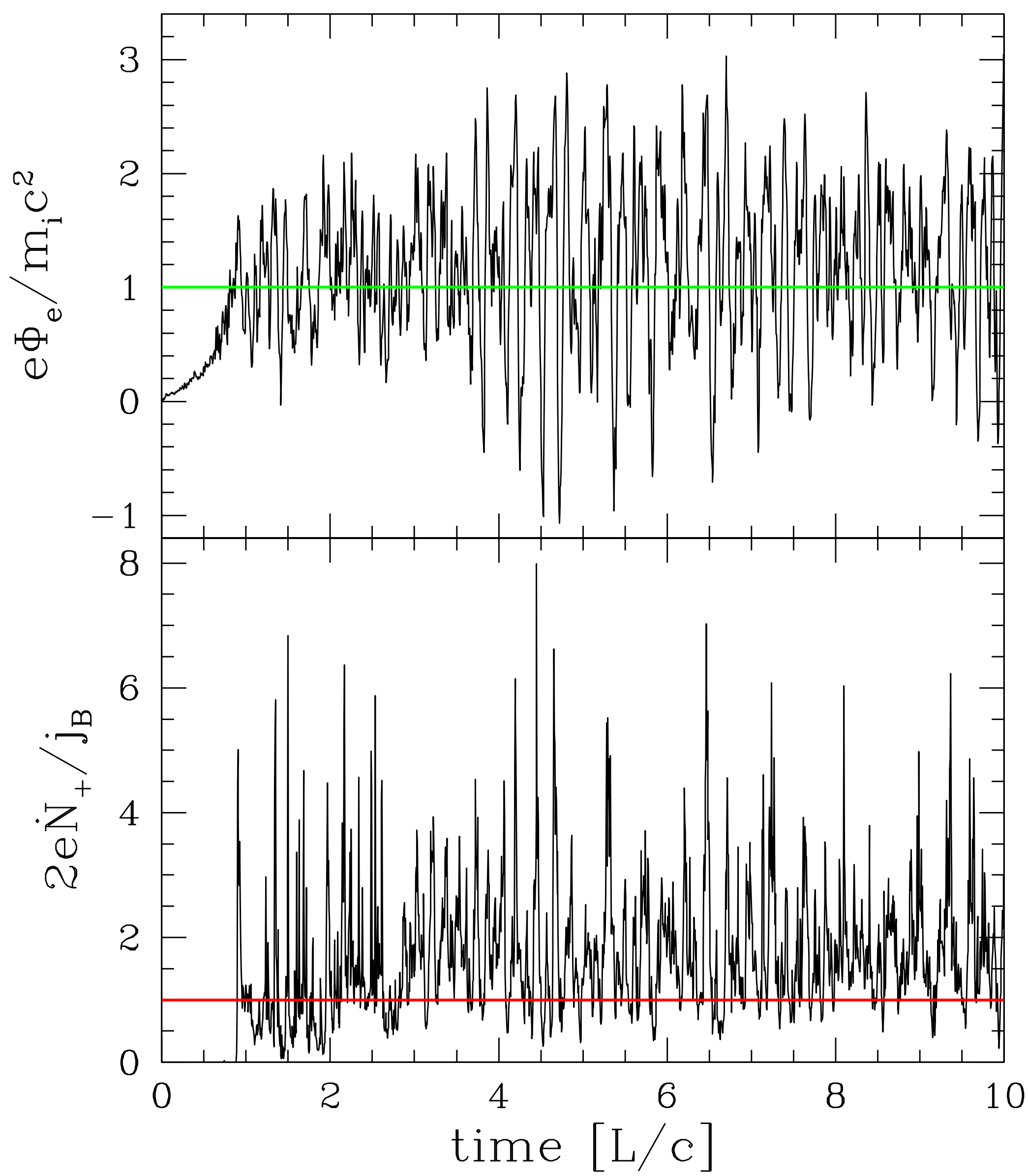

Fig. 7.— Relaxation of the circuit during the first 10 light-crossing times. The circuit parameters are: $m_i = 10m_e$, $j = 10^4 j_*$, $\gamma_{\rm res} = m_i/m_e$. Model A is used for pair production (infinite window above $\gamma_{\rm res}$ with free path $l_{\rm res} = 0$). A quasi-steady fluctuating state is established after a few L/c.

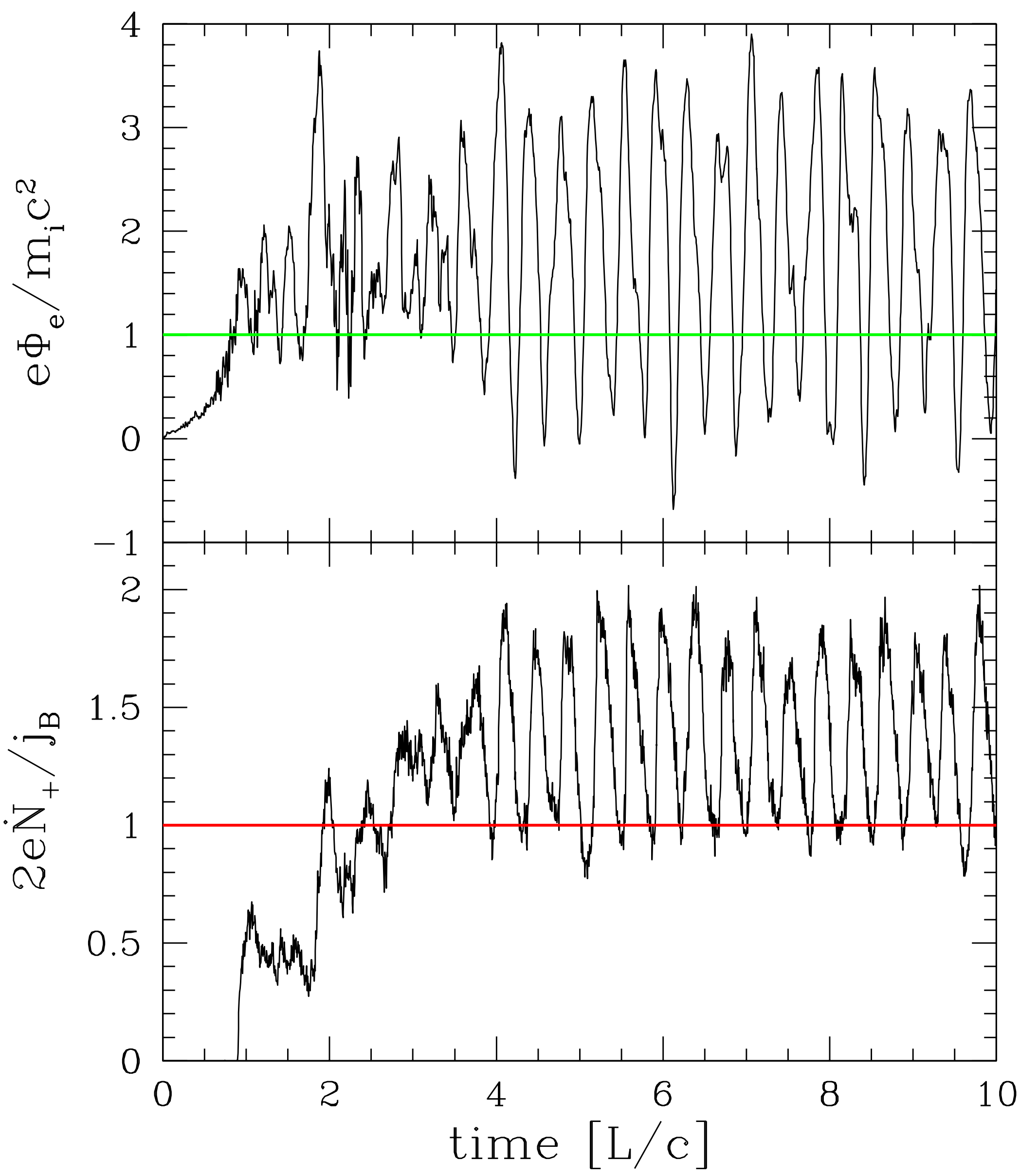

Fig. 8.— Same as Fig. 7, but Model B is used for pair production: narrow window $\gamma_{\rm res} < \gamma_e < 2\gamma_{\rm res}$ with free path $l_{\rm res} = L/3$.

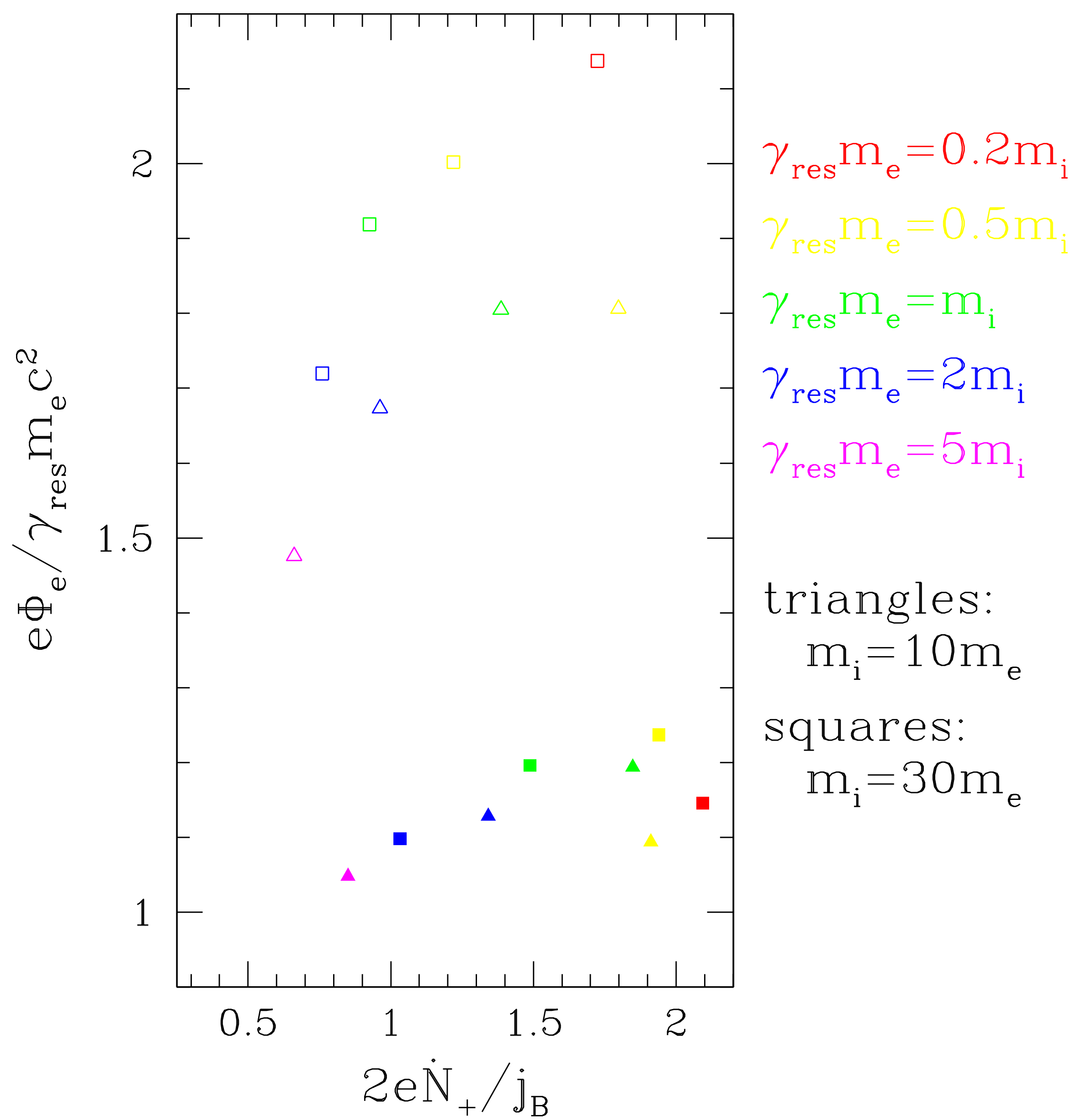

Fig. 9.— Circuits with $m_i/m_e = 10, 30$ and various values of $\gamma_{\rm res}$ ranging from $m_i/5m_e$ to $5m_i/m_e$. Here $\bar{\Phi}_e$ is the time-averaged voltage and $2\dot{N}_+$ is the time-averaged rate of $e^{\pm}$ creation in the circuit. Model A of pair production is shown by open symbols, and Model B by filled symbols.

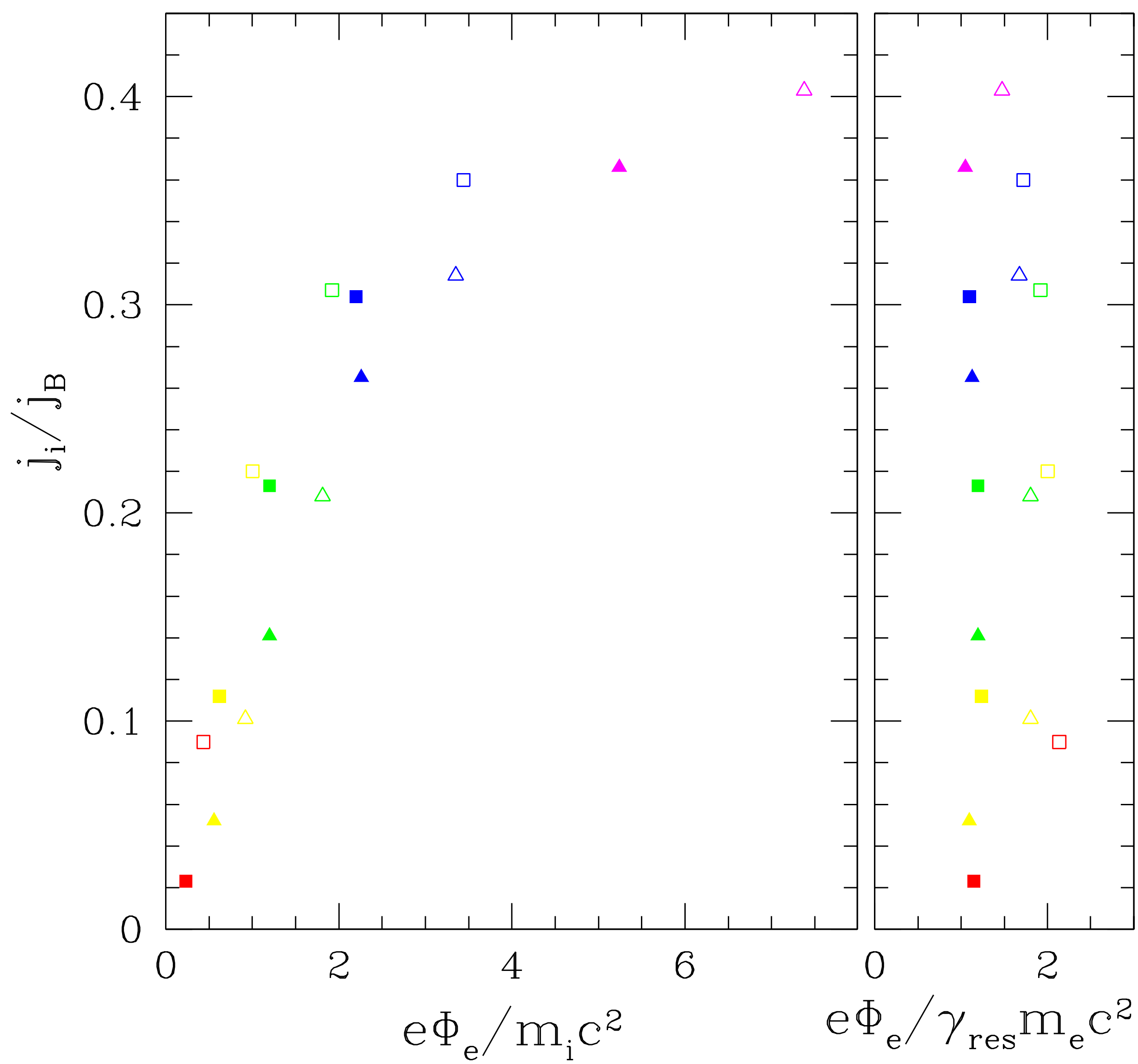

Fig. 10.— Fraction of the electric current carried by ions vs. voltage, for the same set of models as in Fig. 9. Colors have the same meanings. In the left panel voltage is taken in units of $m_i c^2$, and in the right panel in units of $\gamma_{\rm res} m_e c^2$.

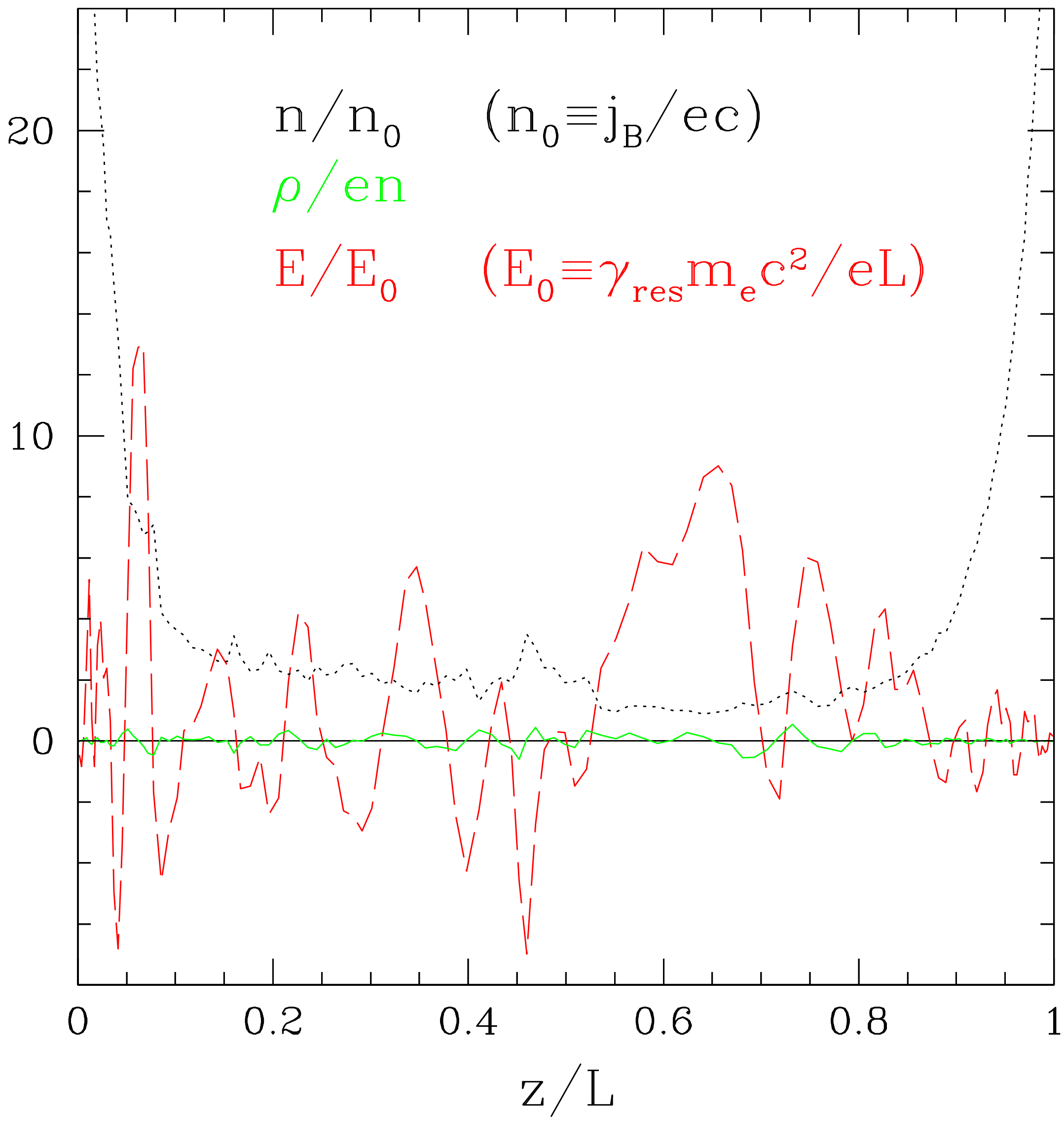

Fig. 11.— Snapshot of the circuit with $\gamma_{\rm res} = m_i/m_e = 10$ and $j_B = 10^4 j_*$ ($\lambda_{\rm D}/L = 10^{-2}$). Model A is assumed for $e^{\pm}$ creation. The three curves show particle density $n = n_i + n_e + n_p$ (dotted), charge density $\rho = e(n_i - n_e + n_p)$ (solid), and electric field E (long-dash).

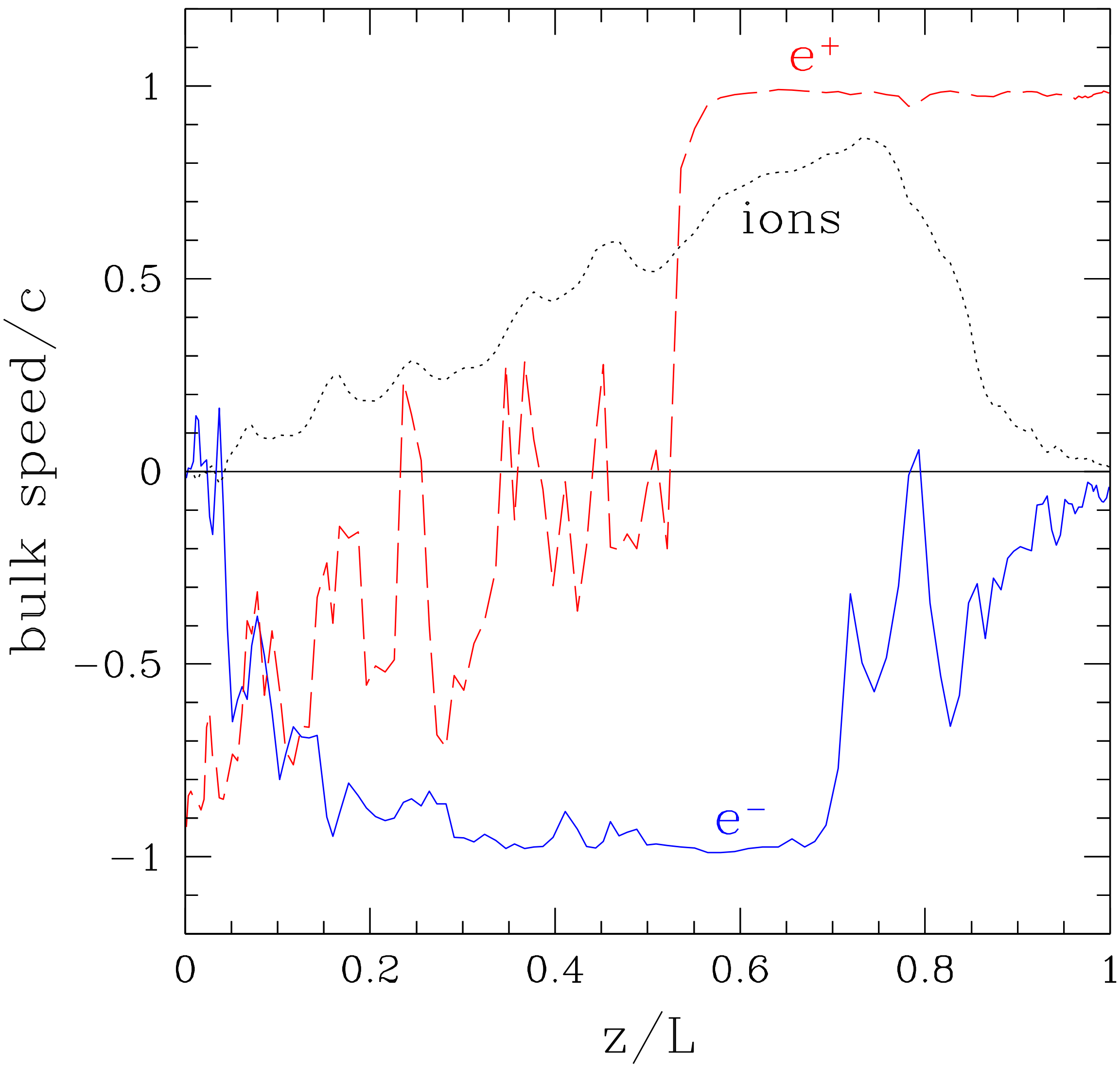

Fig. 12.— Mean velocities of ions, electrons, and positrons as a function of position in the circuit. The mean velocities v_X are related to densities n_X of the three species $X = i, e, p$ by $v_X = j_X/\bar{v}_x$ where j_X is the current carried by species X. The snapshot is taken of the same model and the same time as Fig. 11.

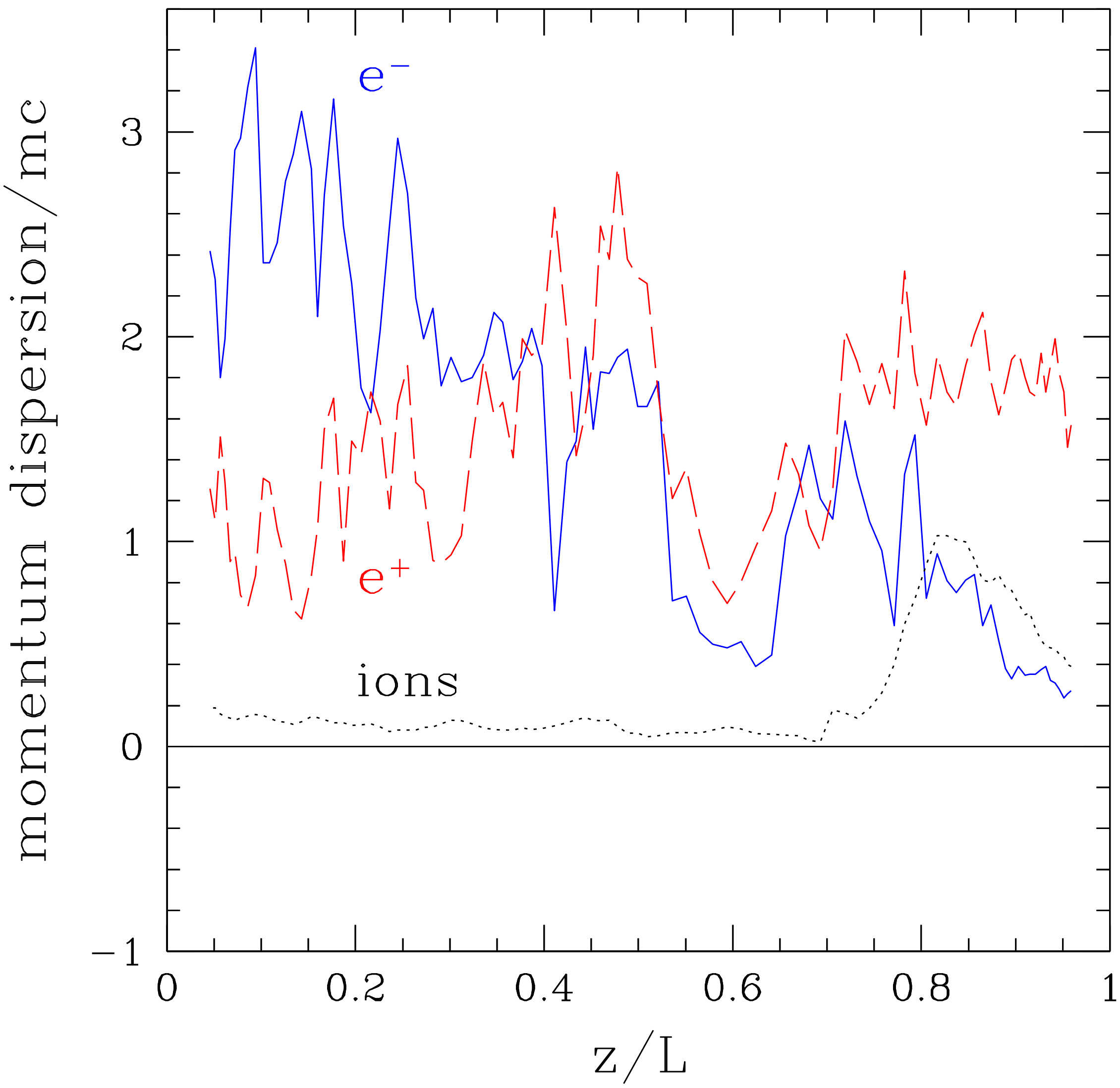

Fig. 13.— Dispersion of momentum (around the mean bulk momentum) for ions, electrons, and positrons as a function of position in the circuit. The snapshot is taken of the same model at the same time as in Fig. 11. Only the corona is shown ($h < z < L - h$) and the surface layers of height $h = 0.04L$ are excluded from the figure.

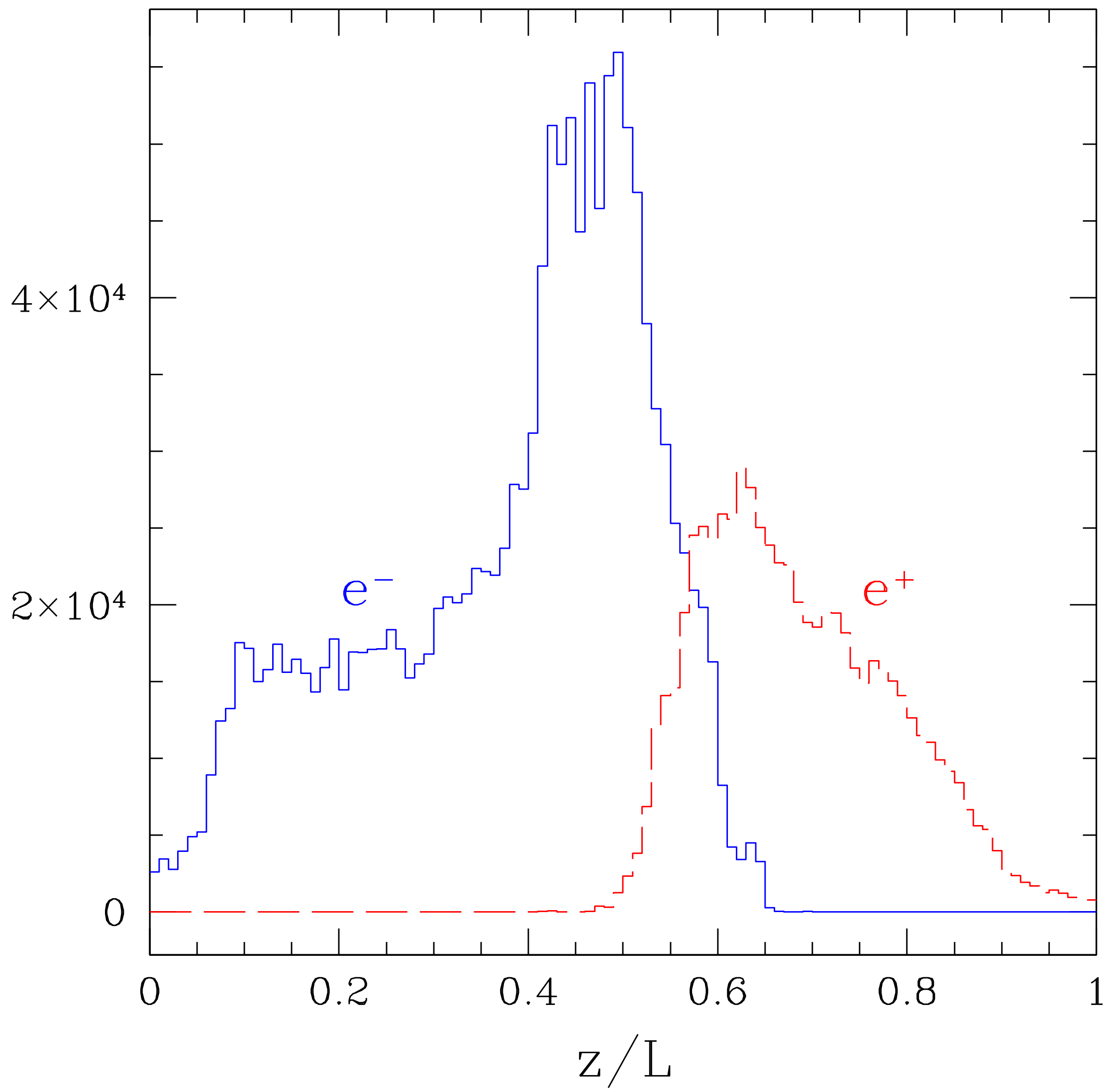

Fig. 14.— Distribution of pair-creation events at $10 < ct/L < 20$ over z. The circuit model is the same as in Figs. 7 and 11-13. The figure shows separately pair creation by accelerated e^- and e^+ (solid and long-dashed curves, respectively).